INVESTIGATION OF WIND EFFECTS ON TALL BUILDINGS
THROUGH WIND TUNNEL TESTING


A THESIS SUBMITTED TO
THE GRADUATE SCHOOL OF NATURAL AND APPLIED
SCIENCES
OF
MIDDLE EAST TECHNICAL UNIVERSITY


BY


BENGİ KAYIŞOĞLU


IN PARTIAL FULFILLMENT OF THE REQUIREMENTS
FOR
THE DEGREE OF MASTER OF SCIENCE
IN
CIVIL ENGINEERING


JUNE 2011

Approval of the thesis:

**INVESTIGATION OF WIND EFFECTS ON TALL BUILDINGS THROUGH WIND TUNNEL TESTING**

submitted by **BENGİ KAYIŞOĞLU** in partial fulfillment of the requirements for the degree of **Master of Science in Civil Engineering Department, Middle East Technical University** by,

Prof. Dr. Canan Özgen                                                         _____
Dean, Graduate School of **Natural and Applied Sciences**

Prof. Dr. Güney Özcebe                                                       _____
Head of Department, **Civil Engineering**

Assist. Prof. Dr. Özgür Kurç                                               _____
Supervisor, **Civil Engineering Dept., METU**

**Examining Committee Members:**

Assoc. Prof. Dr. Uğur Polat                                               _____
Civil Engineering Dept., METU

Assist. Prof. Dr. Özgür Kurç                                               _____
Civil Engineering Dept., METU

Assist. Prof. Dr. Alp Caner                                               _____
Civil Engineering Dept., METU

Assist. Prof. Dr. Oğuz Uzol                                               _____
Aerospace Engineering Dept., METU

Assist. Prof. Dr. Tolga Yılmaz                                             _____
Engineering Sciences Dept., METU

                                                        Date:       09.06.2011

I hereby declare that all information in this document has been obtained and presented in accordance with academic rules and ethical conduct. I also declare that, as required by these rules and conduct, I have fully cited and referenced all material and results that are not original to this work.


Name, Last Name    : Bengi KAYIŞOĞLU

Signature    :

# ABSTRACT

## INVESTIGATION OF WIND EFFECTS ON TALL BUILDINGS THROUGH WIND TUNNEL TESTING

Kayışoğlu, Bengi

M.Sc., Department of Civil Engineering

Supervisor: Assist. Prof. Dr. Özgür Kurç

June 2011, 138 pages

In recent years, especially in the crowded city-centers where land prizes have become extremely high, tall buildings with more than 30 floors have started to be designed and constructed in Turkey. On the other hand, the technical improvements have provided the opportunity of design and construction of more slender structures which are influenced by the wind actions more. If the building is flexible, wind can interact with it so the wind induced oscillations can be significantly magnified. In order to analyze the response of such buildings under wind effects, wind tunnel tests are accepted to be the most powerful tool all over the world. In this study, a series of tests were performed in Ankara Wind Tunnel on a model building in the shape of a rectangular prism. For the similitude of flow conditions, passive devices were designed. The response of the model building was measured through a high frequency base balance which was designed specifically for this case study. Through the tests, the effects of turbulence intensity, vortex shedding and wind angle of attack on the response of the building were questioned. Finally, the results were compared with the results of various technical specifications about wind.

**Keywords:** HFBB, High Frequency Base Balance, Wind, Wind Effects, Wind Loads, Wind Tunnel Testing, Tall Buildings

# ÖZ

## YÜKSEK BİNALARDA RÜZGAR ETKİLERİNİN RÜZGAR TÜNELİ DENEYLERİYLE TESPİTİ

Kayışoğlu, Bengi

Yüksek Lisans, İnşaat Mühendisliği Bölümü

Tez Yöneticisi: Yrd. Doç. Dr. Özgür Kurç

Haziran 2011, 138 sayfa

Son yıllarda ülkemizde, özellikle de arsa fiyatlarının yüksek olduğu şehir merkezlerinde 30 kattan daha yüksek binaların inşaatları oldukça yaygınlaşmaktadır. Ayrıca, tasarım ve yapım aşamalarında kullanılan tekniklerin gelişmesi ve iyileştirilmesi daha az malzeme ve daha küçük yapı elemanı kesitlerinin uygulanmasına olanak sağlamaktadır. Bu durumda ortaya çıkan esnek binalarda rüzgar etkileşimleri gözlenmekte ve bu etkileşimler rüzgar kaynaklı salınımları ciddi miktarlarda arttırabilmektedirler. Rüzgar tüneli deneyleri, binalar üzerindeki rüzgar etkilerinin incelenmesinde dünyada en çok kabul görmüş yöntemdir. Türkiye'de ilk defa yapılan bu çalışma kapsamında kısa test kesiti özelliklerine sahip Ankara Rüzgar Tüneli'nde bir seri test gerçekleştirilmiştir. Akış koşullarının benzerliğinin sağlanması için özel yüzey pürüz elemanları tasarlanmıştır. Deneylerde dikdörtgen prizma şeklinde oluşturulan bir bina modeli üzerindeki rüzgar tesirleri bu proje için tasarlanan yüksek frekanslı taban balans sistemiyle ölçülmüş, rüzgar tesirlerinin türbülans içeriği, periyodik girdap etkisi ve rüzgar vuruş açısından nasıl etkilendiği gözlenmiştir. Son olarak da elde edilen sonuçlar rüzgar yönetmelikleriyle hesaplanan sonuçlarla karşılaştırılmıştır.

**Anahtar Kelimeler:** HFBB, Yüksek Frekanslı Taban Balans Yöntemi, Rüzgar, Rüzgar Etkileri, Rüzgar Yükleri, Rüzgar Tüneli Testi, Yüksek Bina

*To my fiance, Erman Atak and to my family…*

# ACKNOWLEDGEMENTS

# TABLE OF CONTENTS

# LIST OF TABLES

TABLES

# LIST OF FIGURES

FIGURES

# CHAPTER 1

# INTRODUCTION

## 1.1  PROBLEM DEFINITION

Tall buildings have been designed and constructed since the beginning of the twentieth century. In today's world, there are several buildings which have more than a hundred of floors. Design of such buildings has been preferred especially in overcrowded cities where the prices of building lands cost much. In Turkey, construction of buildings that have more than thirty floors has become widespread for the last few years as well. For instance, the highest building in Turkey (236 meters tall) which will be constructed in İstanbul, has been introduced.

Recent improvements in structural analysis and design technologies, developed construction techniques and production of higher strength materials result in the fact that modern buildings can be designed by using smaller structural elements and fewer materials which means that modern buildings are lighter in weight and more flexible when compared with the older ones. An important outcome of these light and flexible buildings is that they get more prone to the wind induced actions. Thus, for a tall building to be safe, remain serviceable and provide comfort to its occupants through its service life time, its behaviour under wind actions should be carefully analysed and necessary precautions should be taken.

As the height of the buildings increases, its vulnerability to wind effects also increases. Particularly, compared with a rigid one, a building with a natural period of more than 1 second, perceives the wind-induced vibrations more. In general, the response of such a flexible building under wind loads can be examined under three categories. First one is about the comfort criterion which is related with the human perception of acceleration. The

top floor acceleration of the designed building should remain below the specified limits in order to provide comfort to its occupants because humans are sensitive to vibrations to the extent that they feel unsafe. Second category regarding the building response under wind load is the expression of the dynamic loads induced by wind as equivalent static loads or as time dependent series. These equivalent loads should be formed such that they produce maximum forces considering the random behaviour of the wind. Final category is related with the cladding design. Compression and suction forces acting on the outer surfaces of the buildings should carefully be determined considering also the localized effects. Approach of calculating pressure for the design of cladding system is different than the pressure determination in equivalent static loads because in the design of the cladding system, rather than the average values, the maximum and minimum values in a short period of time are more dominant.

Detailed investigation of wind effects on tall buildings requires consideration of the building geometry, direction of the wind and topographic factors. Researches conducted in the last 20 years show that the response of the building in the across wind and torsional directions are at least substantial as the response in along wind direction (Mendis, et al., 2007). There are some analytical procedures in literature that are utilised to solve the along wind response of buildings; however, there are no such relations defined in full for the across wind or torsional components or for the local pressure effects. Consequently, a widely accepted and effective tool for the determination of all these components is performing wind tunnel tests (Holmes, 2005). Moreover, wind tunnel tests provide the opportunity to analyse structures with extraordinary geometries which is not possible by using the traditional methods which employ equivalent static loads estimated from wind pressures multiplied by some constants that are derived for ordinary shapes.

In the design of a building, the designer must obey the rules given in the technical specifications adopted for the relevant country. Two examples for the most widely used standards particularly for wind actions on structures are ASCE 7-05 (by American Society of Civil Engineers) (ASCE 7-05, 2005) and Eurocode 1 (by European Committee for Standardization) (Eurocode 1, 2005). These standards offer some procedures for the determination of response of buildings under wind loads; however, they are valid only for buildings in rectangular prismatic or cylindrical shapes. In addition, these techniques ignore the interaction of the building with the structures in its vicinity. Another issue that is underlined in the standards is that the described procedures can be applied only to the buildings that are less than 200 meters in height (ASCE 7-05, 2005). For the special

circumstances such as for a taller building in different geometry or for the one which have other structures that may affect its own behaviour under wind actions, the standards force the designer to utilize the results of wind tunnel tests. On the other hand, in Turkey, the official specification regarding the load actions on structures is TS 498 (TS 498, 1987). In the wind load part of TS 498, the descriptions were adopted from DIN 1055 in 1972 and it has not been updated since then. In this standard, wind load effects are determined by applying the equivalent static loads on the building and solving the system. Concepts of the cladding design or the local pressure effects or wind tunnel test necessities are not covered. These deficiencies are mostly resolved by the guideline called "İstanbul Yüksek Binalar Rüzgar Yönetmeliği (İYBRY)" (İYBRY, 2009). As well as ASCE 7-05 and Eurocode 1, İYBRY also forces the designers to conduct a wind tunnel test for the buildings which need a more comprehensive and sensitive investigation regarding the wind issue.

As a result, main aim of this study is to review the literature for determination of wind induced response of tall buildings by means of performing a series of wind tunnel tests since it has become a necessity for design of tall buildings. Another aim is to analyze the nature of wind in a more elaborate way than the traditional approaches used in Turkey. After the wind tunnel tests and relevant analysis, the results are compared with some technical specifications for the purpose of assigning the required improvements in the study.

## 1.2   LITERATURE SURVEY

This chapter is devoted to the studies related to the history and the theoretical developments of wind effects on tall buildings. Firstly, the wind effects on tall buildings will be introduced. Secondly, the history of wind tunnels will be discussed and finally, the special data acquisition system widely used in the wind tunnel tests, *High Frequency Base Balance* (H-FBB) will be explained.

### Wind Effects on Tall Buildings

Tall buildings which have low natural frequencies are very sensitive under wind loads. Inevitably, in the design of these structures, wind effects play a major role. When a tall building is exposed to wind, it experiences oscillations which result in member forces, displacements and accelerations not only in the along-wind direction but also in the across-wind and torsional directions. These response quantities have great importance regarding

both the ultimate capacity of the building and its serviceability. In other words, ultimate capacity of a building is related with the balance between load carrying capacities of the structural members and the member forces that occur whereas serviceability is associated with the accelerations since human beings perceive oscillations such that they feel unsafe and uncomfortable. Another wind related issue is that for the design of the glazed cladding systems and roofs of the buildings, the local extremes of pressure occurring due to wind should be carefully analyzed (Mendis, et al., 2007).

Unlike streamlined bodies that are similar to a water drop, the geometries of buildings are most probably bluff bodies with sharp and flattened fronts. Therefore, in order to understand the behaviour of a building under wind loads, flow around bluff bodies should be carefully studied. Flow around a bluff body does not follow a tangential pattern. Instead, in the separation layers, highly unstable and turbulent vortices are formed. These vortices create a response of the body that is full of uncertainties (Holmes, 2005).

Traditionally, wind loads are treated as static and deterministic lateral loads acting on the buildings which cause response in along-wind direction only. The above mentioned vortices forming at the back of the body, however, can lead to forces in transverse (across-wind) direction if the natural frequency of the building is small. In addition, the asymmetric pressure distribution among the building originates torsional response and twist. Thus, these three major components of response should be examined for a more elaborate understanding of behaviour of the building under wind loads (Holmes, 2005).

In literature, for the along-wind response, there are several closed form analytical solutions related with bluff body aerodynamics and random vibration theory; whereas, for the across-wind and torsional ones, experimental studies are necessary (Holmes, 2005). Especially, after a certain height of the buildings, design standards are forcing the designers to conduct a wind tunnel test (ASCE 7-05, 2005) (Eurocode 1, 2005). With the help of wind tunnel tests, the statistical properties of the along wind, across wind, and torsional responses can be obtained. Through the data obtained from the wind tunnel tests, the design base force quantities (base shear and moment), top acceleration and the equivalent static load representations can be achieved which are the necessary parameters for the design of a building.

Human perception to wind induced vibrations of tall buildings is an important issue that should be carefully and accurately determined during the design of such buildings. Human beings are very sensitive to vibration to the extent that they feel uncomfortable and unsafe

even if these vibrations cause very little member forces. Consequently, the design of most tall buildings is governed by the serviceability design criteria rather than the strength and ultimate capacity issue.

Human perception is directly related with the acceleration of the oscillations. There are various studies performed by researchers about this issue in physiological and psychological ways (Irwin, 1978) but there is no generally accepted comfort criteria given in the design standards. In the following, there will be given some guidelines about the human perception and comfort criteria in the design of buildings in Table 1.1 (Mendis, et al., 2007). In the table, the upper limits were recommended by Irwin (1978).

**Table 1.1 Human perception levels**

| LEVEL | ACCELERATION $(m/s^2)$ | EFFECT |
|:---:|:---:|:---|
| 1 | <0.05 | People cannot perceive motion. |
| 2 | 0.0.5-0.1 | a) Sensitive people can perceive motion. |
| | | b) Hanging objects may move slightly. |
| 3 | 0.1-0.25 | a) Majority of people can perceive motion. |
| | | b) Level of motion may affect desk work. |
| | | c) Long-term exposure may produce motion sickness. |
| 4 | 0.25-0.4 | a) Desk work becomes difficult or almost impossible. |
| | | b) Ambulation still possible. |
| 5 | 0.4-0.5 | a) People strongly perceive motion. |
| | | b) Difficult to walk naturally |
| | | c) Standing people may lose balance. |
| 6 | 0.5-0.6 | Most people cannot tolerate motion and are unable to walk naturally. |
| 7 | 0.6-0.7 | People cannot walk or tolerate motion. |
| 8 | >0.85 | Objects begin to fall and people may be injured. |

*History of Wind Tunnels*

Wind tunnel testing is an experimental tool that has been used to examine the aerodynamic effects of wind on a solid object since the end of the nineteenth century. The first attempts for building up such kind of a laboratory was resulted from the need of understanding the lift and drag forces acting on surfaces cutting through the atmosphere for the purpose of designing and making a flying machine. Around 1740-1750, an English mathematician, Benjamin Robins employed the idea of moving the air past an object that is stationary for the purpose of simulating its movement in the air. He arranged a system that consists of a whirling arm of 4 ft long and a falling weight attached to a pulley. The idea was to obtain a wind speed at the tip of the arm where the model was mounted. After Robins, in 1804, Sir George Cayley made improvements in the design of his whirling arm system and built a small glider (Baals, et al., 1981). But due to the centrifugal forces, the aircraft models on the end of a whirling arm were prone to very high turbulence. Hence, reliable relative velocity between the model and air could not be determined. Moreover, it was rather hard to set up instruments and measure small forces exerted on models while they were moving with high speeds. As a result, the need for more extensive testing equipment has aroused.

This brings the first enclosed wind tunnel invented and operated by Francis Herbert Wenham, a Council Member of the Aeronautical Society of Great Britain in 1871 (Baals, et al., 1981). Since then, the wind tunnel testing techniques have been widely used in aeronautical engineering. In addition, for the revolutions in auto industry and for civil engineering structural design purposes, wind tunnel tests had become invaluable tools.

Reports in the literature stated that the use of wind tunnels in the design of man-made structures, i.e. civil engineering structures date back to 1742 to 1759. First attempts can be summarized as inspections on small scale models mounted on rotating disks in open environment. Getting some measurements from the wind tests started approximately 150 years later, in 1894-1895; wind induced pressures were measured on simple building models in Denmark. The test was performed in a gas works smoke stack. In the wall of this stack, in a test section with 0.23 x 0.11 m in cross section and 1.02 m in length was constructed and flow was induced to a small building model. From 1890s to 1950s, in wind tunnel tests for model buildings and mass-transport studies only, pressure measurements were performed. On the other hand, these wind tunnels were not properly designed to simulate natural winds. The relevant wind tunnel studies performed at the National Physical Laboratory and at Colorado State University have indicated the fact that in order to provide a well-established

simulation of a structure's behaviour under wind loading, the exposed wind should essentially be similar to the natural one. This brings the necessity of atmospheric boundary-layer flow (Cermak, 2003). Atmospheric boundary layer is the thickness where the wind speed profile reaches a constant magnitude.

As a result, the first wind tunnel capable of creating atmospheric boundary layer was designed during 1955-1957 and its construction was finished in 1962 at Colorado State University. Its long test section (29.3 m) together with the heating and cooling capacities make it possible to develop thick turbulent boundary layers and simulate the natural wind properties (Cermak, 2003). The first major boundary layer wind tunnel study for a tall building was performed in this wind tunnel in Colorado State University for the design of the twin towers of the World Trade Centre, New York, in the mid 1960s (Holmes, 2005). During 1980-1995, several boundary layer wind tunnels (BLWT) with some advanced properties such as simulating wind and wave forces for offshore structures or automated surface roughness creation system for the simulation of different wind profiles were constructed in University of Western Ontario (Canada), Monash University (Australia), the Public Works Research Institute in Tsukubu (Japan) (Cermak, 2003).

In Turkey, unfortunately there is no boundary layer wind tunnel with a long test section at present. But, there is one with a short test section in Ankara which belongs to TÜBİTAK-SAGE, called Ankara Wind Tunnel (AWT). Although Mustafa Kemal ATATÜRK gave the directions for the design and construction of a wind tunnel for aircraft industry works, the starting of the project was after his death in 1947 and the construction were finished in 1950. The wind tunnel, however, was not functional until it was delegated to TÜBİTAK-SAGE in 1994. For AWT to work properly, several improvements were made in order to fulfil the technological necessities. At the end of these enhancement processes during 1994-1998, it started to serve for numerous projects of aeronautical and automotive industries and for Turkish Armed Forces (Tübitak Savunma Sanayii Araştırma ve Geliştirme).

AWT is a closed circuit wind tunnel with 3.05 x 2.44 m test section and 6.1 m length. Its 750 kW power make it possible to achieve 90 m/sec of wind speed in the test section. The general overview of Ankara Wind Tunnel is presented in Figure 1.1. For such tunnels with short test section lengths, the creation of atmospheric boundary layer is only possible with the use of surface roughness elements.

| 1 | Test section |
| 2 | Outlet diffuser |
| 3 | First rotational ailerons (two-layers) |
| 4 | Rotor and conditioner ailerons |
| 5 | Second ailerons |
| 6 | Second rotational ailerons (two-layers) |
| 7 | Flow regulator baffles |
| 8 | Rest room and collector |
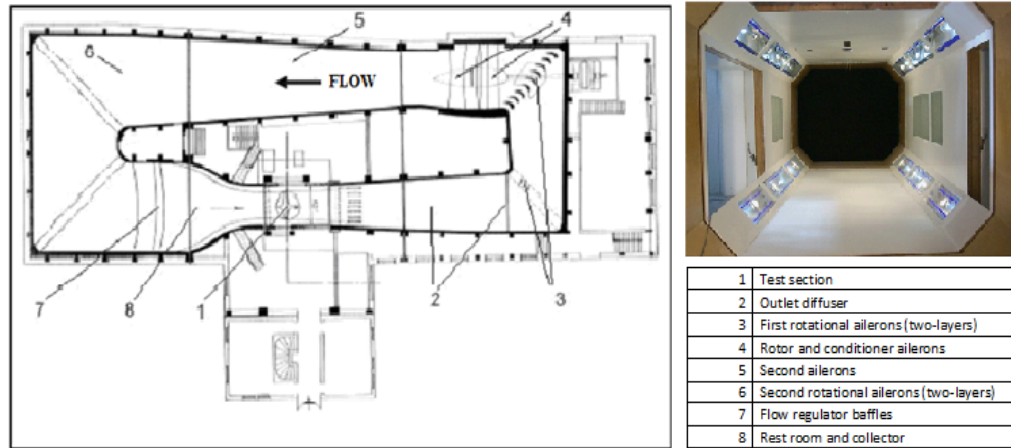
**Figure 1.1 Plan drawing of AWT (on left) and test section (on right) (Tübitak Savunma Sanayii Araştırma ve Geliştirme)**

*Types of the Wind Tunnel Experiments for Tall Buildings*

In order to analyze the effects of wind on high rise buildings, three types of experiments are generally conducted.

- ⇒ Synchronous multi-pressure scanning system (SM-PSS)
- ⇒ High frequency base balance (H-FBB)
- ⇒ Aeroelastic model tests

The types of the wind tunnel tests that are based on the pressure fluctuations on the models are the SM-PSS tests. These kinds of tests have been conducted since 1986 (Fuji, et al., 1986). The main idea in this type is to measure the time series of instantaneous pressure distributions occurring on the exterior surfaces of the model utilizing pressure tubes mounted on it. The other types of information such as the base force components (shear and moments) can be indirectly obtained relating them to the pressure measured. Since the pressure fluctuation monitoring is the basis of the SM-PSS tests, they are mostly preferred for the pressure based design works such as the cladding design and the design of large-area roof systems. SM-PSS tests are very useful in the development and improvement works of the building design specifications since the codes approach to wind loading problems from the pressure point of view. In the standards while converting the wind pressure to resultant forces, some constant drag coefficients are utilized which can be more specific and detailed by the application of such tests. In spite of these advantages of pressure tests, their usage

8

may be debatable for some high-rise buildings because the space necessary for the accommodation of pressure tubing for taps may be insufficient if the model structure is slender. Actually, the fundamental difference between SM-PSS and H-FBB is that unlike SM-PSS tests, base force components of the model are directly measured in H-FBB tests through special data acquisition systems which seems more practical since the major parameters in the design of a building are the base force components. In both of SM-PSS and H-FBB tests, the models are rigid made up of balsa wood, polystyrene foam or thin-walled plastic (Gamble, 2003) hence wind/structure interaction cannot be determined from these two tests. For this purpose, aeroelastic tests are conducted.

When a lightly damped, low mass and highly flexible structure experiences wind-induced oscillations, the deformations in turn lead to amplifications in the wind loads that the structure feels. This phenomenon is known as wind/structure interaction and it may result in aeroelastic instability with a possible unfavourable consequence such as inadmissible deformations/accelerations or it may also result in lesser extreme effects than predicted (Cermak, 2003). Eventually, performing aeroelastic model tests is the only tool in order to determine the effects of wind/structure interaction for such structures. In this type of tests, the model of the structure is prepared so that it represents the dynamic properties of the actual structure, i.e. stiffness and damping characteristics. Through this test, the level of damping required to reduce the magnitudes of the damping response quantities to admissible and tolerable values can be identified.

As an expected result, aeroelastic model tests give the most reliable data about the behaviour of the structure under wind loading. It is, however, usually preferred for special structures such as very slender and tall buildings or long span bridges due to its cost. Despite the several advantages of the other two techniques, high frequency base balance is preferred in many wind tunnel laboratories because it is cost effective compared with the other two; it provides directly the time series data for the base force components which is the main goal in the design of buildings, and it is straightforward to apply since it just contains a rigid model connected to the data acquisition devices at the bottom. (Tschanz and Davenport, 1983)

Another issue on conducting a test on a scaled model in order to predict the response of an actual structure is to ensure the similitude. Similitude requires matching of the shape of the wind profile and the turbulence. Wind has a profile that has zero speed on the ground and increasing logarithmically up to a height which is named as the boundary layer height. After

this height, the speed of the wind remains almost constant. *Turbulence* is a flow regime which includes rapid variation of pressure and velocity both in space and time (Simiu, et al., 1978). Due to these variations, turbulence problems should be solved in a probabilistic way. Therefore, turbulence is measured by its statistical properties such as standard deviation or root mean square. The term *turbulence intensity* is the ratio of the standard deviation to the mean value of the turbulence. Turbulence intensity is directly related to the surface roughness. In other words, as the surface roughness increases turbulence intensity also increases. As a result, it is concluded that turbulence intensity decreases with height above the ground (Holmes, 2005). *Turbulence length* is a physical quantity that describes the size of the region containing eddies, i.e. size of the gusty region. In the design standards, both of the shape of the wind profile and the turbulence intensities are defined (ASCE 7-05, 2005) (Eurocode 1, 2005) (İYBRY, 2009). In a wind tunnel test, the aim is to match these quantities. For this reason, *special boundary layer creation elements* are designed which are the tools used to generate the similar wind profile and turbulence intensity in nature. The scale of the model comes from the ratio of this boundary layer height in the tunnel's test section to the one in nature (Shojaee, et al., 2009).

### *High Frequency Base Balance (H-FBB) System*

High frequency base balance is a type of a data acquisition and processing system that consists of ultra-sensitive force measurement arrangements. Although the first time this technique is used dates back to 1960s it has become a widely used wind engineering tool for the last 20 years (Cermak, et al., 1970).

Some of the pioneers of direct force measurement applications in wind engineering are Dr. Jack Cermak, Dr. Alan G. Davenport and Dr. Ahsan Kareem. Dr. Jack Cermak is one of the owners and establishers of Cermak Peterka Petersen, Inc. (CPP) together with Dr. Jon Peterka and Dr. Ron Petersen. His field of studies includes modeling of boundary-layer winds, structural responses to wind, and the atmospheric transport of pollutants, snow, sand, and water (2005). Dr. Alan Garnett Davenport (1932-2009), was a professor of University of Western Ontario. He established the Boundary Layer Wind Tunnel Laboratory in 1965 where the design processes of many tall buildings and bridges are handled such as Sears Tower in Chicago and Tsing Ma Bridge in Hong Kong (2005). Dr. Ahsan Kareem is one of the establishers of the aerodynamic loads database called *NatHaz* which is available on internet. This site has become a valuable tool for the preliminary design works of the

buildings regarding wind issue since 2000 and it was recently introduced in the Commentary of ASCE 7-05 (ASCE 7-05, 2005) as an alternative method to determine the dynamic effects of wind actions on buildings (Kareem, et al., 2009).

In the recent applications, the balance system constitutes of ultra sensitive load cells for the purpose of measuring the five base response components that are basically the moments about the three orthogonal axes (x,y,z) and the two base shears as time series. Note that for the definition of wind loads, uplift is not a concern. Figure 1.2 presents a sketch of a typical balance system taken directly from (Cermak, 2003). As it can be seen from the vertical section A-A given in Figure 1.2, the building model is mounted to the balance system through an aluminium tube passing through its inside. The response of the model is directly transferred to the gages by the use of this tube. The mounting plate is written to be a turntable since the tests are performed for several wind angles of attack. Several angles of attack should be considered because the worst case is not necessarily one of the perpendicular directions and there is not necessarily a single worst case. Depending on the limit state, for instance deflection limit states or internal force limit states, the angle of attack that creates the greatest influence may vary (Hart, et al., 1983).
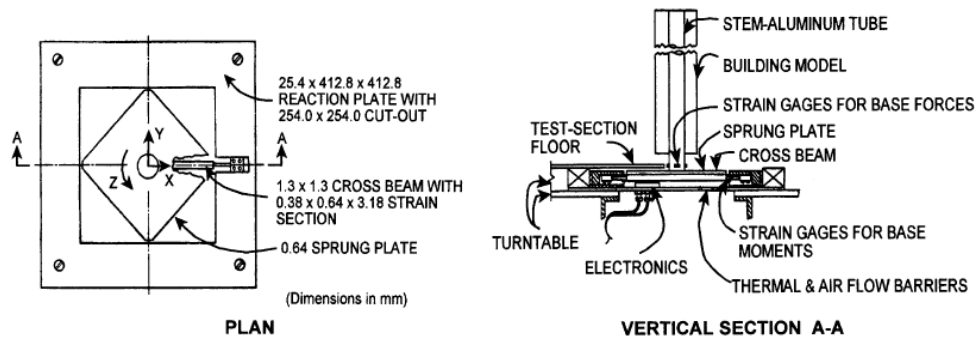


**Figure 1.2 High-frequency base balance (Cermak, 2003)**

H-FBB has replaced use of the aeroelastic model tests because its application is easier and it is more cost efficient. The reason for the cost efficiency is that, unlike the aeroelastic models, the only requirement of this test is a low mass and rigid model of the actual structure mounted on a highly sensitive and stiff force balance. Low mass and high rigidity are the requirements for the models that are used in H-FBB tests. Therefore, the mostly preferred materials are balsa wood, polystyrene foam and thin-walled plastic (Gamble, 2003). The balance system used for data gathering should have high stiffness as well for it

not to participate in the response. The most widely used material for the production of the balance system is aluminium. Despite these advantages, it may be insufficient for special design projects because H-FBB tests do not take the negative aerodynamic effect which is an increase in dynamic excitation into account which may become an essential issue for the projects where very high wind speeds are considered or where the structure is extremely flexible and in consequence experiences large lateral deflections (Cermak, 2003).

Simultaneous measurements of the five base response components provide data for several applications. First, the output of H-FBB tests is utilised for expressing the dynamic loads in terms of equivalent static loads which is directly related with the fundamental mode shape of the structure. Since the fundamental mode shape of a high rise building is usually almost linear, the generalized forces for the translational modes are proportional to the base bending moment. With this assumption, base moments can easily be represented as storey shear forces. Another measurement is the base shear force which gives information about the shape of the distribution of dynamic loads on the building whether it is trapezoidal or parabolic, etc. Obviously, the torsional measurements supply data to understand the torsional response of the building under wind loading. However, linear mode shape assumption must be corrected in the case of torsional response calculations. The correction is a function of base moments and shears (Cermak, 2003). The building that is analyzed through H-FBB tests should have a linear mode shape. Otherwise, even the test can be conducted in a similar manner; the results must be corrected considering the actual mode shapes (By the ASCE Aerospace Division Task Committee on Wind Tunnel Studies of Buildings and Structures, 1996).

The results obtained from single H-FBB test gives preliminary information for other design projects as well provided that the model geometrical properties match. This is a fact for the H-FBB tests because the goal of achieving the worst design force quantities is fulfilled through some statistical operations. Hence, the aim of conducting the tests is to acquire the statistical properties of the base force resultants instead of their actual values. Some examples for these properties can be mean, standard deviation, autocorrelation function and spectral density function. In 2000, a database called "Nathaz Aerodynamic Loads Database" was established and has been accessible on internet since then. It is comprised of high-frequency base balance measurements that are conducted on isolated high rise building models.

## 1.3 OBJECTIVES AND SCOPE

Under the scope of the thesis study, a series of wind tunnel tests are performed in Ankara Wind Tunnel. In this experimental work which is conducted in Turkey for the first time, the wind load effects on a rectangular building model are investigated. The main objectives are listed below.

- Ankara Wind Tunnel has a test section that is comparatively short. As a result of this fact, special boundary layer creation elements are designed in order to create a wind profile similar to the one in nature. During the test, the wind speed all along the height of the test section is measured using a hot-wire anemometer system.

- The response of the model building which is made up of polystyrene foam is monitored by a special data acquisition system, *High Frequency Base Balance System (H-FBB)*. This system is designed such that it is capable of reading the two base moments with the help of load cells. It is mounted underneath the tunnel floor and connected to the model through an aluminium rod which is glued by epoxy to the inside of model.

- The test is performed for two types of exposure categories defined in ASCE 7-05 (ASCE 7-05, 2005). They are named as B and C which refer to the city centres and open areas respectively. The aim is to understand the effect of the environmental conditions on the behaviour of the building.

- The test is repeated for several angles of attack specifically in exposure C. This time the objective is to investigate the influence of the wind direction on the response of the building.

- Utilising the data gathered by H-FBB system, the randomness of the base moments in the along-wind and across-wind directions are obtained in terms of some statistical parameters such as mean, standard deviation and power spectral density function. Finally, the design base moments, equivalent static loads and the top accelerations are determined for each of the tests.

- The results obtained from Ankara Wind Tunnel case study are compared with the ones determined from the technical specifications ASCE 7-05 (ASCE 7-05, 2005), Eurocode 1 (Eurocode 1, 2005) and İYBRY (İYBRY, 2009) and with the aerodynamic loads database, NatHaz (Kareem, et al., 2000).

# CHAPTER 2

# THEORETICAL BACKGROUND

## 2.1 INTRODUCTION

This chapter is devoted to the theoretical concepts regarding wind engineering. The scope of this study covers the response of a tall building under wind loads. Therefore, in this chapter, the items which build up response of the building are investigated one by one, which are the along-wind, across-wind and torsional responses. The theoretical background of the analytical solutions is explained. Unlike along-wind ones, there is no closed form analytical solutions for across-wind and torsional responses. Hence, in those two, only some concepts will be introduced.

The behaviour of a tall building under lateral loads can be satisfactorily represented by a single degree of freedom system (SDOF) (Holmes, 2005). The response of a building is basically related to forces, i.e. equivalent loads and corresponding member forces and displacements or accelerations as the derivatives. These two main components are associated with survivability and serviceability design criteria respectively. As a result, force-related and displacement-related quantities will be dealt with in this chapter.

## 2.2 THEORY

In order to understand the behaviour of a building that is exposed to wind, the concept of bluff body aerodynamics and random vibration theory should be studied carefully. Bluff body is a body which has a broad, flattened front. Unlike a streamlined body which has a rounded shape similar to a water drop, the flow around a bluff body does not follow a

tangential pattern. Instead, a separation of the flow at the leading edge corners generates high shear and vorticity. Flow around a bluff body is demonstrated in Figure 2.1. The vortices create a response on the body that is full of uncertainties (Holmes, 2005). Tschanz and Davenport approach the problem on the basis of random vibration theory (Tschanz, et al., 1983). In other words, the wind forces or the relevant responses of buildings are treated as stationary random processes and expressed in terms of their statistical properties such as means, standard deviations, correlations and power spectral density functions. Thus, in order to calculate the response of a building the wind speed profile and its turbulence intensity in the relevant environment must be determined.
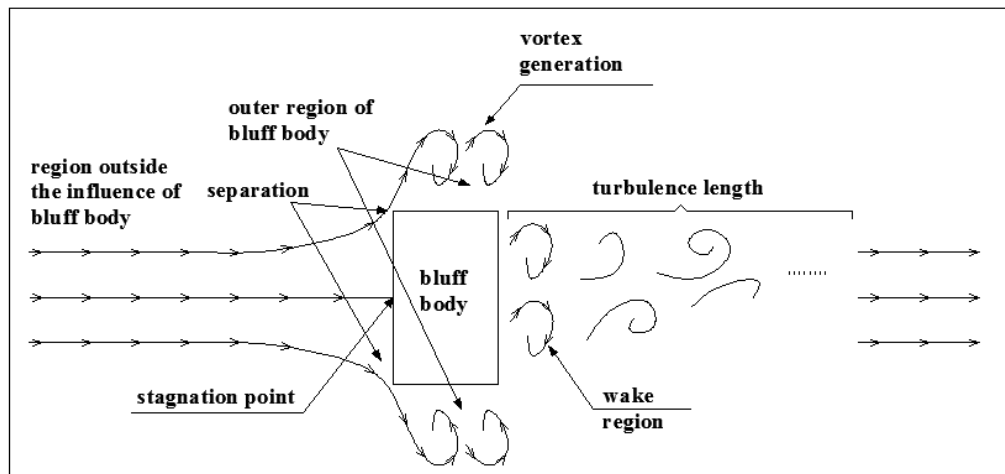


**Figure 2.1 Flow around a bluff body**

*Mean Wind Speed Profile*

At the Earth's surface, the wind flow is affected by friction. After a certain height, the frictional effects become negligible, thus the wind speed remains constant. The region where the wind speed varies is called "Atmospheric Boundary Layer" (Simiu, et al., 1978). Boundary layer thickness is related with the roughness length, $z_0$ of the terrain. In design codes, different terrains with different roughness lengths are categorized and known as exposure categories. Some examples for the exposure categories can be listed as open terrain, terrain with small and isolated obstructions and city centres. Mean wind profiles are

reasonably expressed by *power law*. It has no theoretical basis but widely used in wind engineering problems (Holmes, 2005). Equation of power law is given below.

$$\bar{U}(z) = \bar{U}_{10} \left( \frac{z}{10} \right)^{\alpha} \tag{2.1}$$

The terms in Equation (2.1) are;

- $\bar{U}(z)$ : Mean wind speed at height z;
- $\bar{U}_{10}$ : Mean wind speed at 10 m of height;
- z: Height;
- α: Constant related with the roughness length and height range as in Equation (2.2)

$$\alpha = \frac{1}{log_e(z_{ref}/z_0)} \tag{2.2}$$

The terms in Equation (2.2) are;

- $z_{ref}$: reference height that is specifically defined in design codes
- $z_0$: roughness length

***Turbulence Intensity***

The wind flow fluctuates both in time and space. Therefore, wind flow is not *laminar*; it is turbulent except some wind flows that are in relatively low speeds under specific temperature conditions. Turbulence is a significant concept in structural engineering due to three major reasons. First, turbulence affects the shape of the wind profile. Second, turbulence influences the wind flow around a structure and hence the wind forces that the structure is exposed to. Finally, the fluctuations in the wind flow regime generate dynamic effects in flexible structures, i.e. long span bridges or tall buildings (Simiu, et al., 1978). The turbulence in a flow is usually described with *turbulence intensity* which is defined as the ratio of the standard deviation of the wind speed to its mean (Equation 2.3).

$$I_u = \frac{\sigma_u}{\bar{U}} \tag{2.3}$$

In Equation (2.3), $I_u$ is the turbulence intensity. $\sigma_u$ stands for the standard deviation of the wind speed. $\bar{U}$ is mean value of the wind speed. In other words, since coefficient of variation is defined as the ratio of standard deviation of a random variable to its mean,

turbulence intensity is actually the coefficient of variation of the wind speed. In order to compare turbulence for different environments, talking with the coefficient of variations is more meaningful than the means or standard deviations alone because it provides a normalization which diminishes the effects of magnitudes and units.

### *Bluff Body Aerodynamics*

Response of a bluff body to surrounding air flow is described by *Bernoulli's equation* as follows;

$$p + \frac{1}{2}\rho_a U^2 = a \ constant \tag{2.4}$$

The terms in Equation (2.4) are:

- $p$: Pressure of flow;
- $\rho_a$: Density of air;
- $U$: Velocity of flow

Response of the bluff body under wind loading depends on the pressure occurring on its faces. Looking at Figure 2.1, if the pressure and velocity on the outer regions of the bluff body ($p$ and $U$ respectively) and the ones outside the influence of the body are denoted by $p_0$ and $U_0$, they can be related to each other as;

$$p + \frac{1}{2}\rho_a U^2 = p_0 + \frac{1}{2}\rho_a U_0^2 \tag{2.5}$$

According to Holmes (Holmes, 2005), both of the outer region and the region outside the influence of the body can be assumed to be regions of zero viscosity and vorticity. Hence Equation (2.5) could be written.

Rearranging Equation (2.5), the surface pressure on the body, meanly $p-p_0$ can be expressed as

$$p - p_0 = \frac{1}{2}\rho_a(U_0^2 - U^2) \tag{2.6}$$

In almost every technical specification, for the sake of simplicity, pressure on the bluff body due to wind is generally expressed by using a pressure coefficient, $C_p$ to the velocity part of the Bernoulli's equation written for the region outside the influence of the body. That is,

$$p - p_0 = C_p \frac{1}{2} \rho_a U_0^2 \tag{2.7}$$

Combining Equations (2.6) and (2.7), $C_p$ can be expressed as;

$$C_p = \frac{\frac{1}{2}\rho_a(U_0^2 - U^2)}{\frac{1}{2}\rho_a U_0^2} = 1 - \left(\frac{U}{U_0}\right)^2 \tag{2.8}$$

From Equation (2.8), it is seen that, at the stagnation point (Figure 2.1), which is defined as the point on the body where velocity is zero, the pressure is the same as the one outside the body. In other words, $C_p$ is equal to one. The highest expected pressure coefficients on the windward face are usually less than one. In the regions where flow velocity is greater than $U_0$, in other words, where separated flow takes place, $C_p$ may be negative. There, Bernoulli's equation is not valid due to high vorticity; however, if U is taken as the velocity of the flow that is just outside the wake region (region of vortex generation in Figure 2.1), the equation can give very reasonable solutions (Holmes, 2005).

Both the fluctuating nature of wind flow in atmospheric boundary layer and the unstable nature of the flow around a bluff body cause the pressure on the body to be highly unstable and fluctuating. Assuming *quasi-steady* behaviour around the bluff body, the fluctuating pressure on the body is believed to follow the same variation characteristics of longitudinal wind velocity. Therefore, by using Equation (2.7) and putting p(t) instead of p-p₀ which stands for the pressure on the face of the body, the fluctuating pressure can be expressed as;

$$p(t) = C_{p0} \frac{1}{2} \rho_a (U(t))^2 \tag{2.9}$$

$C_{p0}$ is used to denote quasi-steady pressure coefficient. U(t) represents the fluctuating wind velocity outside the bluff body.

A general approach to the random excitation problems is decomposition of the wind velocity, wind pressure or wind induced response quantities into their mean and fluctuating components. This is the basis of 'gust-*factor approach*' used in design codes (Davenport, 1967).

The velocity can be separated into its mean and fluctuating components, $\bar{U}$ and u'(t) respectively as in Equation (2.10).

$$U(t) = \bar{U} + u'(t) \tag{2.10}$$

Inserting Equation (2.10) into Equation (2.9) results in;

$$p(t) = C_{p0} \frac{1}{2} \rho_a (\bar{U} + u'(t))^2 \tag{2.11}$$

Or, in expanded form;

$$p(t) = C_{p0} \frac{1}{2} \rho_a (\bar{U}^2 + (u'(t))^2 + 2\bar{U}u'(t)) \tag{2.12}$$

p(t) can also be separated into its mean and fluctuating components as $\bar{p}$ and p'(t);

$$\bar{p} = C_{p0} \frac{1}{2} \rho_a \bar{U}^2 \tag{2.13}$$

$$p'(t) = C_{p0} \frac{1}{2} \rho_a [(u'(t))^2 + 2\bar{U}u'(t)] \tag{2.14}$$

Since $u'(t)^2$ is small compared with $2\bar{U}u'(t)$, it can be neglected (Holmes, 2005). In that case, Equation (2.14) can be rewritten as;

$$p'(t) = C_{p0} \rho_a [\bar{U}u'(t)] \tag{2.15}$$


***Along-wind response of buildings***

A building is usually considered as a single degree of freedom (SDOF) system to investigate its along-wind response. For this purpose, the equation of motion for a SDOF system is written as;

$$m\ddot{x}(t) + c\dot{x}(t) + kx(t) = F(t) \tag{2.16}$$

The parameters of this equation are;

- m: Mass of the system;
- c: Damping of the system;
- k: Stiffness of the system;

- F(t): Force applied to the system (aerodynamic drag force in this case);
- x(t): Deflection response of the system;
- $\dot{x}(t)$: Velocity of the system;
- $\ddot{x}(t)$: Acceleration of the system

The dynamic properties interrelation of a single degree of freedom system that is represented by a simple mass-spring-damper (Figure 2.2) is briefly explained in the following equations.
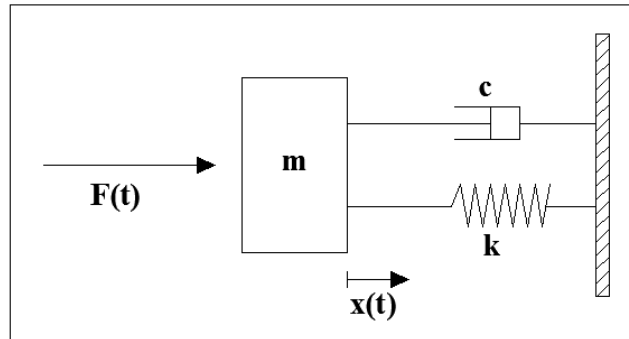


**Figure 2.2 Simplified Dynamic Model of a Single Degree of Freedom System**

Two essential parameters which relate the dynamic properties of a single degree of freedom system are fundamental frequency and structural damping ratio, i.e. $f_1$ (in Hertz) and $\xi$ respectively. (Clough, et al., 2003).

$$f_1 = \frac{1}{2\pi} \sqrt{\frac{k}{m}} \tag{2.16}$$

$$\xi = \frac{c}{2\sqrt{mk}} \tag{2.17}$$

In order to solve the equation of motion, first of all, force applied to the system, F(t) should be derived by making use of the pressure resultant obtained in Equation (2.15). By definition, force is the product of pressure and the area that it has an impact. If A is used to denote the exposure area, meanly the area of windward face of the structure, F(t) can be written as;

$$F(t) = A(\bar{p} + p'(t)) \tag{2.18}$$

$$F(t) = AC_{p0} \frac{1}{2} \rho_a (\bar{U}^2 + 2\bar{U}u'(t)) \tag{2.19}$$

Similarly, mean and fluctuating components of the wind force can be expressed as;

$$\bar{F} = AC_{p0} \frac{1}{2} \rho_a \bar{U}^2 \tag{2.20}$$

$$F'(t) = AC_{p0} \rho_a [\bar{U}u'(t)] \tag{2.21}$$

In order to write the fluctuating component of wind force in terms of mean wind force, first the squares of the force components are taken;

$$\bar{F}^2 = \frac{1}{4} A^2 C_{p0}^2 \rho_a^2 \bar{U}^2 \bar{U}^2 \tag{2.22}$$

$$F'(t)^2 = A^2 C_{p0}^2 \rho_a^2 \bar{U}^2 u'(t)^2 \tag{2.23}$$

When $A^2 C_{p0}^2 \rho_a^2 \bar{U}^2$ term is left alone, Equation (2.23) can be rewritten as follows;

$$A^2 C_{p0}^2 \rho_a^2 \bar{U}^2 = \frac{F'(t)^2}{u'(t)^2} \tag{2.24}$$

Then, inserting Equation (2.24) into Equation (2.22) will give;

$$\bar{F}^2 = \frac{1}{4} \frac{F'(t)^2}{u'(t)^2} \tag{2.25}$$

When Equation (2.25) is revised to leave the fluctuating force term alone on the left side;

$$F'(t)^2 = \frac{4\bar{F}^2}{\bar{U}^2} u'(t)^2 \tag{2.26}$$

In random vibration theory, the equation of motion for force excited systems are solved easier in frequency domain compared with the time domain analytical solution techniques. Some important concepts regarding the random vibration theory are defined and explained in Appendix A.

Let $S_F(f)$ and $S_U(f)$ be the spectral densities of wind force and velocity, respectively, normal distribution assumption and the linearity property of spectral density function allow Equation (2.27) to be written in the following form since $\frac{4\bar{F}^2}{\bar{U}^2}$ term is actually a constant.

$$S_F(f) = \frac{4\bar{F}^2}{\bar{U}^2} S_U(f) \tag{2.27}$$

In Equation (2.27), 'f' stands for frequency in Hertz.

Equation (2.27) describes the relation between the wind force, meanly the *drag force* and the wind flow velocity. Thus, in order to derive the relationship between the deflection response of the system, x(t) with the drag force, x(t) can be decomposed into its mean and fluctuating components as;

$$x(t) = \bar{x} + x'(t) \tag{2.28}$$

The relation between the mean drag force and mean deflection response is as follows;

$$\bar{F} = k * \bar{x} \tag{2.29}$$

In random vibration theory, the spectral densities of the applied force and the response are directly related through a *mechanical admittance function*. Explicitly,

$$S_x(f) = \frac{1}{k^2} |H(f)|^2 S_F(f) \tag{2.30}$$

The terms in Equation (2.30) are;

- $S_x(f)$: Spectral density function of displacement response;
- k: Stiffness of the system;
- $|H(f)|^2$: Mechanical admittance function;
- $S_F(f)$: Spectral density function of drag force

Mechanical admittance function for a SDOF system as shown in Figure 2.2 can be expressed as follows;

$$|H(f)|^2 = \frac{1}{\left[1 - \left(\frac{f}{f_1}\right)^2\right]^2 + 4\xi^2 \left(\frac{f}{f_1}\right)^2} \tag{2.31}$$

When Equations (2.27) and (2.30) are combined, the spectral density function of the deflection response can be related to the spectral density of the wind velocity.

$$S_x(f) = \frac{1}{k^2} |H(f)|^2 \frac{4\bar{F}^2}{\bar{U}^2} S_U(f) \tag{2.32}$$

Equation (2.32) applies to structures which have small windward face areas comparatively. For structures with large areas, *aerodynamic admittance function*, $\chi^2$(f) is introduced to

account for the correlation of velocity fluctuations over the whole large face area. For such a case, Equation (2.32) becomes;

$$S_x(f) = \frac{1}{k^2} |H(f)|^2 \frac{4\bar{F}^2}{\bar{U}^2} \chi^2(f) S_U(f)$$ (2.33)

Analytically, the aerodynamic admittance function can be obtained by using the correlation properties of the upwind velocity fluctuations. Vickery (Vickery, 1965) performed an experimental study for obtaining the aerodynamic admittance function and this study is usually preferred instead of using analytical solutions that involves several assumptions (Holmes, 2005). This experimental data obtained by Vickery is presented in Figure 2.3. In the figure, the symbol 'A' stands for the windward face area of the structure. Note that for small A, $\chi(f)$ approaches to one as expected.
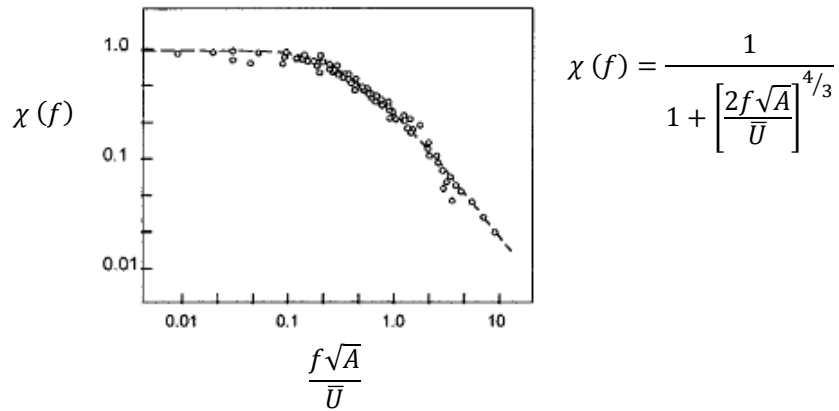


Figure 2.3 Aerodynamic Admittance – Experimental Data and Fitted Function
(Vickery, 1965)

In order to determine the variability of the response in a more meaningful way, first of all, variance is expressed in terms of the spectral density function in Equation (2.34).

$$\sigma_x^2 = \int_0^\infty S_x(f) df$$ (2.34)

Inserting Equation (2.34) into (2.33) will give more explicit form for the variance of deflection.

$$\sigma_x^2 = \int_0^\infty \frac{1}{k^2} |H(f)|^2 \frac{4\bar{F}^2}{\bar{U}^2} \chi^2(f) S_U(f) df$$ (2.35)

23

Taking the square of Equation (2.29) and combining it with Equation (2.35) will give;

$$\sigma_x^2 = \int_0^\infty |H(f)|^2 \frac{4\bar{x}^2}{\bar{U}^2} \chi^2(f) S_U(f) df \tag{2.36}$$

If Equation (2.36) is multiplied and divided by $\sigma_U^2$ and the constant terms are taken outside of the integral, the equation can be rewritten as follows;

$$\sigma_x^2 = \frac{4\bar{x}^2 \sigma_U^2}{\bar{U}^2} \int_0^\infty |H(f)|^2 \chi^2(f) \frac{S_U(f)}{\sigma_U^2} df \tag{2.37}$$

The calculations in Equation (2.37) are nothing but an area underneath a function computation. Therefore, for the sake of simplicity, Equation (2.37) can be approximated as superposition of two components, i.e. the background response, B and the resonant component, R. This approximation is used widely in technical specifications in order to analyze along-wind response of the structure as well.

$$\sigma_x^2 \cong \frac{4\bar{x}^2 \sigma_U^2}{\bar{U}^2} [B + R] \tag{2.38}$$

Equation (2.38) can be rearranged involving the turbulence intensity definition stated in Equation (2.3) ($I_u$) as follows;

$$\sigma_x^2 \cong 4\bar{x}^2 I_u^2 [B + R] \tag{2.39}$$

$$B = \int_0^\infty \chi^2(f) \frac{S_U(f)}{\sigma_U^2} df \tag{2.40}$$

$$R = \chi^2(f_1) \frac{S_U(f_1)}{\sigma_U^2} \int_0^\infty |H(f)|^2 df \tag{2.41}$$

Equation (2.39) shows that the variance of the displacement response of the system increases with increasing turbulence intensity which means that highly turbulent flows cause unstable responses.

The background response, B represents the quasi-steady response caused by the flow under the natural frequency of the structure whereas the resonant response, as the name implies, is a dynamic response of the structure. For many ordinary structures with average rigidity, background response is higher than the resonant response; however, for slender ones, resonant responses dominate.

*Across-wind response of buildings*

The across-wind response of buildings is mainly due to vortex shedding and there has not been a complete analytical solution technique that accurately represents the across wind response yet since the analytical computations are based primarily on Bernoulli Equation which loses its validity in case of vorticity (Holmes, 2005). Vortex shedding is defined as the unsteady flow that occurs in special flow velocities in bluff body aerodynamics. In this flow, vortices (spinning and turbulent flow of fluid) are formed at the back of the body (See Figure 2.1). As each vortex is shed from the bluff body, a periodic, strong and unsteady cross wind force is induced on it. The pressure distribution created by the vortices around the body is asymmetric. This asymmetry causes alternating transverse forces. The oscillations will be in transverse direction (across-wind direction) if the body is flexible (Mendis, et al., 2007).

For a given structure, oscillations resulted from vortex shedding have a dominant frequency that is defined by a non-dimensional number, called *Strouhal number, St*. It is expressed as;

$$St = \frac{f_s L}{\bar{U}} \tag{2.42}$$

In this equation, $f_s$ is the frequency of vortex shedding, L is the width of the bluff body that is the dimension of the building perpendicular to wind, $\bar{U}$ is the mean velocity of the approaching wind.

In case the frequency of the building coincides with the vortex shedding frequency, resonance would occur resulting in large amplitude displacements. This phenomenon is known as *the critical velocity effect*. This situation can lead to very large oscillations and possibly failure of the structure.

Strouhal number of a particular structure depends on its cross sectional properties and whether it has sharp corners or curved. If it has a curved section, Strouhal number varies with another non-dimensional number in fluid mechanics, *Reynolds number*. In literature, there are some definitions of Strouhal number for various cross-sections (Holmes, 2005). Figure 2.4 presents Strouhal number variation with the aspect ratio of rectangular sections.
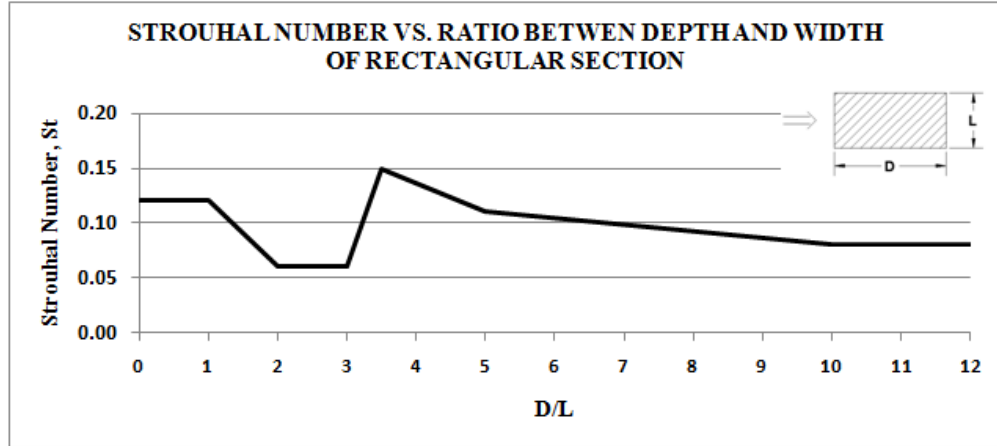
**Figure 2.4 Strouhal number vs. ratio between depth and width of rectangular section (Eurocode 1, 2005)**

In the design of the high rise buildings, the idea is to avoid coincidence of the natural frequency of the structure with the vortex shedding frequency obtained by using the relevant Strouhal number taken from Figure 5 and using Equation (2.42).

### *Torsional response*

Especially, when considering the top accelerations or deflections of the building under wind loading, the torsional response plays a significant role. Non-uniform pressure distributions resulting from vortex shedding, non-symmetric geometrical properties, eccentricities between the elastic and geometric centres of the structure or coupled mode shapes can be listed as the main causes of torsional response of a tall building under wind loading.

Torsional response of tall buildings has been investigated through several aeroelastic model tests in boundary layer wind tunnels since 1980s. Studies by Isyumov and Poole (1983), Lythe and Surry (1990), Cheung and Melbourne (1992), and Zhang et al (1993) are some of the pioneers of this issue.

In order to relate the mean torque to the mean wind pressure, a coefficient called '*mean torque coefficient*', $\bar{C}_{mz}$ can be defined as follows.

$$\bar{C}_{mz} = \frac{\bar{M}_T}{\frac{1}{2}\rho_a \bar{U}^2 L_{max}^2 H} \tag{2.43}$$

The terms in Equation (2.43) are;

- $\bar{C}_{mz}$ : mean torque coefficient;
- $\bar{M}_T$ : mean torque;
- $\rho_a$ : density of air;
- $\bar{U}$ : mean velocity of the approaching wind;
- $L_{max}$ : maximum projected width of the cross section;
- $H$: height of the building

Lythe and Surry (1990) performed several wind tunnel tests on building models with ordinary and extraordinary shapes. They determined a mean value of 0.085 and a standard deviation of 0.04 for the above stated parameter, $\bar{C}_{mz}$ (Lythe, et al., 1990). Cheung and Melbourne (1992) have related the mean torque coefficient to the ratio of the minimum projected width of the section to maximum one by performing several wind tunnel tests. The result that they have obtained is presented in Figure 2.5. They have concluded that the highest value of $\bar{C}_{mz}$ for any section most probably arises when the angle of attack is about 60-80 degrees from the normal to the widest building face (Cheung, et al., 1992).
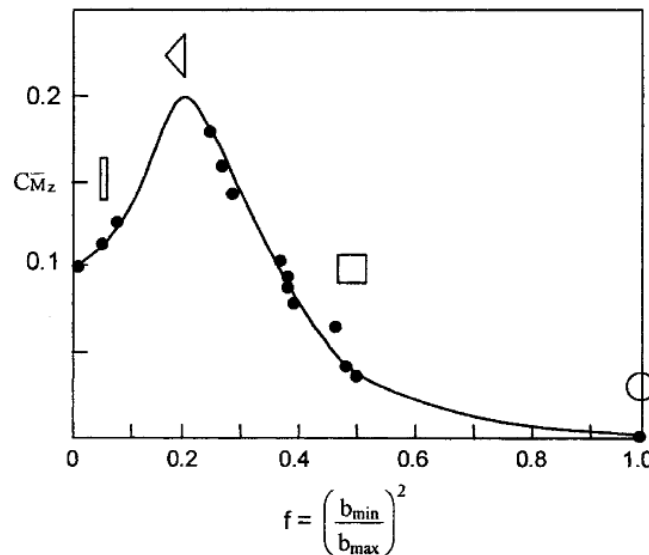


**Figure 2.5 Mean torque coefficients for various cross sections (Cheung, et al., 1992)**

Isyumov and Poole (1983) performed several wind tunnel tests on building models with square sections and with rectangular sections with a 1:2 ratio in order to determine the main

contributing component to the fluctuating torque. The results of their studies showed that main contributions to the fluctuating torque in case of the square section models and rectangular ones if wind direction is parallel to the long side came from the pressures on the side faces. This brings the conclusion that the fluctuating torque can be predicted from the mean torque that is calculated analytically using the quasi-steady assumption. In the remaining case, i.e. rectangular section models and wind direction is parallel to the short edge; the main contributions are from the rear face due to vortex shedding. In this case, the analytical prediction is not valid due to the limitations of the quasi-steady assumption in high vorticity (Isyumov, et al., 1983).

According to Zhang et al (1993), a small eccentricity in the elastic centre of a building from its geometric and mass centre causes a large increase in the mean twist angle and the dynamic torsional response. For example, a shift by 10% in the elastic centre of a building with square cross section may double the torsional effects (Zhang, et al., 1993).

***Wind - Induced Response Analysis through H-FBB Technique:***

H-FBB (High Frequency Base Balance) Technique is an experimental procedure in which the model base force components are measured during the wind tunnel test and the other response quantities are calculated using the base moment data. In the conventional response analysis, the response quantities are calculated based on the top deflection which is primarily based on the linear mode shape assumption. Therefore, in the conventional method, mode shape correction calculations are required to adjust the results if the mode shape of the building under consideration is other than linear. On the other hand, in H-FBB, the effects of non-ideal mode shapes are rather negligible since base bending moments directly accommodate for them. (Zhou. et al, 2002) According to Davenport, (Davenport, 1966) the maximum dynamic and static base bending moment response of a tall building can be represented by the following expression (gust response factor approach) assuming that base bending moment is a stationary Gaussian process;

$$\hat{M} = \bar{M} + g\sigma_M \tag{2.44}$$

In Equation (2.44), $\hat{M}$ and $\bar{M}$ are the expected maximum and mean of the base bending moment respectively; $g$ is the peak factor and $\sigma_M$ is the root mean square (standard deviation) of moment. By definition, the root mean square (RMS) of the base bending

28

moment can be determined as in Equation (2.45) where, $S_M(f)$ is the power spectral density function of the fluctuating base moment.

$$\sigma_M = \left( \int_0^\infty S_M(f)df \right)^{1/2} \tag{2.45}$$

For the sake of simplicity in the solution of the integral calculations in Equation (2.45) and to be more elaborate, the base bending moment is decomposed into two components which are background component, $\hat{M}_B$ and the resonant component, $\hat{M}_R$ (Zhou, et al., 2003). When Equation (2.44) is rewritten using the two fluctuating components;

$$\hat{M} = \bar{M} + \sqrt{\hat{M}_R^2 + \hat{M}_B^2} \tag{2.46}$$

For the closed form determination of the extreme maximum value of the resonant component, the excitation is assumed to be represented by *white noise* near the natural frequency of the building (Zhou, et al., 2003). White noise is an imaginary type of a random process which has a spectral density function (Figure 2.6) that is constant for all frequencies. It is imaginary because it is impossible to realize it physically but it is widely used for the sake of simplicity in the idealization of the complex engineering problems (Wirsching, et al., 1995).
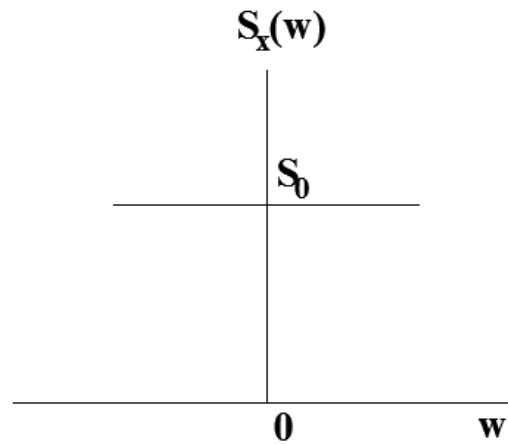


**Figure 2.6 Spectral density function of white noise**

Expected maximum response of a process is simply described by the summation of the mean of the process with its standard deviation times a peak factor which depends on the time interval for which this expected maximum value is calculated. If the process under

consideration is a mean zero process, its expected maximum is directly the peak factor times its standard deviation (Holmes, 2005). Extreme value for the resonant component which is a mean zero process can be expressed as;

$$\widehat{M}_R = g_R * \sigma_{MR} \tag{2.47}$$

Similar to Equation (2.45), $\sigma_{MR}$ can be calculated as;

$$\sigma_{MR} = \left( \int_0^\infty S_{MR}(f) df \right)^{1/2} \tag{2.48}$$

In Equation (2.48), $S_{MR}(f)$ is the power spectral density function of the response of the single degree of freedom system and $f$ is the frequency. Recall that tall building is mathematically idealized by a SDOF system. In random vibration theory, the spectral density of the response of a SDOF system is related to the power spectral density function of the excitation through a transfer function as given in Equation (2.51). Note that in Equation (2.51) the frequency terms are expressed through cyclic frequencies using the relation given in Equation (2.50). Thus, the PSD functions will also be expressed in terms of cyclic frequencies. They can be converted to each other through Equation (2.49)

$$\sigma^2 = \int_{-\infty}^{\infty} S(w) dw = \int_0^\infty 2 * 2\pi * S(f) df \tag{2.49}$$

$$w = 2\pi * f \tag{2.50}$$

$$S_{MR}(w) = |H(w)|^2 * S_M(w) \tag{2.51}$$

In Equation (2.51), the terms are;

- $S_{MR}(w)$: PSD of the response;
- $H(w)$: Transfer function;
- $S_M(w)$: PSD of the excitation. Since the excitation is assumed to be shown by white noise, $S_M(w) = S_0$

*Transfer function* is a function that is used to define a relationship between the input and output of a system. It is useful for solving a single degree of freedom system in frequency domain. For example, if the input of a single degree of freedom system is force and the required output is displacement; the displacement can easily be determined by simply multiplying force with relevant transfer function definition. The transfer function of the above mentioned problem is the one described for "Base-excited systems: Relative motion problems" (Wirsching, et al., 1995). In Equation (2.52), the transfer function is presented in

complex number form. The parameters in Equation (2.52) are as follows: m is the mass, k is the stiffness and c is the damping of the SDOF system.

$$H(w) = \frac{mw^2}{(k-mw^2)+icw} = \frac{k}{(k-mw^2)+icw}$$
(2.52)

Therefore, by using white noise approximation Equation (2.48) becomes;

$$\sigma_{MR} = \left(\int_{-\infty}^{\infty}| H(w)|^2 * S_0 \, dw\right)^{1/2} = S_0\left(\int_{-\infty}^{\infty}| H(w)|^2 \, dw\right)^{1/2}$$
(2.53)

In order to solve the integration calculations in Equation (47), *Residue Theorem* will be used (Wirsching, et al., 1995). According to Residue Theorem, the integration given in Equation (2.54) can be evaluated through the given formulations in Equation (2.55).

$$I = \int_{-\infty}^{\infty}|K(w)|^2 dw \quad where \ K(w) = \frac{B_0+iwB_1}{A_0+iwA_1-w^2A_2}$$
(2.54)

$$I = \frac{\pi[A_0B_1^2+A_2B_0^2]}{A_0A_1A_2}$$
(2.55)

As a result, if Equation (2.53) can be written similar to Equation (2.54), $\sigma_{MR}$ can easily be calculated using Equation (2.55). So, equating H(w) to K(w), the constant terms can be determined as in the following expressions.

$$\frac{k}{(k-mw^2)+icw} = \frac{B_0+iwB_1}{A_0+iwA_1-w^2A_2}$$
(2.56)

$B_0 = k$; $B_1 = 0$; $A_0 = k$; $A_1 = c$; $A_2 = m$. Hence, the result of the integration in Equation (2.53) is;

$$I = \frac{\pi[k0^2+mk^2]}{kcm} * S_0$$
(2.57)

Then, combining Equations (2.16), (2.17) and (2.57);

$$\sigma_{MR}^2 = I = \frac{\pi^2 f_1 S_0}{\xi}$$
(2.58)

In Equation (2.58), the parameter $S_0$ is the value of the constant PSD approximation of the excitation and it is written relating the circular frequency. Note that white noise approximation is done in the vicinity of the natural frequency of the building. Therefore, in a more elaborate form of engineering representation, power spectral density function (PSD) can be written as;

$$S_M(f_1) = 2 * 2\pi * S_M(w_1) = 4\pi * S_0$$
(2.59)

In other words, $S_0 = S_M(f_1)/4\pi$ 　　　　　　　　　　　　　　　　(2.60)

When Equations (2.58) and (2.60) are combined, $\sigma_{MR}$ can be written as;

$$\sigma_{MR} = \sqrt{\frac{\pi}{4\xi} f_1 S_M(f_1)}$$ 　　　　　　　　　　　　　(2.61)

Finally, Equation (2.47) can be revised as;

$$\hat{M}_R = g_R * \sqrt{\frac{\pi}{4\xi} f_1 S_M(f_1)}$$ 　　　　　　　　　　(2.62)

In the above given equation, $g_R$ is the resonant peak factor and determined as in Equation (2.63) (Zhou, et al., 2003), (ASCE 7-05, 2005). It was originated by A.G. Davenport in 1964. (Davenport, 1964).

$$g_R = \sqrt{2\ln(f_1 T)} + 0.5772/\sqrt{2\ln(f_1 T)}$$ 　　　　　　　(2.63)

In Equation (2.63), T is the observation time and it is taken as 3600 seconds in the design standards (ASCE 7-05, 2005), (Eurocode 1, 2005) and (İYBRY, 2009). This value of 3600 seconds or in other words, 1 hour is chosen based on the experimental observations that "at periods of about one hour, a spectral gap exists, which separates microscale from mesoscale motions." (Hart, et al., 1983).

Similar to Equation (2.47), the extreme value for the background component can be expressed as;

$$\hat{M}_B = g_B * \sigma_{MB}$$ 　　　　　　　　　　　　　　　　(2.64)

In Equation (2.64), $g_B$ is the peak factor for background component and usually taken as a value between 3-4 (Zhou, et al., 2003); $\sigma_{MB}$ is the root mean square of the background component and is simply the standard deviation of the base bending moment which is measured during the test.

Measured data of base bending moment and torque can be distributed to each floor in order to determine the equivalent static wind loads by using the expressions below (Zhou and Kareem, 2003) in Equations (2.65) and (2.66) written for bending moment and torsion cases respectively.

$$\hat{P}_R(z) = \hat{M}_R \frac{m(z)\phi_1(z)}{\int_0^H m(z)\phi_1(z).zdz}$$ 　　　　　　　(2.65)

32

$$\hat{P}_{R,T}(z) = \hat{T}_R \frac{I(z)\phi_1(z)}{\int_0^H I(z)\phi_1(z)dz} \tag{2.66}$$

In Equations (2.65) and (2.66), $\hat{P}_R$ is the resonant component of the equivalent static wind load; $\hat{P}_{R,T}$ is the resonant component of the equivalent loads from torsional moments; $m(z)$ is the mass per unit height; $\hat{T}_R$ is the resonant component of torque; $I(z)$ is the mass moment of inertia per unit height; $\phi_1(z)$ is the fundamental mode shape and H is the total height of the building. By simply applying these equivalent loads one by one to the building and performing structural analysis, any of the structural response quantities can be calculated. For each, one resonant and one background component are computed. Then, by taking the square root of the sum of the squares of the two components, the resultant value can be determined. However, for the acceleration response, only the resonant component is dominant (Zhou, et al., 2003). Calling the top peak acceleration of the building by $\hat{\ddot{Y}}$, the relevant expressions can be written for the bending moment and torsion cases as in Equations (2.67) and (2.68) respectively.

$$\hat{\ddot{Y}}(z) = \frac{\int_0^H \hat{P}_R(z)\phi_1(z)dz}{\int_0^H m(z)\phi_1^2(z)dz}\phi_1(z) \tag{2.67}$$

$$\hat{\ddot{Y}}(z) = \frac{\int_0^H \hat{P}_{R,T}(z)\phi_1(z)dz}{\int_0^H I(z)\phi_1^2(z)dz}\phi_1(z) \tag{2.68}$$

Finally, in order to determine the root mean square of the acceleration, the value of $\hat{\ddot{Y}}$ should be divided by the resonant peak factor, $g_R$ that is calculated as in Equation (2.63) (Zhou, et al., 2003).

In order to simplify the wind induced response analysis procedure described, for each of the along wind bending, across wind bending and torsional responses, a non-dimensional power spectrum is generated (Figure 2.7) in which the horizontal axis is $fB/U_H$ and the vertical axis is $fS_M(f)/\sigma_M^2$ where f is frequency in Hertz; $B$ is the building width that is perpendicular to wind; $U_H$ is the mean wind velocity evaluated at the building height, H; $S_M(f)$ is power spectral density function of the moment; and $\sigma_M$ is the root mean square of the moment. In short, $fS_M(f)/\sigma_M^2$ is called non dimensional moment coefficient, $C_M(f)$.
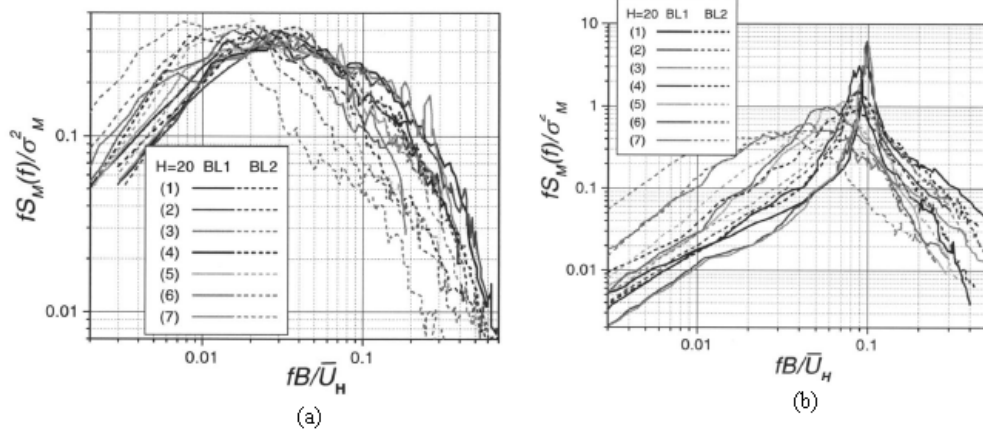
**Figure 2.7 Normalized Spectra (a) in along-wind direction (b) in across wind direction**
**(Zhou, et al., 2003)**

The normalized spectra are created using the wind tunnel test information and model building properties. Then for the actual building, the values of $fB/U_H$ are determined by putting the fundamental frequency of the building in the relevant direction in the place of f and the building plan dimension, B and the design wind speed $U_H$ in along wind and across wind directions. When these values are entered in the relevant spectra, the corresponding non-dimensional moment coefficients can be achieved. After that, the background and resonant components can be simply determined utilizing the following procedure.

- Coefficient of variation of the moment, $\sigma_{C_M}$;

$$\sigma_{C_M} = \frac{\sigma_M}{\bar{M}_{model}}$$ (2.69)

- Background component of the base bending moment, $\hat{M}_B$;

$$\hat{M}_B = g_B * \sigma_{C_M} * \bar{M}$$ (2.70)

- Resonant component of the base bending moment, $\hat{M}_R$;

$$\hat{M}_R = g_R * \sigma_{C_M} * \bar{M} * \sqrt{\frac{\pi}{4*\xi} C_M(f_1)}$$ (2.71)

In Equations (2.69), (2.70) and (2.71), the terms $\bar{M}_{model}$ and $\bar{M}$ are the mean moment obtained for model and the mean reference moment for the real building respectively. $C_M(f_1)$ is the value that is read on the vertical axis of the relevant normalized power

34

spectrum for corresponding normalized frequency which is obtained using the natural frequency of the building, $f_1$. $\bar{M}_{model}$ is the average base bending moment so it is the mean of the data measured during the test. On the other hand, $\bar{M}$ can be calculated using Equation (2.72).

$$\bar{M} = \int_0^H 1/2 C_D \rho \bar{U}(z)^2 Bz dz \tag{2.72}$$

In Equation (2.72), $\rho$ is the density of air; B is the width of the building normal to wind; H is the height of the building. (Figure 2.8) After the mean reference moments and the resonant and background components are determined, the design base moment, $M_d$ can be obtained as;

$$M_d = \bar{M} + \sqrt{\hat{M}_B^2 + \hat{M}_R^2} \tag{2.73}$$
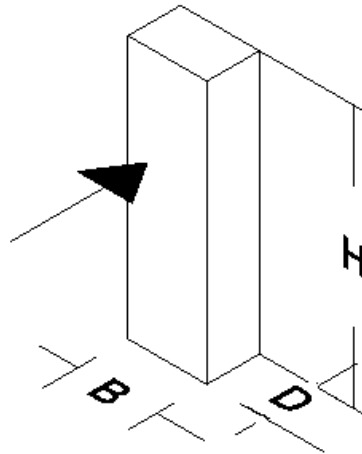


**Figure 2.8 Geometrical properties of the building**

For other response quantities of interest, equivalent static loads can be specified through the determined base bending moment components and by applying structural analysis techniques.

# CHAPTER 3


# DESIGN AND ANALYSIS OF PASSIVE DEVICES


## 3.1   INTRODUCTION


In nature, wind speed profile changes according to environmental conditions such as the geographical properties, surface roughness, and the intensities of the obstacles. On the surface of the Earth, wind speed is affected by the frictions on the ground but as height increases, these friction effects diminish leading to a constant wind speed at a certain elevation. This layer, where the wind profile is under the influence of the surface roughness is known as *atmospheric boundary layer (ABL).* In ABL, flow velocity displays rapid fluctuations and high turbulence. The thickness of this layer is around 200 m in open terrain whereas it reaches 1000 m in condensed urban areas.

It is crucial to simulate the natural wind properties in the wind tunnel tests for reliable results. Thus, creation of the atmospheric boundary layer becomes an important issue. Such wind tunnel tests are generally conducted in special wind tunnels, called 'Boundary Layer Wind Tunnels (BLWT)' which have relatively long test sections of 15 to 20 meters (Cermak, 1982). In BLWT, a thick boundary layer wind profile or the appropriate turbulence levels can be achieved through the long test sections. For wind tunnels having short test sections, boundary layer can still form through the use of special surface roughness elements on the base of the test section. These surface roughness elements, generally called *passive devices*, can be designed in many shapes but the most frequently used ones are grids, barriers, fences, spires and cubes (Simiu, et al., 1978).

Ohya (Ohya, 2001), Counihan (Counihan, 1973), (Counihan, 1969), Cook (Cook, 1973), Cermak et al (Cermak, 1995), (Cermak, 1982), Garg et al (Garg, et al., 1997) and Irwin (Irwin, 1981) are the pioneers of the researches about atmospheric boundary layer simulation elements. These studies date back to 1960s and 1970s (Holmes, 2005).

This chapter is devoted to the design and analysis of the surface roughness elements. In the following parts, design calculations and theoretical background of the design of passive devices will be presented. Then, the design is verified with computational fluid dynamics simulations. As a final section, the tunnel measurements are presented and compared with numerical results and ASCE 7-05 definitions.

## 3.2   DESIGN OF PASSIVE DEVICES

In the design of surface roughness elements, the basic idea is to have similarity between the natural wind profile characteristics and the one in the wind tunnel. Basic criteria for kinematic, dynamic, and thermal similarities are able to be provided through conservation equations of mass, momentum and energy. In order to achieve "exact" similarity between the model and the prototype, the some dimensionless parameters are defined in literature. Here, they are briefly expressed.

*Reynolds Number:* is a dimensionless parameter that is determined from the ratio of the internal forces to the viscous forces. Although the number was named by Osborne Reynolds in 1883 who popularized the use of it, it was actually first introduced by George Gabriel Stokes in 1851 (Potter, et al., 2002). Reynolds Number is computed as follows:

$$Re = \frac{U_0 L_0}{\nu_0} \tag{3.1}$$

The terms in equation (3.1) are:

- $U_0$: Velocity of the fluid;
- $L_0$: Characteristic linear dimension;
- $\nu_0$: Kinematic viscosity of the fluid.

*Richardson Number:* is a dimensionless parameter which expresses the ratio of potential energy to kinetic energy. It gives a rough idea about the expected air turbulence (Potter, et al., 2002).

$$Ri = \frac{\Delta T_0}{T_0} \frac{L_0 g}{U_0^2}$$ (3.2)

The terms in equation (3.2) are:

- $\Delta T_0$: Temperature change;
- $T_0$: Initial temperature;
- $L_0$: Characteristic linear dimension;
- $g$: Gravitational acceleration;
- $U_0$: Velocity of the fluid.

*Rossby Number:* (also known also as Kibel number) is a dimensionless parameter which expresses the ratio of inertial forces to the Coriolis forces which is caused by rotation of the Earth. It demonstrates which forces dominate the system (Potter, et al., 2002).

$$Ro = \frac{U_0}{L_0 \Omega_0}$$ (3.3)

The terms in equation (3.3) are:

- $U_0$: Velocity of the fluid;
- $L_0$: Characteristic linear dimension;
- $\Omega_0$: Angular frequency of planetary rotation.

*Prandtl Number:* is a dimensionless parameter that expresses the ratio of the viscous diffusion rate to the thermal diffusion rate (Potter, et al., 2002).

$$Pr = \frac{\nu_0 \rho_0 c_{p0}}{k_0}$$ (3.4)

The terms in equation (3.4) are:

- $\nu_0$: Kinematic viscosity of the fluid;
- $\rho_0$: Density of the fluid;
- $c_{p0}$: Specific heat;
- $k_0$: Thermal conductivity.

*Eckert Number:* is a dimensionless parameter that expresses the dissipation by relating the flow's kinetic energy and enthalpy (Potter, et al., 2002).

$$Ec = \frac{U_0^2}{c_{p0(\Delta \bar{T})_0}}$$
(3.5)

The terms in equation (3.5) are:

- $U_0$: Velocity of the fluid;
- $c_{p0}$: Specific heat;
- $(\Delta \bar{T})_0$: Characteristic temperature difference of the flow.

In addition to the dimensionless numbers, boundary conditions that are needed for "exact" similarity are:

1) Surface roughness and temperature at ground level;
2) Flow structure above the atmospheric boundary layer or drainage current;
3) Zero pressure gradients in the direction of mean flow;
4) Sufficient upwind fetch to establish equilibrium of the simulated atmospheric boundary layer with surface boundary conditions;
5) Height of an inversion layer, if present.

Under standard atmospheric and gravity conditions, wind tunnel testing entails fundamental scale violations for the Reynolds number. Richardson number is needed only for thermal similarity. Atmospheric boundary layer is actually independent of the geotropic wind effect hence it can be modelled without matching Rossby number. The Prandtl number criterion is automatically satisfied in wind tunnel simulation and finally, the Eckert number is essential only for compressible flows (Shojaee, et al., 2009). This quick review of the dimensionless numbers defined in fluid mechanics indicate that in ordinary wind tunnels "exact" similarity of the entire atmospheric boundary layer is almost impossible. Therefore, instead of matching the dimensionless numbers, geometric scaling of the boundary conditions is tried to be satisfied. For the neutral atmospheric boundary layer similitude considerations, the theory introduced by Cermak (Cermak, 1995) makes use of the only variables defined on the ground surface such as the surface roughness height, $z_0$, and the friction velocity, $u_*$. As a result, in order to achieve the atmospheric boundary layer simulation studies, the surface roughness characteristics and the natural wind profile should be analysed. Ground surface

characteristics are determined based on the vegetation, natural topography and the constructed facilities, in other words the ground coverage.

There are several definitions with minor variations, for the ground surface roughness categories in wind engineering studies (ASCE 7-05, 2005), (Eurocode 1, 2005). In this study, the description given in the design guideline provided by the American Society of Civil Engineers, ASCE was utilised (ASCE 7-05, 2005). According to ASCE 7-05, the ground coverage properties are classified under three exposure categories which are named as Exposure B, C and D. Exposure B applies to urban and suburban areas with closely spaced obstructions which have the size of single-family dwellings that prevail in the upwind direction for a distance of at least 792 m. Exposure D stands for flat, unobstructed areas and offshore regions which prevail in the upwind direction for a distance greater than 1524 m. Remaining exposure category C, applies for the cases where exposure B or D does not suitably fit.

*Wind speed profile definition*

Wind speed profiles are defined by using *power law* as given in equation (3.6).

$$\frac{U}{U_\infty} = \left(\frac{z}{\delta}\right)^\alpha \qquad (3.6)$$

In Equation (3.6), $U$ is wind speed in the relevant height $z$; $U_\infty$ is wind speed after the atmospheric boundary layer is reached. It is the basic wind speed chosen for design with a certain gust effect according to the climatic conditions in the relevant location; $z$ is the height; $\delta$ is the height of the atmospheric boundary layer depending on the exposure category; $\alpha$ is a constant depending on the exposure category.

In this study, the analyses are made for the three exposure categories defined in ASCE 7-05. The parameters of the power law for each of them are given in Table 3.1; and shapes of wind speed profiles for each of them are presented in Figure 3.1.

**Table 3.1 Terrain exposure constants (ASCE 7-05, 2005)**

| EXPOSURE CATEGORY | POWER LAW CONSTANT, $\alpha$ | ATMOSPHERIC BOUNDARY LAYER HEIGHT, $\delta$ (m) |
|---|---|---|
| B | 1/4.0 | 365.76 |
| C | 1/6.5 | 274.32 |
| D | 1/9.0 | 213.36 |
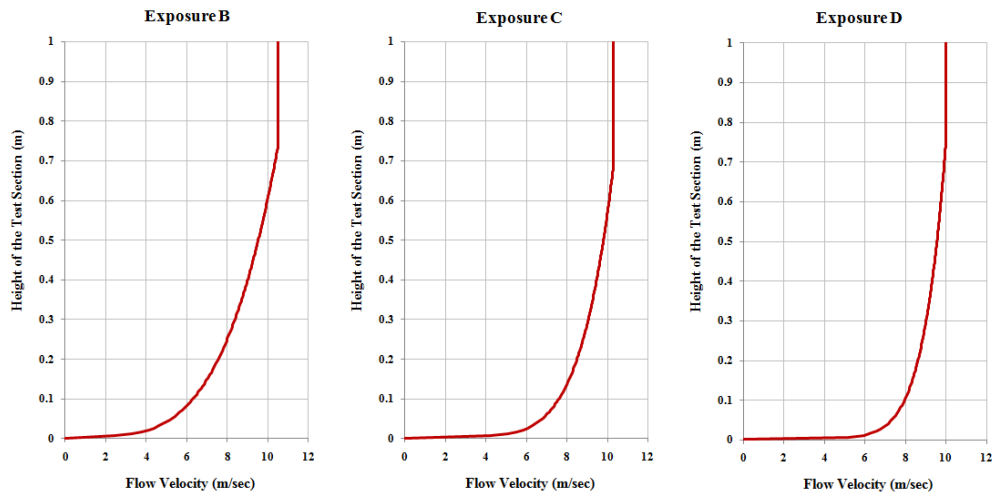


**Figure 3.1 Wind speed profiles for Exposures B, C and D defined in ASCE 7-05**

*Design Methodology for Spires and Roughness Elements*

The object of achieving the desired boundary layer properties upstream of the test section in short wind tunnel, spires should be designed at the inlet and roughness elements, meanly cubes should be placed on the wind tunnel floor. Simiu and Scanlan (Simiu, et al., 1978) proposed the following procedure for the design of spires, which are geometrically defined as in Figure 3.2. This is an empirical procedure in which first of all the desired boundary layer thickness in the tunnel is decided ($\delta$). Then, after the constant parameter, $\alpha$ defined for the relevant exposure category is selected; the height of the spire, h is calculated using Equation (3.7). Finally, the base width of the spire is determined using Figure 3.2. There, H is used to symbolize the height of the wind tunnel test section.
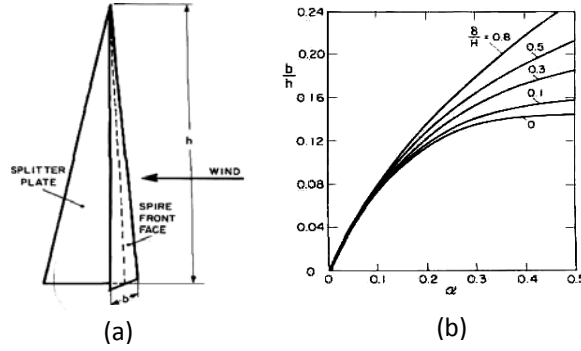
**Figure 3.2 a) A typical spire configuration b) Spire base width variation with power law exponent (Simiu, et al., 1978)**

$$h = 1.39 \frac{\delta}{(1+\alpha/2)} \tag{3.7}$$

For a system designed using this procedure, the desired atmospheric boundary layer most probably occurs 6h downstream from the spires. Hence, the spires should be placed 6h upstream from the building model.

For the complete simulation of the atmospheric boundary layer, spires sometimes may not be sufficient. In such circumstances, the wind tunnel test section floor should be covered by cubes with height k and spacing D such that;

$$\frac{k}{\delta} = e^{\frac{2}{3}\ln\left(\frac{D}{\delta}\right) - 0.1161\sqrt{\frac{2}{C_f} + 2.05}} \tag{3.8}$$

$$C_f = 0.136 \left[\frac{\alpha}{1+\alpha}\right]^2 \tag{3.9}$$

Equation (3.9) is only valid in the range of 30<αD²/k³<2000.

As a remark, although similitude in atmospheric boundary layer can be achieved through the design of the passive devices, similarity in turbulence levels generally cannot be satisfied in short wind tunnels.

### *Results of Numerical Simulation*

Under the scope of the Ankara Wind Tunnel case study, design of the surface roughness elements for each of the exposure categories B, C and D in ASCE 7-05 were performed. Hence, first of all the atmospheric boundary layer thicknesses, δ were taken from Table 3.1. Then, a preliminary scale factor was assumed considering height of the test section. By

using the above mentioned procedure, designs of the surface roughness elements were made. During the calculations, basic wind speed was taken as 10 m/sec which is the smallest flow velocity that can be stabilized in AWT. After the dimensions of the surface roughness elements were determined, it was tested that whether the desired wind profile was achieved in the test section or not using the commercially available computational fluid dynamics software, *ANSYS Fluent*. The number of computational cells used in the software in order to mesh the system was between 1.3 and 1.7 million tetrahedral cells. Results were obtained by solving RANS equations using κ-ε turbulence model, with standard pressure, second order momentum, turbulent kinetic energy and turbulent dissipation rate computations.

The scale of the model that is used in the wind tunnel test is determined from the ratio of the boundary layer thickness obtained in the tunnel to the atmospheric boundary layer height given in Table 3.1. As an initial attempt in all of the three exposure categories, the scale of the model was assumed to be 1/400 which is the most widely preferred one in literature. The design results for this first iteration are given in Table 3.2. The spacing between the cubic roughness elements, D is selected as 0.2 m for each of the cases.

In Table 3.2, δ is used for the thickness of the atmospheric boundary layer for the relevant exposure category that is determined from Table 3.1 and scaled with the assumed factor of 1/400. The other parameters, b refers to the base width, h is the height of the spire and k is the height of the cubes. Splitter means the width of the splitter plate attached to the spire (Figure 3.2). Lateral is used for the lateral distance of the splitter plate. X is the factor of h that is used to express the distance from the spires where the atmospheric boundary layer is reached instead of using 6h generalization and $\Gamma$ is the distance downstream from the spires where the atmospheric boundary layer is reached. ($\Gamma = X*h$)


**Table 3.2 The boundary layer characteristics and the geometries of the passive devices for 1/400 scale factor**

| Exposure | δ (m) | X | h (m) | b (m) | Splitter | Lateral | k | $\Gamma$ | Number of Spires |
|----------|-------|-----|-------|-------|----------|---------|--------|------|------------------|
| B | 0.914 | 4.5 | 1.129 | 0.120 | 0.282 | 0.565 | 0.0356 | 5.08 | 4 |
| C | 0.686 | 4.5 | 0.885 | 0.107 | 0.221 | 0.443 | ~ 0 | 3.98 | 5 |
| D | 0.533 | 6.0 | 0.702 | 0.064 | 0.175 | 0.351 | ~ 0 | 4.21 | 6 |

Figure 3.3 and Figure 3.4 given below show the results of the computational simulations for the 1/400 scale model prepared for each of the exposure categories. Effects of the spires and roughness elements on the flow regime are clearly identifiable in Figure 3.3. For Exposure B, the individual wakes of the spires are identifiable up to about 2 m downstream of the test section entrance. These wakes as well as the disturbances created by the cubical roughness elements start to mix out and create a thick boundary layer near the wall. For the other two exposures, because of the missing roughness elements, individual spire wakes persist much longer.

Figure 3.4 represents the velocity contours downstream of the spires at the cross sections corresponding to the Γ values given in Table 3.2. The numerically predicted velocity profile and the one determined from the power law are given on the right column. The computational fluid dynamics (CFD) results show that although the required boundary layer profile is very well obtained for Exposure C, for Exposures B and D the desired power law boundary layer profiles cannot be reproduced exactly by the designed spire and roughness configurations. Although the reliability of the CFD outputs can also be questionable, current results still indicate that the inlet configurations for Exposures B and D may not be appropriate for the experiments.
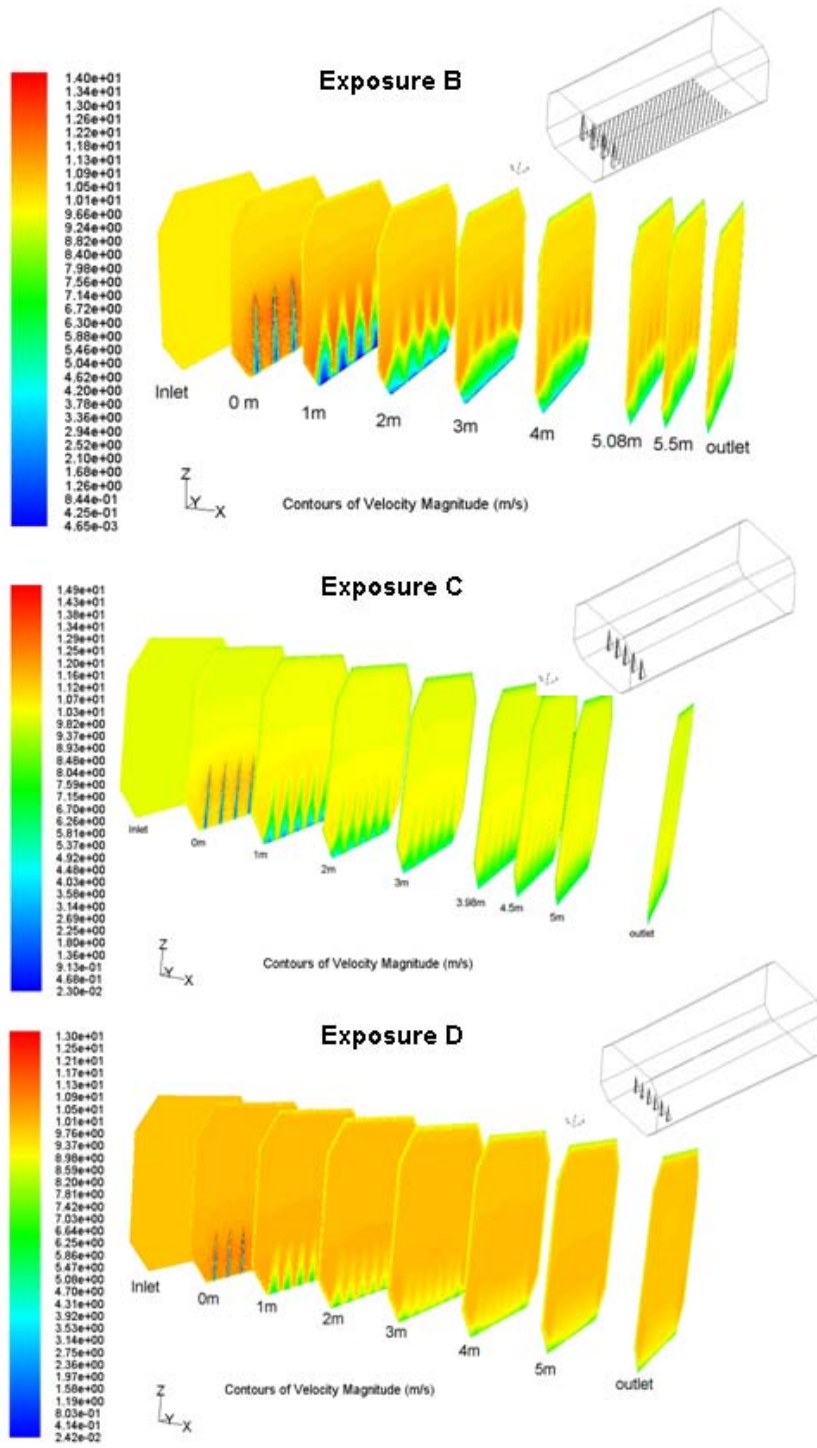
**Figure 3.3 Contours of wind speed for exposures B, C and D (1/400 scale) at various cross sections downstream of the test section inlet (Shojaee, et al., 2009)**
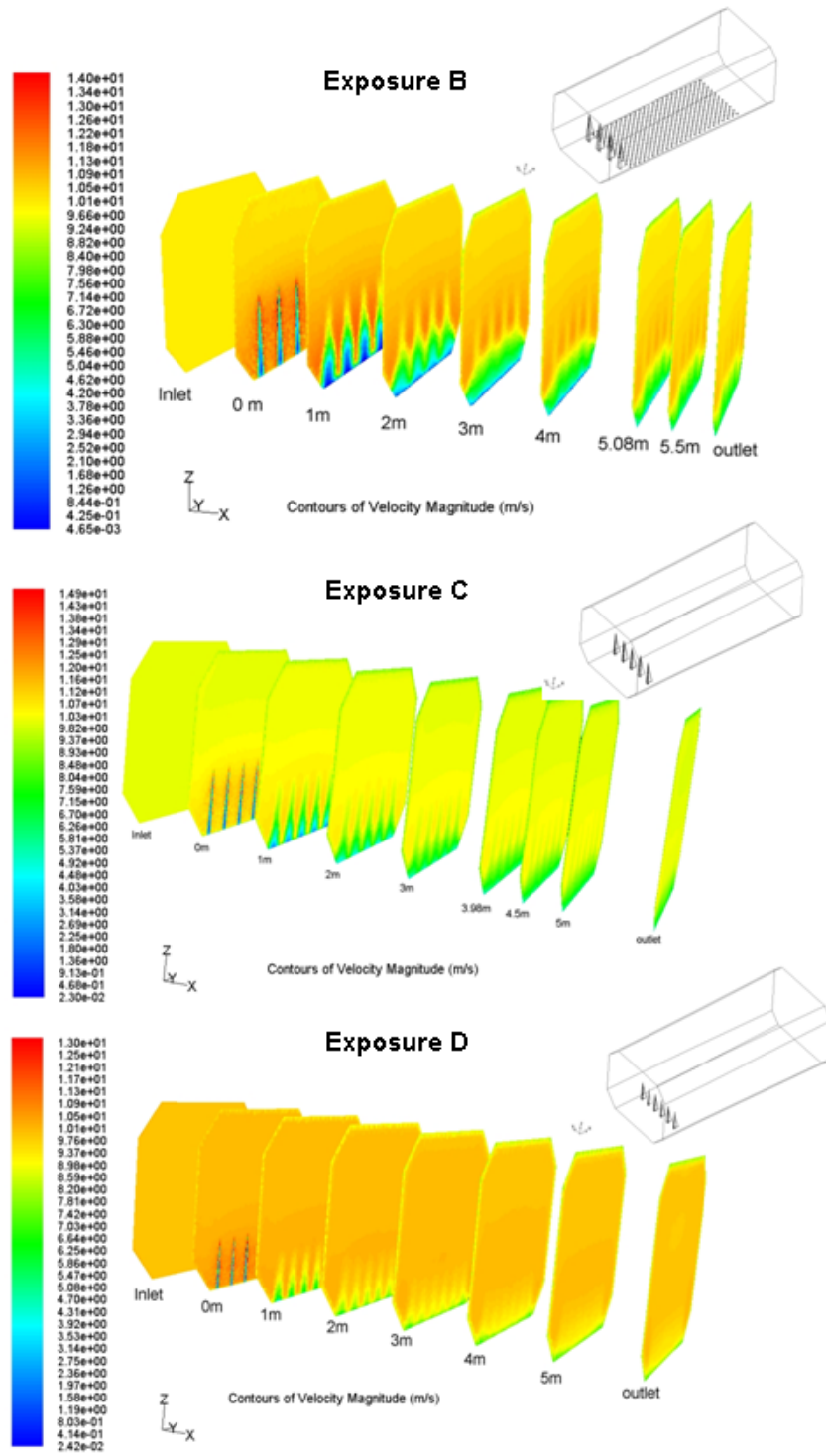
**Figure 3.4 Contours of wind speed downstream of the spires at the cross sections corresponding to the Γ values given in Table 3.2 (Shojaee, et al., 2009).**

In order to produce more appropriate inlet configurations for Exposures B and D, the spires and roughness elements are re-designed with different scale factors. In this second iteration, the scale factors for Exposures B and D are chosen such that the desired boundary layer heights are about 30% of the tunnel height, similar to the case for Exposure C in the first design iteration. This study resulted in scale factors of 1/500 and 1/285 for Exposures B and D, respectively. The geometrical parameters for the re-designed spires and roughness elements are presented in Table 3.3 and the velocity contours downstream of the spires at the cross sections corresponding to the relevant $\Gamma$ values are presented in Figure 3.5 for exposures B and D.

**Table 3.3 The boundary layer characteristics and the geometries of the passive devices for the second iteration**

| Exposure | $\delta$ (m) | X | h (m) | b (m) | Splitter | Lateral | k | $\Gamma$ | Number of Spires |
|----------|------|-----|-------|-------|----------|---------|-------|------|-----------|
| B | 0.731 | 4.5 | 0.904 | 0.158 | 0.226 | 0.452 | 0.033 | 4.07 | 5 |
| D | 0.747 | 4.5 | 0.983 | 0.091 | 0.246 | 0.492 | ~ 0 | 4.43 | 5 |

The finalized design configurations for each of the exposure categories are summarized in Table 3.4 below. As a surface roughness element, cube is required only in Exposure B. In the other two, the height of the cubes, k has come out to be zero implying that there is no need to them. On the other hand, five spires have been designed in different dimensions. The boundary layer thickness in the tunnel is around 0.7 m in each of the categories which is approximately 30% of the tunnel height that is 2.44 m.

The predicted and desired power law velocity profiles along the tunnel height present a better agreement compared with the first design iteration. As a result, it was decided that these geometrical inlet configurations given in Table 3.4 were used in the building model experiments in AWT. For this purpose, all three inlet configurations of the surface roughness elements corresponding to the three exposure categories were manufactured as shown in Figure 3.6 below. The cubes were located in a staggered pattern.
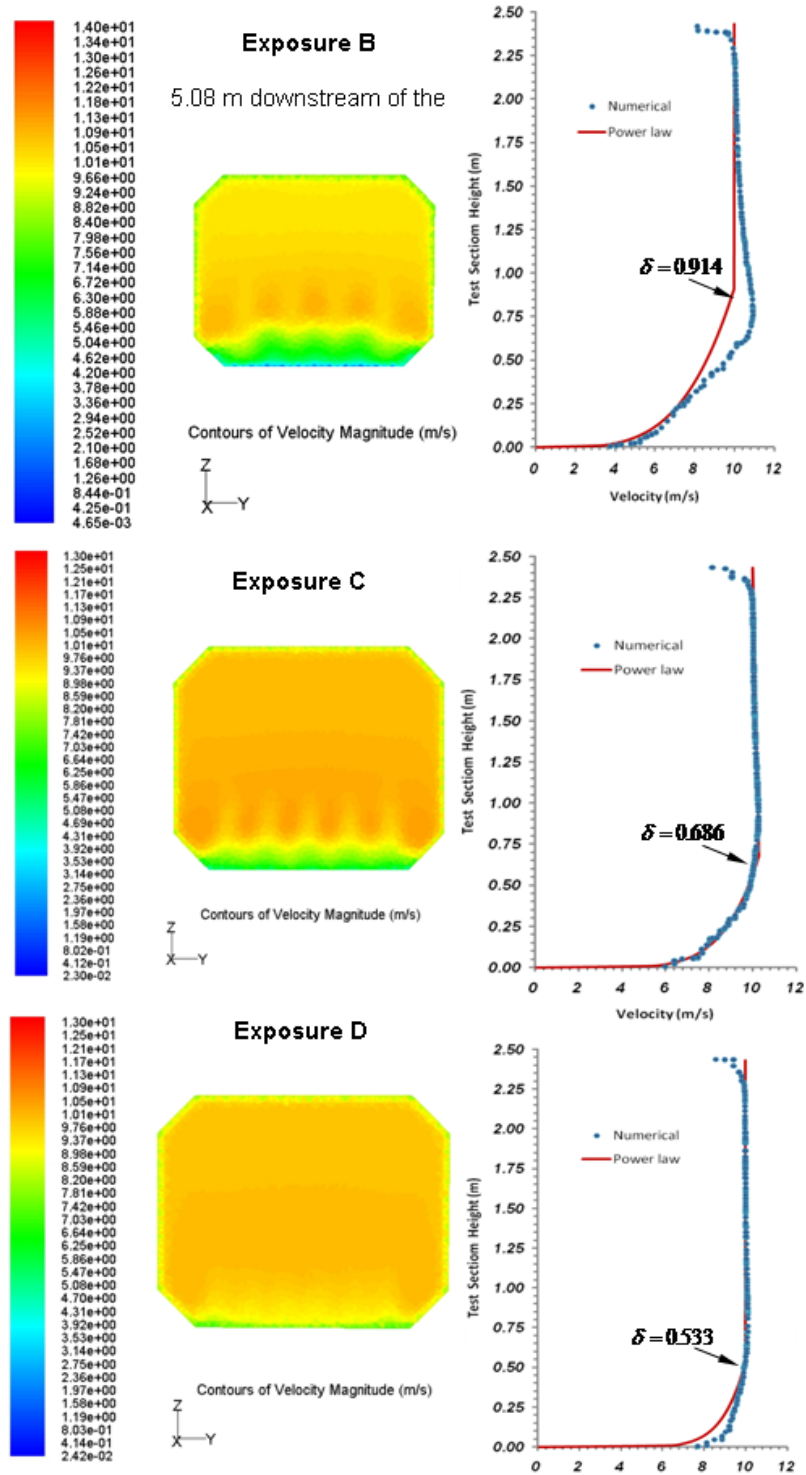
**Figure 3.5 Contours of wind speed for the re-designed inlet configurations downstream of the spires on cross sections corresponding to the Γ values given in Table 3.3 (Shojaee et al., 2009).**

**Table 3.4 Geometrical properties for the finalized design of surface roughness elements**

| Parameters | Exposure B | Exposure C | Exposure D |
|---|---|---|---|
| $\delta_{natural}$ (m) | 365.76 | 274.32 | 213.36 |
| Scale Factor | 1/500 | 1/400 | 1/285 |
| $\delta_{tunnel}$ (m) | 0.731 | 0.686 | 0.747 |
| $\alpha$ | 1/4.0 | 1/6.5 | 1/9.0 |
| k (m) | 0.033 | ~ 0 | ~ 0 |
| Number of Spires | 5 | 5 | 5 |
| h (m) | 0.904 | 0.885 | 0.983 |
| b (m) | 0.158 | 0.107 | 0.091 |
| X | 4.5 | 4.5 | 4.5 |
| Splitter | 0.226 | 0.221 | 0.246 |
| Lateral | 0.452 | 0.443 | 0.492 |
| $\Gamma$ | 4.07 | 3.98 | 4.43 |
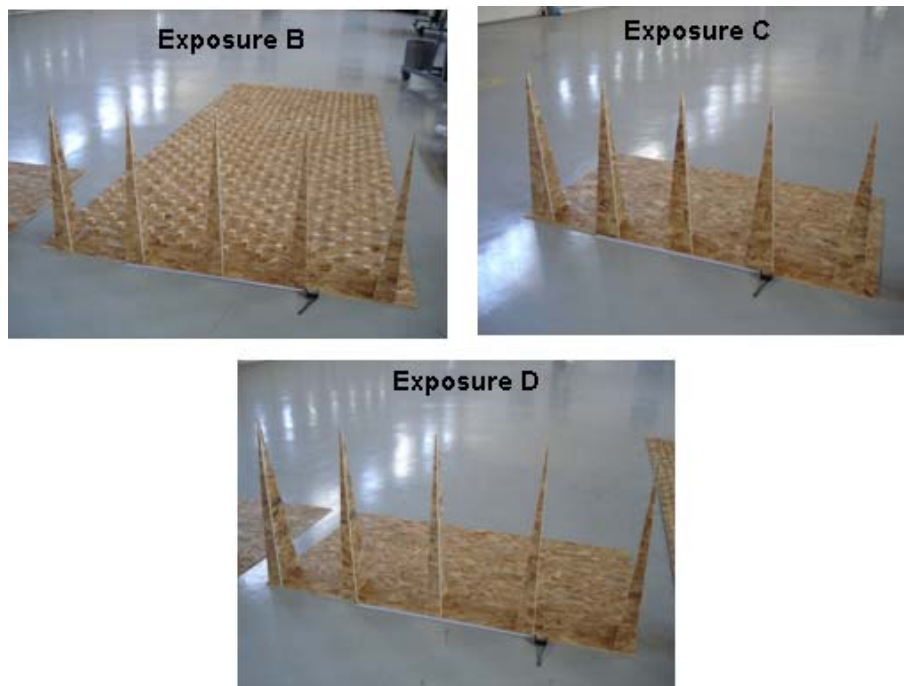


**Figure 3.6 Photograph of the manufactured spires and roughness element configurations for the three exposure categories. (The tape on the photographs shows 1 m length.)**

## 3.3 MEASUREMENTS IN ANKARA WIND TUNNEL TEST

The surface roughness elements designed for three exposure categories were placed in Ankara Wind Tunnel and tested whether they successfully create the desired wind profile or not. Location of the surface roughness elements in the tunnel are presented in Figure 3.7 for each of the exposure categories. As a first step, the manufactured configurations are mounted on the floor of the test section $\Gamma$ distance away from the location of the model of the building and 10 m/sec wind speed was provided in the tunnel. Wind speed depending on height was measured utilising a hot wire anemometer system which was attached to a three level mobilizing traverse system placed beneath the floor of the test section as given in Figure 3.8 on the left. By the help of this traverse configuration, the anemometer system was capable of measuring the wind speed in every 5 mm up to a 1 m of height. Before the data gathering operation has initiated, measurement system was calibrated. In Figure 3.8 on the right, a photograph taken during the measurements is presented.
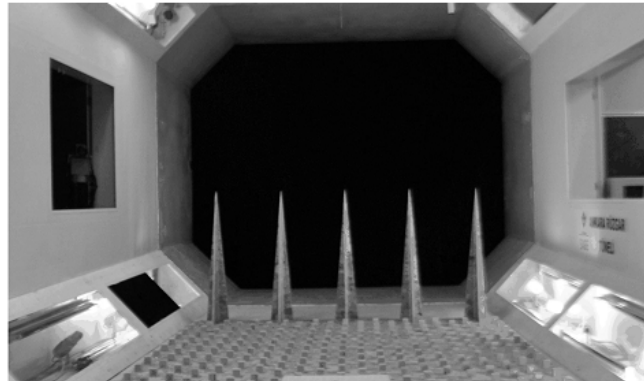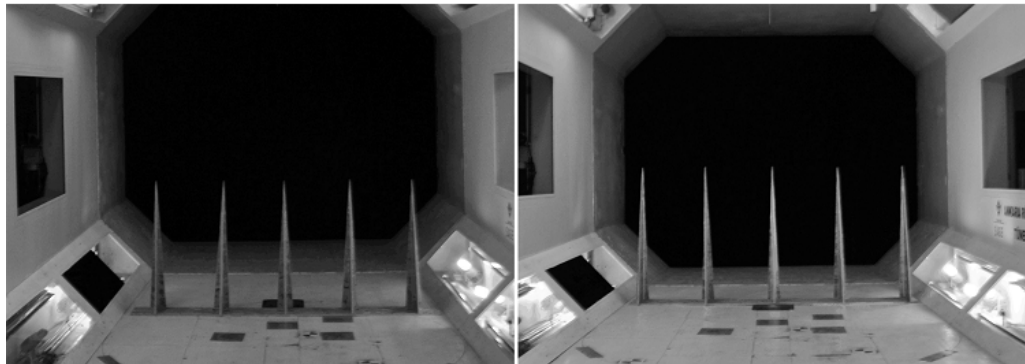


Figure 3.7 Location of surface roughness elements in the tunnel

**Figure 3.8 Photographs of the traverse system and hot wire anemometer system taken during the test**

The results of the experiments are investigated in terms of wind speed profiles and the turbulence intensity levels. Turbulence intensity is a parameter that demonstrates the variability of the flow velocity and it is determined utilising Equation (3.10).

$$I_u = \frac{\sigma_u}{\overline{U}}$$ (3.10)

In equation (3.10), $I_u$ is the turbulence intensity; $\sigma_u$ is the root mean square of the velocity and $\overline{U}$ represents the mean flow velocity.

The turbulence level of the empty tunnel, the one measured during the test and the definition of ASCE for each exposure categories are presented in Figure 3.9. When the tunnel is empty, the turbulence intensity is approximately 3% in average which is considerably low when compared with the ASCE 7-05 definitions. Surface roughness elements placed at the inlet of the test section caused an increase of the turbulence intensity as expected. As the roughness of the exposure category increases, i.e. from exposure D to B, the flow gets more turbulent. Within the first 20 cm of height, for exposure B, the turbulence intensity levels

reach to 20-40 % values as a consequence of the utilisation of the surface roughness cubes whereas turbulence intensities are around 10% in the other two categories in which there are spires only.

The experimental results for turbulence intensities are quite similar with the ones defined by ASCE 7-05 (ASCE 7-05, 2005) for the first 50 cm of the test section height but for the higher regions, while ASCE definition remains constant, the test results exhibit a decrease, almost a disappear. This is a consequence of the fact that the spires lose their effects on turbulence after a certain height.
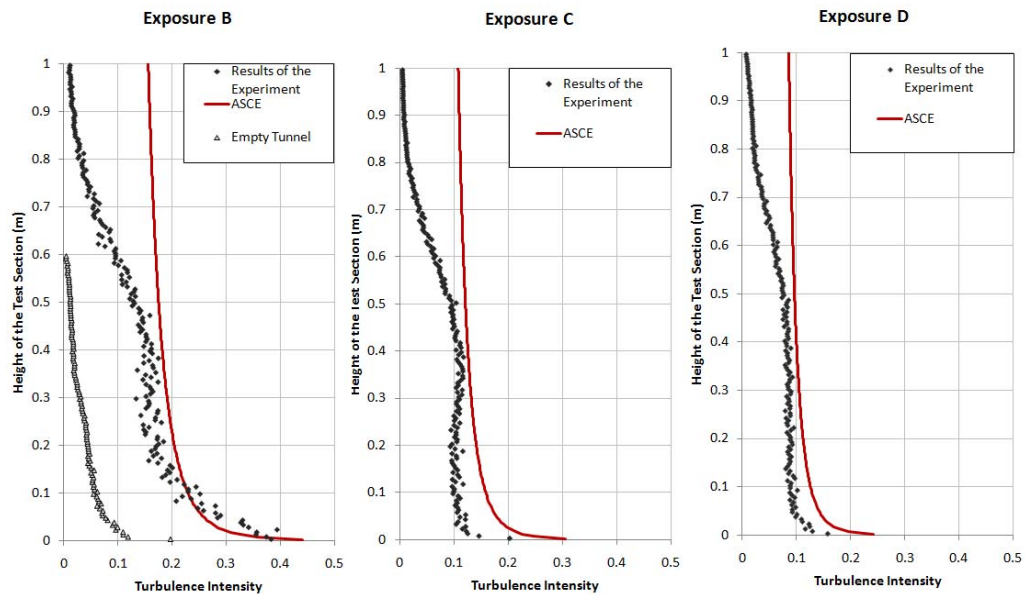


**Figure 3.9 Comparative turbulence intensities of the flow in the tunnel**

In Figure 3.10, the graphs of the wind speed profiles obtained from experiments, numerical modelling and ASCE 7-05 definitions (ASCE 7-05, 2005) are given for each of the exposure categories. The measurements in the empty tunnel indicate that the wind speed gets constant after 35 cm of height. In other words, if no surface roughness elements were used in the tests, the thickness of the atmospheric boundary layer would be 35 cm. By the help of the spires located at the inlet of the test section, the atmospheric boundary layer has occurred at a height that is quite close to the desired values given in Table 3.4 for each of the exposure categories B, C and D. Although the results of the numerical modelling closely fit to the ones defined in ASCE 7-05, measured profiles slightly deviate from them due to the high turbulent effects described in Figure 3.9. This deviation is much greater in exposure B

compared with the other two because of the utilisation of the cubic surface roughness elements. Since the turbulence that occurs around the spires at the wake cannot be fully reflected in the numerical models, such deviations could not be estimated from numerical simulations.
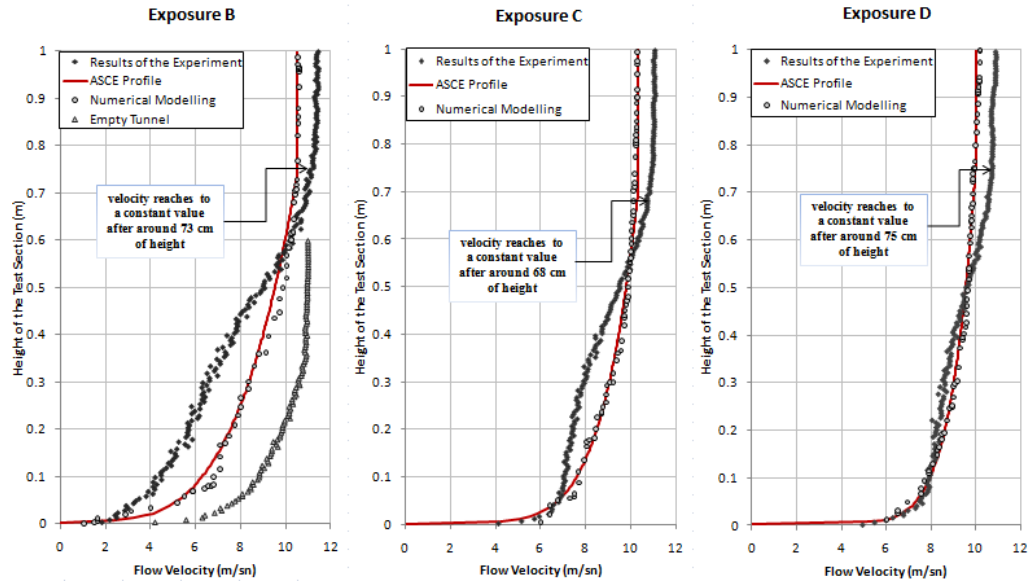


**Figure 3.10 Comparative wind profiles of the flow in the tunnel**

These results emphasize the significance of the length of the test sections of the wind tunnels for the similitude of the atmospheric boundary layers. For the atmospheric boundary layers to be completely modelled in a wind tunnel, the test sections should be around 15 - 20 meters in length (Cermak, 2003). Because the test section of the only wind tunnel in Turkey, AWT is relatively short, the turbulence intensities occurring around the spires cannot completely disappear before the flow reaches to the building model. As a result of this turbulence, a smaller wind speed is obtained compared with the ones defined in ASCE 7-05 (ASCE 7-05, 2005).

Another remarkable consequence is that the wind speed exceeds 10 m/sec after the atmospheric boundary layer is reached approximately at a height of 60 cm. In the high frequency base balance (H-FBB) analysis, instead of the magnitude of the wind speed and the turbulence intensity, their randomness and similarities with the target shapes have the major significance. In conclusion, the results demonstrated in Figures 3.9 and 3.10 are quite admissible for a short-section wind tunnel test and could be utilized for H-FBB tests.

# CHAPTER 4

# ANKARA WIND TUNNEL TESTS

A series of tests were performed on a rectangular building model by using high frequency base balance technique at Ankara Wind Tunnel. The base moments were measured by a base balance system designed and manufactured especially for this study. Ankara Wind Tunnel is a closed circuit wind tunnel with 3.05 x 2.44 m test section and 6.1 m length. Since it has a comparatively short test section, special passive devices were utilized at the inlet of the tunnel to create atmospheric boundary layer and to match the requirements of the wind profile and turbulence intensity. The tests were repeated several times for examining the effects of exposure categories and angle of attack.

## 4.1 DESIGN OF THE BASE BALANCE SYSTEM

In the high frequency base balance (H-FBB) tests, response of the model building is measured through a special data acquisition and processing system that consists of ultra-sensitive force measurement arrangements. Balance system which was designed and constructed particularly for this study is capable of measuring two base bending moments that are orthogonal to each other. In the system, there are four load cells each of which has a capacity of 5 kg; and capable of measuring 50 g of load. Load cells are arranged such that they form the shape of a cross-hair. In other words, two load cells are perpendicularly connected to each other through aluminium beam elements. Thus, two orthogonal base bending moments can be obtained by multiplying the distance between two opposing cells with the axial load measured on them. A photograph of this balance system is presented in Figure 4.1. The photograph on the left in Figure 4.1 is the balance system itself. The rod at its centre is the element used for integrating the model. The system was connected to a data

acquisition system which was located under the test section floor. The photograph on the right in Figure 4.1 presents the placement of the balance system in the tunnel. The floor in the picture is actually the basement of the test section. The rod was passed through the hole on the floor and glued to the model by epoxy through the hole produced in its centre. A major requirement of the balance system is that it should have low mass and high stiffness in order not to participate in the response (Cermak, 2003). In order to fulfil this requirement, aluminium is chosen as the material during design of the balance system. After the assemblage, the system is measured to have a natural frequency of approximately 10 Hertz.
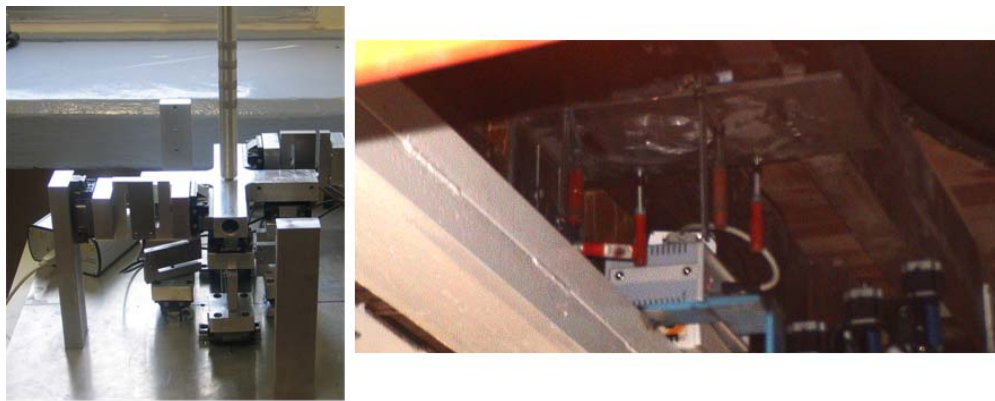


**Figure 4.1 Balance system and its location in the tunnel**

In H-FBB tests, models are required to have low mass and high rigidity. Most widely used materials that satisfy these necessities are balsa wood, polystyrene foam and thin walled plastic (Gamble, 2003). In this case study, polystyrene foam is preferred since it can be supplied and shaped easily. The aluminium rod connected rigidly to the balance system was glued to the model by epoxy. Building model is a rectangular prism of 15 x 20 x 50 cm in size which is equivalent to a building of 60 x 80 x 200 m for a scale of 1/400. (Figure 4.2) This scale was determined particularly for Exposure C defined in ASCE 7-05 (Shojaee, et al., 2009).

**Figure 4.2 Alignment of the model in test section**

## 4.2   TEST RESULTS

The major aim of this study is to investigate the influences of exposure categories and angle of attack on response of the building. Therefore, tests were conducted for exposure categories B and C which represent city centre and open environment in ASCE 7-05, respectively (ASCE 7-05, 2005). In category B tests, only the case of perpendicular wind direction was analyzed, whereas in category C, effects of different angle of attack were investigated through the tests for 0, 15, 30, 45, 60, 75 and 90 degrees. In Figure 4.3, there is a sketch of the system displaying the direction system used in this study. In order to satisfy the repeatability of the tests, each test was performed at least two times. Data acquisition system gathered data with a speed of 100 Hz for a duration of 3 minutes in each test. In other words, the time dependent data is in 0.01 second time interval.

At the end of the tests, the balance system has supplied the axial loads occurring on four load cells. The two opposing ones form a couple for the bending moment in x direction and the two other perpendiculars form one in y direction. (See Figure 4.3) The idea is to simply multiply the axial loads with the distance between them which is measured to be 13 cm. As a result, base moment variations in time for two orthogonal directions are obtained. After that, the statistical properties of each data such as the mean, standard deviation and power spectral density function are calculated. For the calculations, commercially available software's 'MATLAB' and 'Microsoft Office Excel' are used. These parameters are used to

determine the design base moments, equivalent static loads and top accelerations. Design wind speed is selected as 40 m/sec (90 miles/hr) for this study.
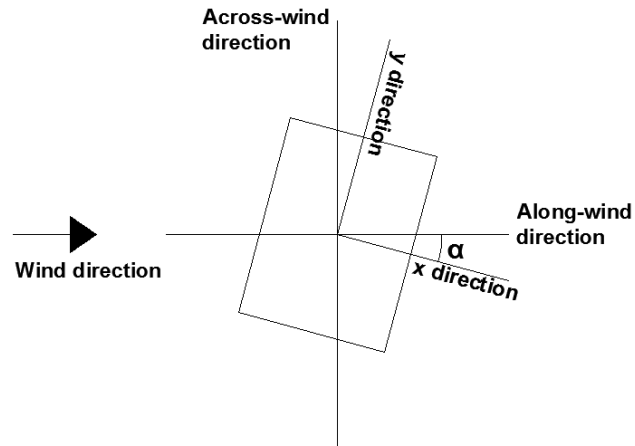


**Figure 4.3 Angle of wind attack**

At the end of the tests, base moment data is obtained as time series. The results for each of the tests are given explicitly in Appendix B but here, base bending moments depending on time in along and across wind directions specifically for the tests made in exposure category C and zero angle of attack are presented in Figures 4.4 and 4.5. Fast Fourier Transforms of the base bending moments are presented in the same figures as well. In both of the FFT's, natural frequency of the base balance system is appearing around a frequency of 10 Hertz with an artificial peak response. In the FFT graph of across wind base moments, there occurs another peak which corresponds to the vortex shedding frequency.
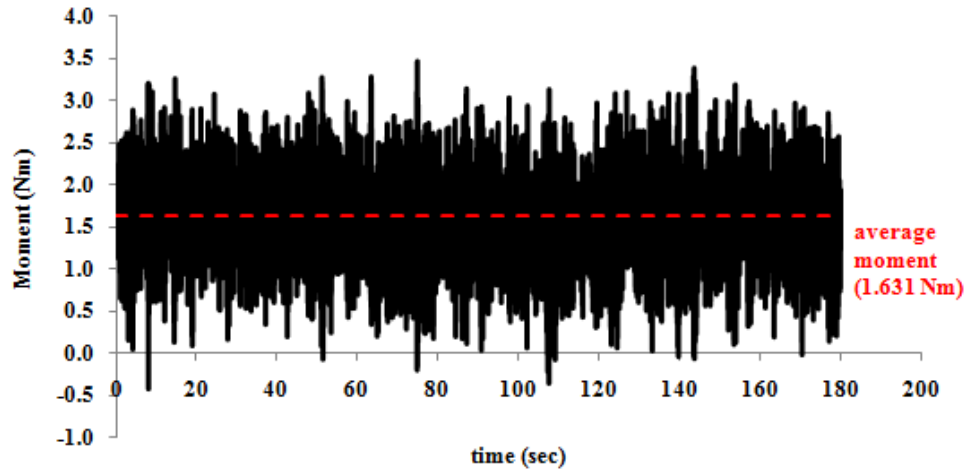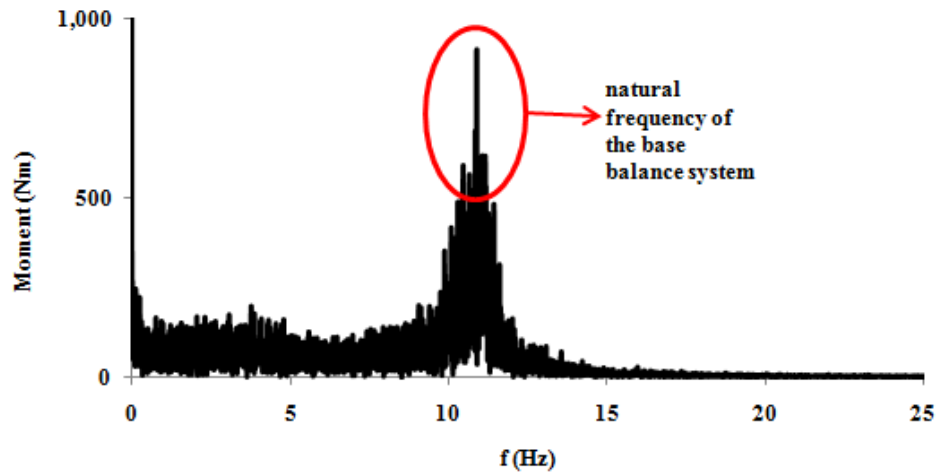
**Figure 4.4 (a) Base bending moment in along wind direction vs. time graph and (b) its Fast Fourier Transform**
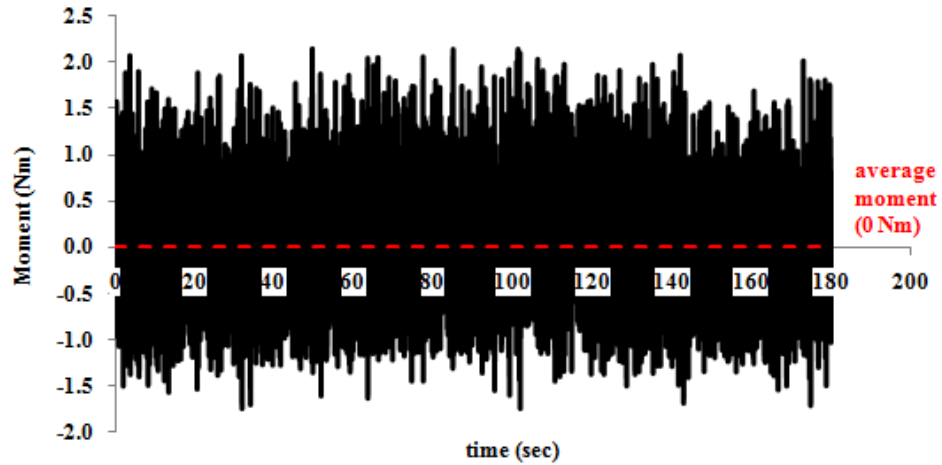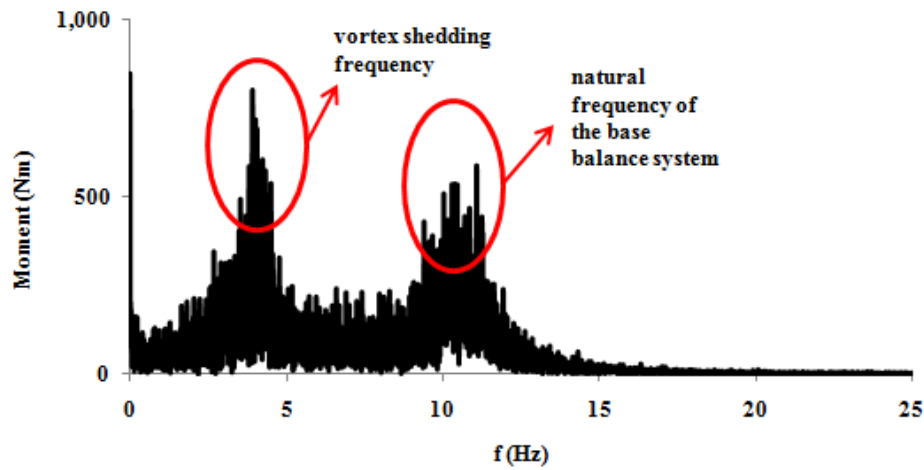
**Figure 4.5 (a) Base bending moment in across wind direction vs. time graph and (b) its Fast Fourier Transform**

Then, in order to implement the results of the wind tunnel test and determine the data necessary for design of the building, normalized wind spectra are generated. The horizontal axis of a normalized wind spectrum is $f * B/U_H$ where; f is the frequency; B is the dimension of the building perpendicular to wind; and $U_H$ is the design wind velocity. On the other hand, vertical axis is $fS_M(f)/\sigma_M^2$ where $\sigma_M$ is the root mean square of the moment; and $S_M(f)$ is the power spectral density function of the moment. $fS_M(f)/\sigma_M^2$ will be in short denoted by $C_M(f)$. These spectra are created in all exposure categories and angles of

59

attack in along wind, across wind, x and y directions. In Figure 4.6, there are the normalized spectra for the tests whose time dependent graphs and FFT's are presented in Figures 4.4 and 4.5. In order to provide a smooth power spectral density function, the time dependent series are divided into 18 parts each of which has 1500 data such that first part starts from 0 second to 14.99 seconds; second part is from 15 seconds to 29.99 seconds; and third part is from 7.48 seconds to 22.47 seconds that sets in between first and second parts. The remaining 15 parts are formed by using the same logic. Therefore, the data is divided into 36 subgroups since the same test is repeated twice in order to show repeatability. Finally, the power spectral density functions are made smoother by using '*moving average*' technique in Matlab where the function of 'smooth' is used with a selected degree of smoothing of 8.

## 4.3 INTERPRETATION OF RESULTS

### Calculation Details for the Tests in Exposure C and 0° Angle of Attack

In order to explain the procedure in the determination of base moments in Table 4.4, calculations performed for Exposure C and 0° angle of attack will be demonstrated in this part. First of all, the physical properties of the building can be listed as;

- Fundamental frequency in x direction, $f_{1x}$ : 0.386 Hertz
- Fundamental frequency in y direction, $f_{1y}$: 0.200 Hertz
- Building bulk density: 250 kg/m$^3$
- Structural damping ratio, $\xi$: 0.02
- Drag coefficient, $C_D$: 1.3
- Air density, $\rho$: 1.25 kg/m$^3$

For survivability design, one hour averaging time, 50 year return period wind speed is recommended to use (Kareem, et al., 2000). Selected design speed of 40 m/s is the basic wind speed at reference height of 10 m in terms of 3 s gust. In order to convert 3 s gust speed to hourly gust speed, ASCE 7-05 defines a relationship such that hourly speed is 0.65 times 3s gust speed. Hence, wind speed at 10 m reference height, $U_{10}$ becomes 40*0.65 that gives 26 m/s. Design wind speed, $U_H$ is defined as wind speed at the top of the building. Recall that $\alpha$ is the power constant defined for each exposure categories specifically (ASCE 7-05, 2005). Relevant normalized spectra are given in Figure 4.6. Then calculations are

presented in bulleted form. These normalized spectra are created using a mean velocity calculated below using Equation (2.1).

$$\rightarrow \quad U_H = U_{10}*(200/10)^{\alpha} = 26*(200/10)^{1/6.5} = 41.222 \text{ m/s}$$



(a)



(b)
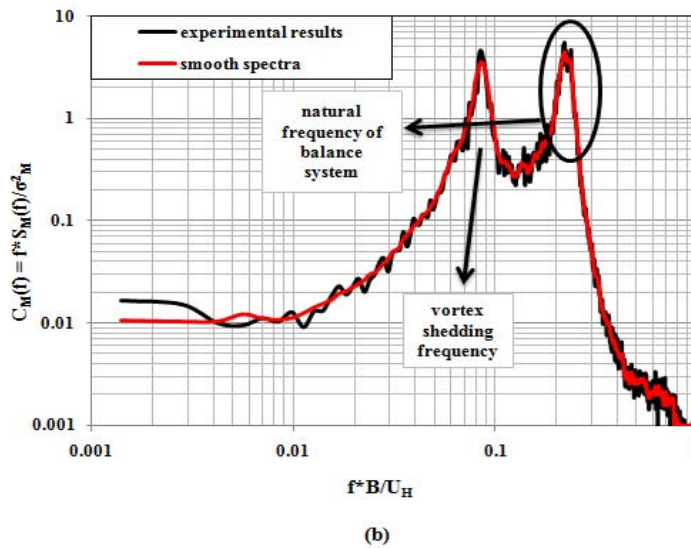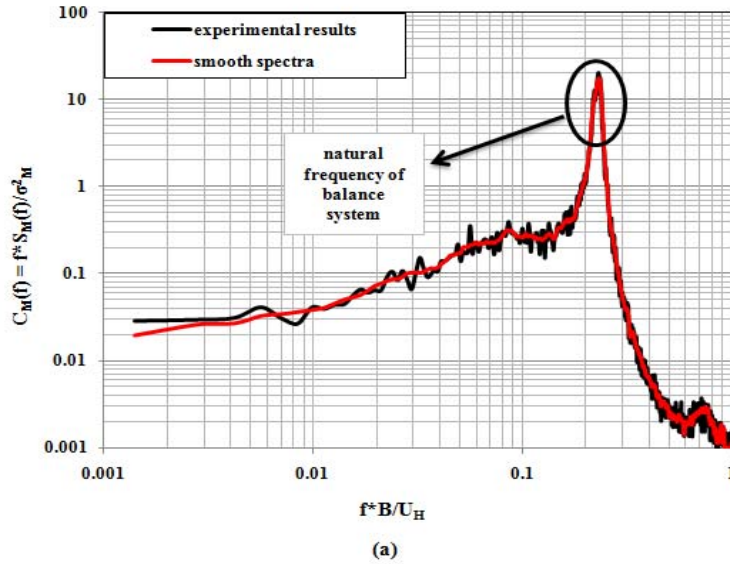
**Figure 4.6 Normalized spectra in (a) along and (b) across wind directions for exposure C and zero angle of attack**

→ $f_{1x}*B/U_H = 0.386*0.20/41.222 = 0.749 \Rightarrow C_M(f_{1x}) = 0.002769$ (Figure 4.6)

→ $f_{1y}*B/U_H = 0.200*0.20/41.222 = 0.388 \Rightarrow C_M(f_{1x}) = 0.006708$ (Figure 4.6)

Statistical parameters of random moment data obtained from base balance are;

→ Root mean square in along-wind or x direction, $\sigma_{Mx} = 0.335$ kNm

→ Root mean square in across-wind or y direction, $\sigma_{My} = 0.464$ kNm

→ Mean moment in along-wind direction, $\mu_{Mx} = 1.631$ kNm

→ Mean moment in across-wind direction, $\mu_{My} = 0$ kNm

→ Normalized standard deviation of moment in along wind direction,
$\sigma_{C_{Mx}} = 0.335/1.631 = 0.206$

→ Normalized standard deviation of moment in across wind direction,
$\sigma_{C_{My}} = 0.464/1.631 = 0.284$

→ Average/mean moment in along wind direction, $\bar{M}$ for actual building is determined using Equation (2.72) in Chapter 2 as **$1.917*10^6$ kNm.**

→ Assuming a background factor of 3 (Zhou, et al., 2003), background component of base moment in along wind direction is $3*0.206*1.917*10^6 = $ **$1.182*10^6$ kNm**

→ Resonant peak factor in both along-wind and across wind directions;
$g_R = \sqrt{2\ln(0.386*3600)} + 0.5772/\sqrt{2\ln(0.386*3600)} = 3.951$

→ Resonant component of base moment in along-wind direction is;
$\hat{M}_R = 3.951 * 0.205 * 1.917 * 10\char`^6 * \sqrt{\frac{\pi}{4*0.02}0.002769} = $ **$0.512*10^6$ kNm**

→ Finally, design base moment in along-wind direction is;
$M_d = \bar{M} + \sqrt{\hat{M}_B^2 + \hat{M}_R^2} = 1.917 + \sqrt{1.182^2 + 0.512^2} = \mathbf{3.205 * 10^6 \, kNm}$

→ Assuming a background factor of 3 again, background component of base moment in across wind direction is $3*0.284*1.917*10^6 = $ **$1.635*10^6$ kNm**

→ Resonant component of base moment in across-wind direction is;
$\hat{M}_R = 3.951 * 0.284 * 1.917 * 10\char`^6 * \sqrt{\frac{\pi}{4*0.02}0.006708} = $ **$1.104*10^6$ kNm**

→ Finally, design base moment in across-wind direction is;
$M_d = \bar{M} + \sqrt{\hat{M}_B^2 + \hat{M}_R^2} = 0 + \sqrt{1.635^2 + 1.104^2} = \mathbf{1.973 * 10^6 \, kNm}$

*Effects of Exposure Category:*

In order to analyze effects of exposure category on response of a building, tests performed for 0° angle of attack in exposure B and exposure C are compared and discussed. In Table 4.1, parameters related with the base moments in both along wind and across wind directions are given for exposure categories B and C. The parameters are average moment of the real building ($\overline{M}$), average moment for the model ($\overline{M}_{model}$), root mean square ($\sigma_M$) and coefficient of variation or the normalized standard deviation of moment ($\sigma_{C_M}$). Equations to calculate these parameters are restated in Equations (4.1) to (4.3).

$$\overline{M} = \int_0^H 1/2 C_D \rho \overline{U}(h)^2 Bhdh \tag{4.1}$$

$$\sigma_M = \sqrt{\frac{\sum(M - \overline{M}_{model})}{n-1}} \tag{4.2}$$

$$\sigma_{C_M} = \frac{\sigma_M}{\overline{M}_{model}} \tag{4.3}$$

In the above equations, $C_D$ represents the drag coefficient and taken as 1.3 for rectangular buildings (Zhou, et al., 2003); H is height of the model building and it is 0.5 m; $\overline{U}(h)$ is the mean wind velocity; and n is the number of data points in time dependent series of the random variable, moment under consideration. In Equation (4.3), the mean moment under consideration is calculated for the along wind direction. In addition, mean moment in the across wind direction is always zero since there is no mean wind velocity acting there and the only reason for the across wind moment is due to vortex shedding (not mean but fluctuating component of moment). While computing the coefficient of variation, the interaction of the base balance's natural frequency, the row data was filtered by utilizing 'band-stop filter'. During this process, the data that has a frequency between 9 Hz and 11 Hz were excluded. (The natural frequency of the balance system was measured to be equal to 10 Hz).

Average base moments and coefficient of variations are calculated in along and across wind directions for exposure categories B and C when the angle of attack, α is 0°. In this case, along direction coincides with the x direction and across wind direction with y. Therefore, dimension of the model building perpendicular to wind, B is 0.2m and the natural frequencies of the building corresponding to the along and across wind directions (x and y)

are 0.386 Hertz and 0.200 Hertz, respectively. Table 4.1 presents the moment parameters for exposures B and C. Superscripts x and y denote along and across wind directions.

**Table 4.1 Resultant moment parameters – Effects of exposure category**

| Exposure Category | Average Moment | Root mean square | Root mean square | Normalized Standard Deviation | Normalized Standard Deviation |
|---|---|---|---|---|---|
| | $(\bar{M}_{model})$ | $(\sigma_M{}^x)$ | $(\sigma_M{}^y)$ | $(\sigma_{C_M}^x)$ | $(\sigma_{C_M}^y)$ |
| **Exposure B** | 1.052 | 0.266 | 0.276 | 0.253 | 0.262 |
| **Exposure C** | 1.631 | 0.335 | 0.464 | 0.206 | 0.284 |

*All dimensions are in N.m*

In Table 4.1, average moment values increase with increasing average wind velocity. In exposure B, average velocity in first 50 cm of the test section height is determined to be 6 m/sec and it is 7.73 m/sec in Exposure C (Figure 3.1 in Chapter 3). The increase in average moment is directly proportional to the square of the average velocity ratios. When the normalized standard deviations are compared, in x direction, it is seen that the value is larger for exposure B due to high turbulence. Note that average turbulence intensity in first 50 cm of height is around 22% in B whereas it is 10.7 % in C. As a result, it is concluded that turbulence intensity directly affects normalized standard deviation, thus the background moment, in along wind direction.

In order to determine the total base moment, the fluctuating moment values should also be calculated since total moment is the summation of the mean moment and the square of sum of squares of the resonant and background components of fluctuating moment as given in Equation (4.6). In Equation (4.4), it is seen that background component is directly related with the average moment and normalized standard deviation but resonant component is related with the power spectral density function of moment as given in Equation (4.5). For this purpose, normalized spectra in along and across wind directions for both exposure categories are computed (Figure 4.7).

64

$$\widehat{M}_B = g_B * \sigma_{C_M} * \overline{M} \tag{4.4}$$

$$\widehat{M}_R = g_R * \sigma_{C_M} * \overline{M} * \sqrt{\frac{\pi}{4*\xi} C_M(f_1)} \tag{4.5}$$

$$M_d = \overline{M} + \sqrt{\widehat{M}_B{}^2 + \widehat{M}_R{}^2} \tag{4.6}$$
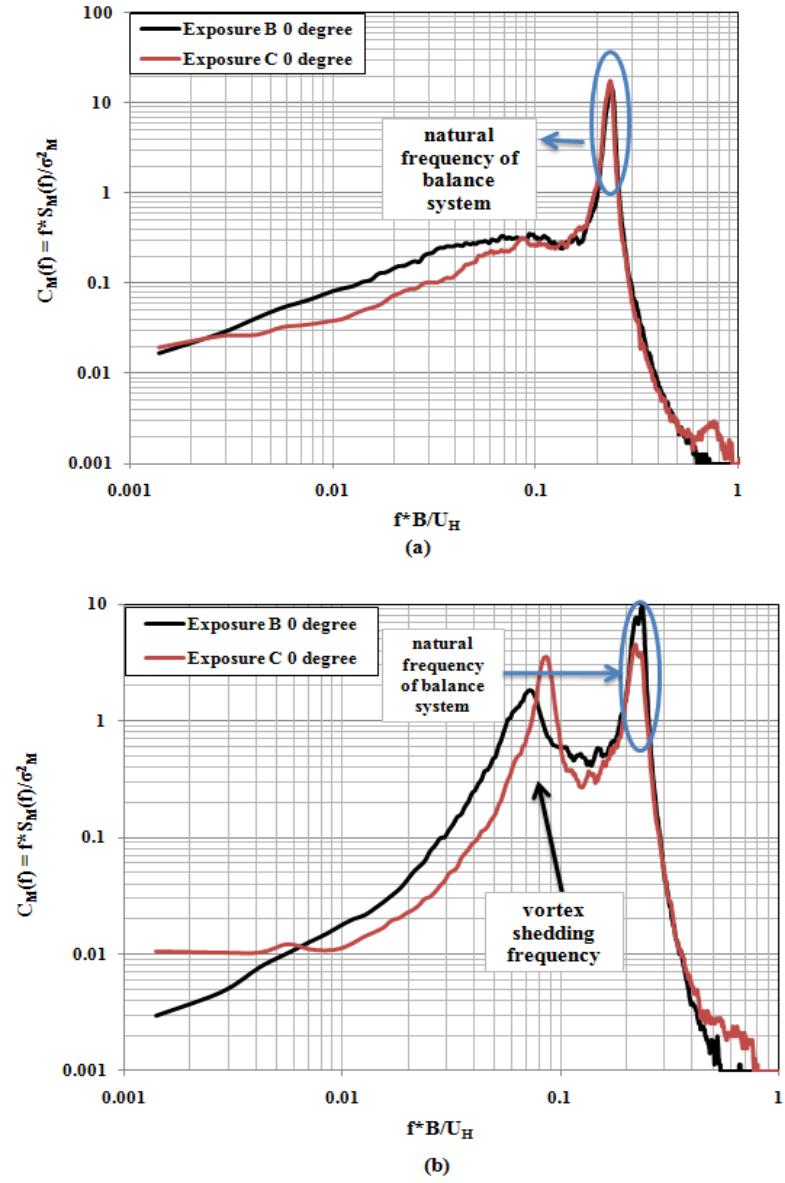


**Figure 4.7 Normalized spectra in (a) along wind and (b) across wind directions for exposure categories B and C**

In the spectra for both directions, around a normalized frequency of 0.23, there occurs a peak which is due to the interaction of natural frequency of the balance system. Using data in this range leads to a biased result. Improving the balance system such that it has a high natural frequency out of the range of modal frequencies of the model may solve this problem. In the spectra of across wind direction there is one more region where response makes a peak which matches with the vortex shedding frequency. Vortex shedding frequency mainly depends on the wind speed and plan geometry of a building. The effect of building geometry is usually described with *Strouhal number* which can be computed by using the following equation.

$$St = \frac{f_s * B}{\bar{U}} \tag{4.7}$$

where, $f_s$ is vortex shedding frequency; $St$ is Strouhal number; B is the dimension of the building perpendicular to wind; and $\bar{U}$ is mean velocity of the approaching wind. Equation (4.7) is actually the horizontal axis of the normalized spectra. According to Eurocode 1 (Eurocode 1, 2005), for rectangular buildings, Strouhal number changes according to the aspect ratio (D/B). Since the building model that was tested has an aspect ratio equal to 0.75, the Stouhal number for steady state flow becomes equal to 0.12 from Figure (2.4). According to the normalized spectra presented in Figure 4.7, Strouhal number for exposures B and C is around 0.07 and 0.09, respectively. The main reasons of the difference between the measured and computed Strouhal numbers are the varying wind speed with respect to height and varying turbulence intensity.

Turbulence intensity is greater in exposure B (22%) than in exposure C (10.7%) since B corresponds to city centre whereas C to open terrain (ASCE 7-05, 2005). Effects of this difference in turbulence are seen in the normalized spectra of across-wind direction around the vortex shedding part. The peak value for more turbulent category B is around 2 whereas it is approximately 3.5 in C. Moreover, shape of the spectra around vortex shedding is sharper in C. As a result, it is observed that higher turbulence intensity decelerates the fluctuations of resonant effects. On the other hand, when the spectra in along-wind direction are examined, it is seen that the building does not experience resonant effects but the fluctuations are primarily based on the pressure differences and hence on turbulence. As a remark, it is seen that in low frequency levels, more turbulent exposure category B leads to higher fluctuations.

*Effects of Angle of Attack:*

In order to investigate the influence of changing wind directions on the response of buildings, the model is tested in exposure C for 7 different angles of attack (0, 15, 30, 45, 60, 75 and 90 degrees). Results are examined firstly on the along and across wind directions (Figure 4.3). In Table 4.3, the resultant base moment components in along wind and across wind directions are shown and in Figure 4.9, change in the normalized standard deviation depending on the angle of attack is presented.

Parameters in Table 4.3 are determined by making statistical calculations for random moment data obtained from the measurements of balance system. Through balance system, moments in the x and y directions of the building are obtained (building perpendicular directions); however, in this part, moments in the along and across wind directions are under consideration. Therefore, random data for moments in along wind and across wind directions should be determined relating them with the x and y direction moments as given in Figure 4.8 and Equations (4.8) and (4.9). Note that during the wind tunnel test, building model is rotated in clockwise direction for each angle of attack, α.

$$M_{along} = M_x * \cos(\alpha) + M_y * \sin(\alpha) \qquad (4.8)$$

$$M_{along} = -M_x * \cos(\alpha) + M_y * \sin(\alpha) \qquad (4.9)$$

In Figure 4.8, $B_r$ is the dimension of the building perpendicular to wind and $D_r$ is one in parallel directions when it is rotated. They are listed in Table 4.2.
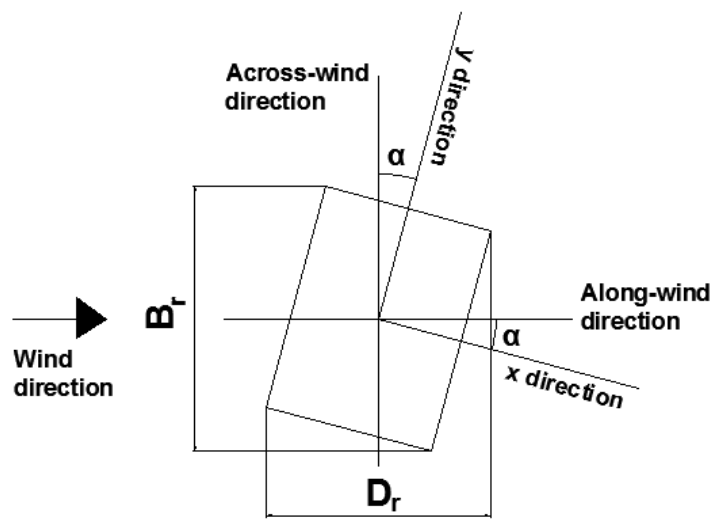


**Figure 4.8 Determination of moment data in along wind and across wind directions**

**Table 4.2 Rotated perpendicular and parallel dimensions**

| α (°) | B$_r$ (cm) | D$_r$ (cm) |
|---|---|---|
| **0** | 20.00 | 15.00 |
| **15** | 23.20 | 19.67 |
| **30** | 24.82 | 22.99 |
| **45** | 24.75 | 24.75 |
| **60** | 22.99 | 24.82 |
| **75** | 19.67 | 23.20 |
| **90** | 15.00 | 20.00 |

**Table 4.3 Resultant Moment Parameters (Model Building) – Effects of angle of attack**

| Angle of Attack | Average Moment | Root mean square | Root mean square | Normalized Standard Deviation | Normalized Standard Deviation |
|---|---|---|---|---|---|
| (°) | $(\bar{M}_{model})$ | $(\sigma_M{}^{along})$ | $(\sigma_M{}^{across})$ | $(\sigma_{C_M}^{along})$ | $(\sigma_{C_M}^{across})$ |
| **0** | 1.631 | 0.335 | 0.464 | 0.206 | 0.284 |
| **15** | 1.473 | 0.277 | 0.282 | 0.188 | 0.191 |
| **30** | 1.520 | 0.257 | 0.154 | 0.169 | 0.101 |
| **45** | 1.650 | 0.280 | 0.126 | 0.170 | 0.076 |
| **60** | 1.493 | 0.266 | 0.161 | 0.178 | 0.108 |
| **75** | 0.997 | 0.170 | 0.120 | 0.170 | 0.120 |
| **90** | 0.965 | 0.189 | 0.223 | 0.196 | 0.231 |

*All dimensions are in N.m*

In Table 4.3, mean moment is the summation of all moment vales in along wind direction divided by the number of data. It should be noted that, mean moment is in along wind direction, across wind mean moment is theoretically zero. Root mean squares in each direction are calculated using the moment data in the relevant direction and utilizing Equation (4.3). Finally, normalized standard deviations are simply root mean squares of the moment in that direction divided by the mean moment in the along wind direction.
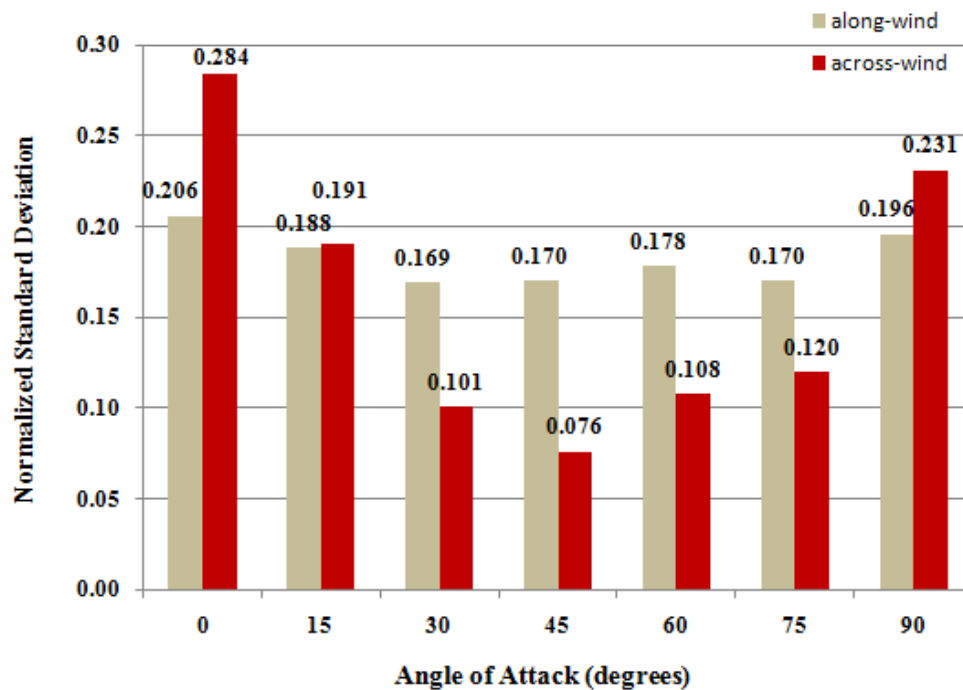


**Figure 4.9 Relationship of normalized standard deviation with angle of attack**

In buildings, main reason of having base bending moments in the across wind direction is vortex generation (Holmes, 2005). The effectiveness of these vortices on building response mainly depends on its architecture, meanly the geometry. This effect can be best visualized if two extreme conditions which are 0° and 90° angles are examined. When the angle of attack is 0°, the dimension of building model perpendicular to wind (B) is 0.2 m, whereas one in parallel direction (D) is 0.15 m. In other words, the aspect ratio of the building according to the wind direction (D/B) is equal to 0.75. When the angle of attack is 90°, the aspect ratio becomes equal to 1.33. In Table 4.3, normalized standard deviation of the across

wind moments in 0° is 0.284 whereas in 90°, it is 0.231. The ratio in the decrease of this quantity is around 23%. Hence, it can be concluded that as D/B ratio increases, effects of the vortices on the building response decrease. When the wind direction is different from the two orthogonal ones that are 0 and 90, the normalized standard deviations in across wind direction decrease significantly. Especially, when the angle is 45°, $\sigma_{C_M}$ is almost ¼ of the one in 0° (See Figure 4.9). On the other hand, no significant effects of angle of attack are observed in the response of building in along-wind direction.

Drag coefficient, $C_D$, is a dimensionless coefficient which explains how much a building resists wind flow actions. Equation (4.1) shows the direct relationship between $C_D$ and $\bar{M}$. Hence, a larger $C_D$ means larger mean moment. Change in the drag coefficient for different angles of attack is presented in Figure 4.10. In order to calculate $C_D$ values in the figure, average moment calculated in the along-wind direction of the building is divided by $B_r$ and then the ratio of this result is divided into the one obtained for 0°.
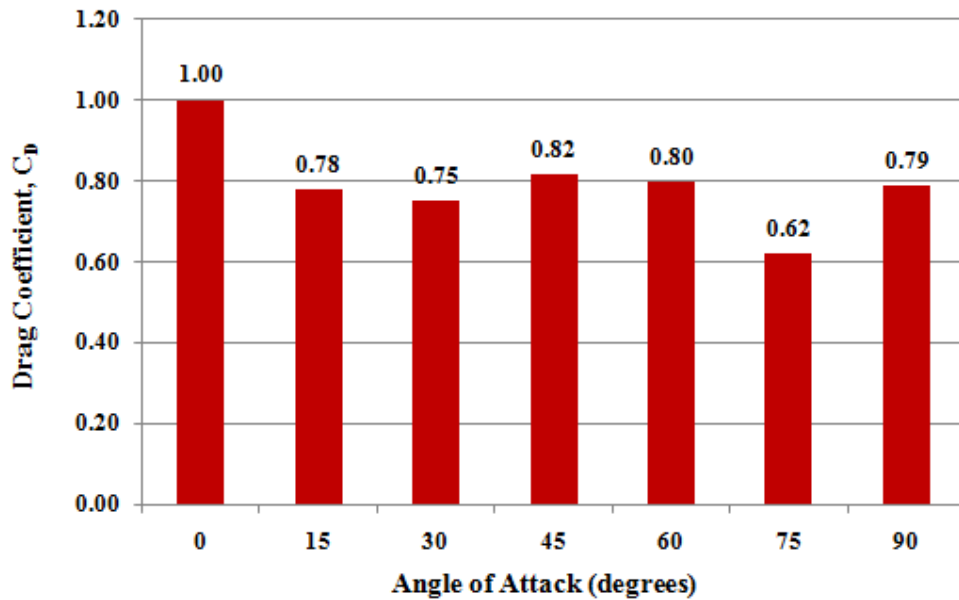


**Figure 4.10 Relationship of Drag Coefficient with Angle of Attack**

In Figure 4.10, a chart presenting drag coefficients in different wind directions is given such that $C_D$ in 0° angle of attack is assumed as 1. It is seen that as D/B ratio increases, the drag

coefficient and hence the resistance of the building to wind actions decreases. For instance, when D/B is changed from 0.75 to 1.33 (from 0° to 90°), $C_D$ decreases in 21%.

In Figure 4.11, normalized spectra in both along wind and across wind directions are computed for different angles of attack. In across wind spectra it is seen that as D/B ratio increases, vortex shedding effects decrease and the width of the peak part widens and smoothens. In along wind direction spectra, no significant effect of D/B ratio is observed.
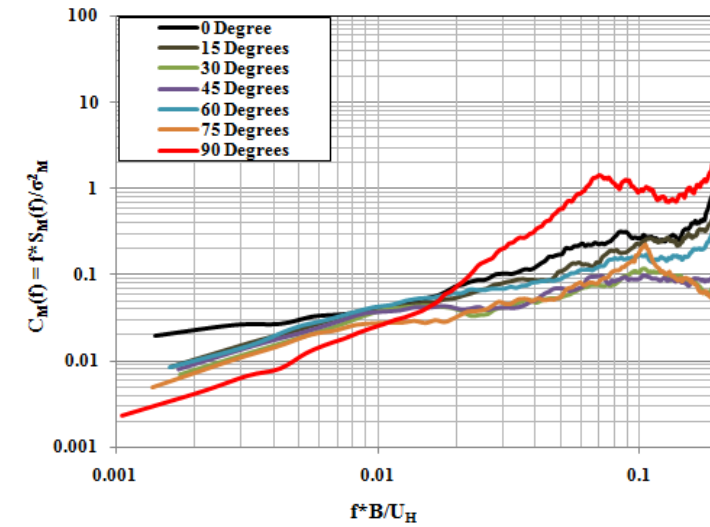


(a)
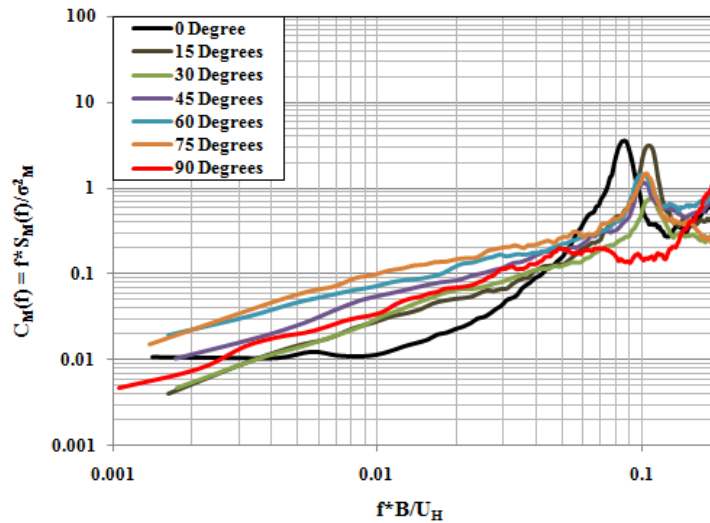


(b)

**Figure 4.11 Normalized spectra in (a) along and (b) across wind directions for different angles of attack**

In the design of buildings, base bending moments in the direction of building's translational mode are more meaningful than the along and across wind directions since the background and resonant components of base moments represent wind building interactions. Therefore, in Table 4.4, base bending moments in the direction of two translational modes (x and y) are listed. Since the bending moments under consideration are in the two translational modes of the building, relevant frequencies in x and y directions are the modal frequencies of the building that are 0.386 Hertz and 0.200 Hertz, respectively. In order to determine the resonant components of the fluctuating part of base moments, necessary normalized spectra in x and y directions were computed and are presented in Figure 4.12. While calculating the average moments, the ones determined in along –wind direction is decomposed into their vectorial components in the relevant x and y directions. (See Figure 4.3) In the calculations, design wind speed is 40 m/sec.
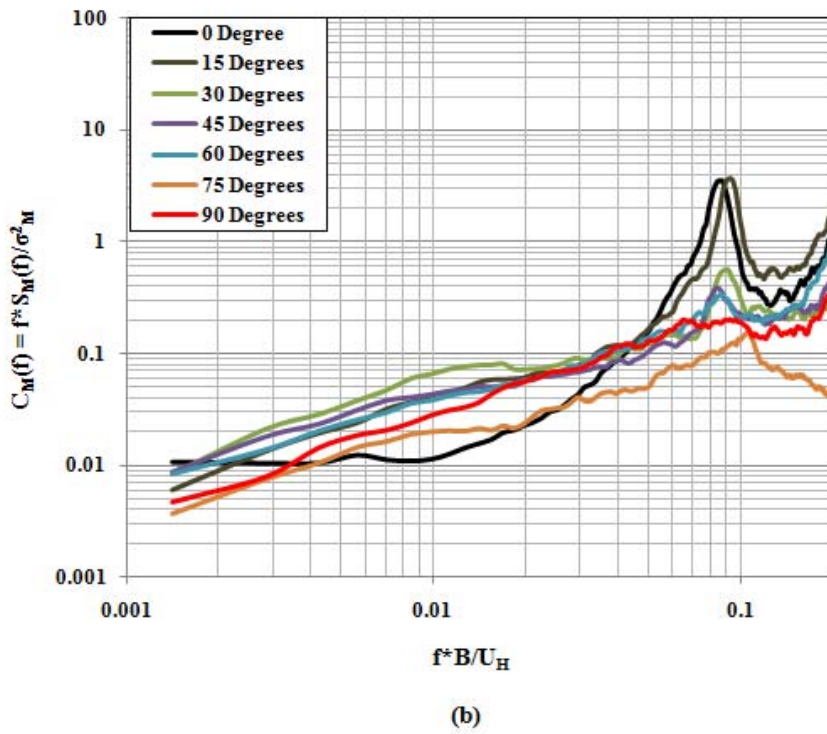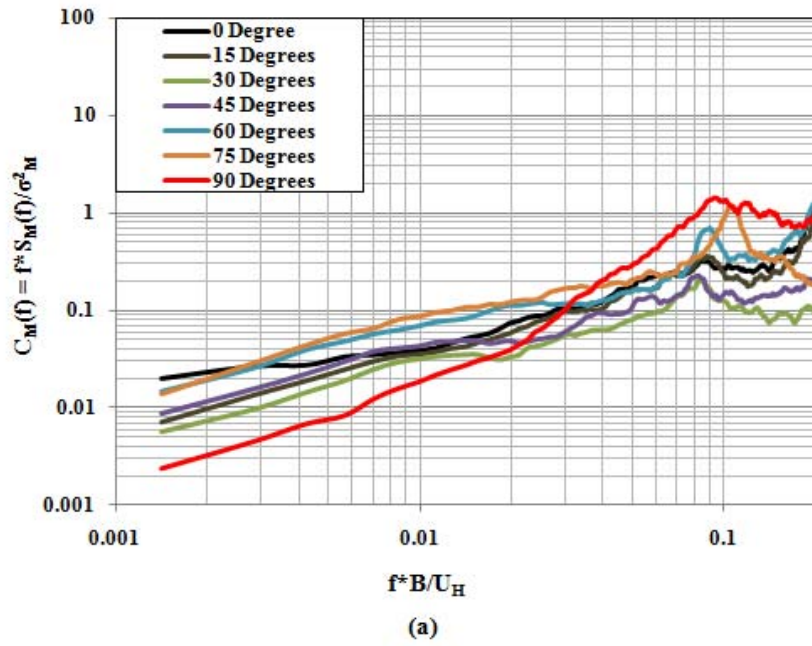
**Figure 4.12 Normalized spectra in (a) x and (b) y directions for different angles of attack**

When the spectra in x direction are examined in Figure 4.12, it is observed that as the degree of angle of attack increases, vortex shedding becomes more effective. This is an expected result since across wind response that involves resonant behavior due to vortex shedding becomes more pronounced. In the normalized spectra created for y direction in Figure 4.12, it is observed that for small angles of attack, vortex shedding frequency is effective but as the degree of angle of attack increases, it diminishes since y direction changes from across wind direction to along wind direction as the building is rotated.

**Table 4.4 Resultant Design Base Moments (Actual Building) – Effects of angle of attack**

| Angle of Attack (°) | X Direction | | | | Y Direction | | | |
|---|---|---|---|---|---|---|---|---|
| | $\bar{M}$ | $\widehat{M}_B$ | $\widehat{M}_R$ | $M_d$ | $\bar{M}$ | $\widehat{M}_B$ | $\widehat{M}_R$ | $M_d$ |
| 0 | 1.917 | 1.182 | 0.512 | *3.205* | 0.000 | 1.635 | 1.104 | *1.973* |
| 15 | 2.148 | 1.228 | 0.343 | *3.423* | 0.576 | 1.071 | 0.804 | *1.915* |
| 30 | 2.060 | 1.101 | 0.078 | *3.164* | 1.189 | 0.624 | 0.666 | *2.102* |
| 45 | 1.677 | 0.909 | 0.237 | *2.616* | 1.677 | 0.667 | 0.522 | *2.524* |
| 60 | 1.102 | 0.736 | 0.272 | *1.887* | 1.909 | 0.700 | 0.464 | *2.749* |
| 75 | 0.488 | 0.417 | 0.145 | *0.929* | 1.821 | 0.434 | 0.902 | *2.822* |
| 90 | 0.000 | 0.997 | 0.994 | *1.408* | 1.438 | 0.845 | 0.266 | *2.324* |

*All dimensions are in $10^6$ kN.m*

In Table 4.4, $\bar{M}$ is average moment that is calculated using Equation (2.72) in Chapter 2; but in this case, $B_r$ is used instead of B in the expression since $B_r$ represents the width of building that is perpendicular to wind. Then the resultant mean moment is decomposed into its components in x and y directions using Equations (4.8) and (4.9) since it is the moment in along-wind direction. $\widehat{M}_R$ and $\widehat{M}_B$ are resonant and background components of fluctuating part of the base moments. They are determined utilizing Equations (2.71) and (2.72) in Chapter 2 respectively. Finally, $M_d$ is the design base moment which is calculated summing

mean moment with the square root of sum of square of the resonant and background components (Equation (2.73) in Chapter 2). When Table 4.4 is analyzed, it is seen that unlike the traditional approaches, maximum base moment does not necessarily occur in the perpendicular directions. For instance, in x direction, maximum design base moment has occurred in 15° angle of attack. Specifically, this increase is due to larger mean moment that is caused from the fact that area of building which is exposed to wind is larger. ($B_r > B$) Except the 90° results, resonant components of base moments are largest when D/B ratio is minimum which is expected because it was observed before that as D/B ratio increase, effects of vortex shedding decreases. The resonant component of the moment in x direction for 90° angle of attack is calculated to be very high compared with the others because the amplitude of the normalized spectra is very high around the relevant normalized frequency.

In calculations, basic wind speed at a reference height of 10 m in terms of 3 s gust is used which corresponds to 40 m/s of speed. As a design philosophy, force based response quantities of a building are considered under the title of *survivability design* and ones related with human comfort, specifically top accelerations are analyzed under the scope of *serviceability design*. The difference between these two types appears in the selection of design wind speeds. It is a common approach to use one-hour averaging time with 50 year return period for survivability design calculations and one-hour averaging time with 10 year return period for serviceability design (ASCE 7-05, 2005), (Zhou, et al., 2003).

### *Determination of Equivalent Static Loads*

Calculations for equivalent static loads are made by using one-hour averaging time, 50 year return period design wind speed (Survivability design). In order to determine equivalent static loads, Equation (2.65) in Chapter 2 is used with a linear mode shape and constant mass per unit height assumptions. Explicitly, the equations that are utilized are given below;

$$\hat{P}_R(z) = \hat{M}_R \frac{m(z)\phi_1(z)}{\int_0^H m(z)\phi_1(z).z dz} \tag{4.10}$$

$$\hat{P}_B(z) = \bar{P}(z)\frac{\hat{M}_B}{\bar{M}_x} \tag{4.11}$$

$$\bar{P}(z) = \frac{1}{2}C_D\rho U(z)^2 B \tag{4.12}$$

In Equations (4.10), (4.11) and (4.12), $\hat{P}_R(z)$, $\hat{P}_B(z)$, $\bar{P}(z)$ are resonant component, background component and mean equivalent loads, respectively; $\phi_1(z)$ is the mode shape and assumed as linear ($\phi_1(z) = z/H$); m(z) is mass per unit height which is determined as floor area times the unit weight of the building that is assumed to be 250 kg/m³. Therefore, m(z) is constant and B*D*250 = 80*60*250 = $1.2*10^6$ kg/m. $C_D$ is the drag coefficient and assumed to be 1.3. $\hat{M}_B$ is the background component of the base bending moment. $\bar{M}_x$ is the mean base bending moment in x direction. Finally, U(z) is the wind profile which is defined in Figure 3.1, ASCE profile in Chapter 3 (ASCE 7-05, 2005). In the following figures, equivalent wind loads for each of the tests are demonstrated. Note that due to linear mode assumption, graphs for resonant components of the equivalent loads are linear; however, mean load distributions and background components of the equivalent loads are parabolic due to shape of the wind profile. As a result, shape of the equivalent loads is parabolic in each of the tests.
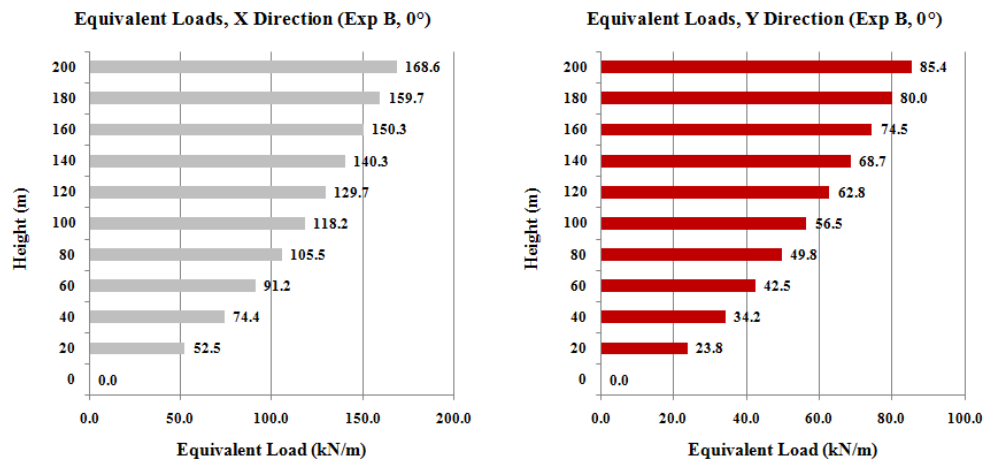


**Figure 4.13 Equivalent loads for exposure B and 0° angle of attack**
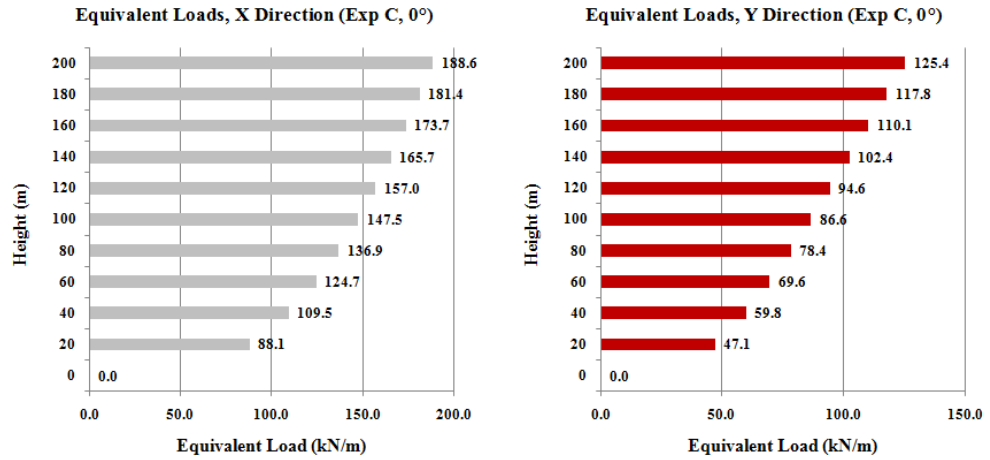
**Figure 4.14 Equivalent loads for exposure C and 0° angle of attack**
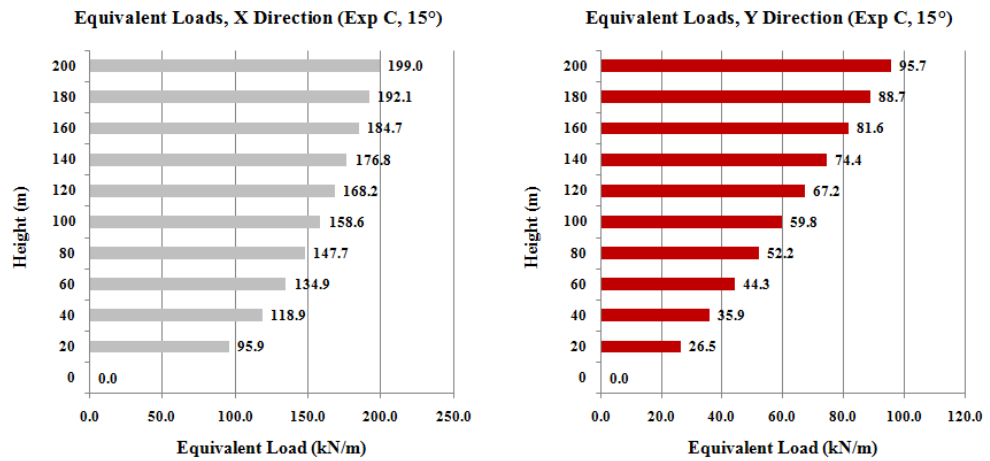


**Figure 4.15 Equivalent loads for exposure C and 15° angle of attack**
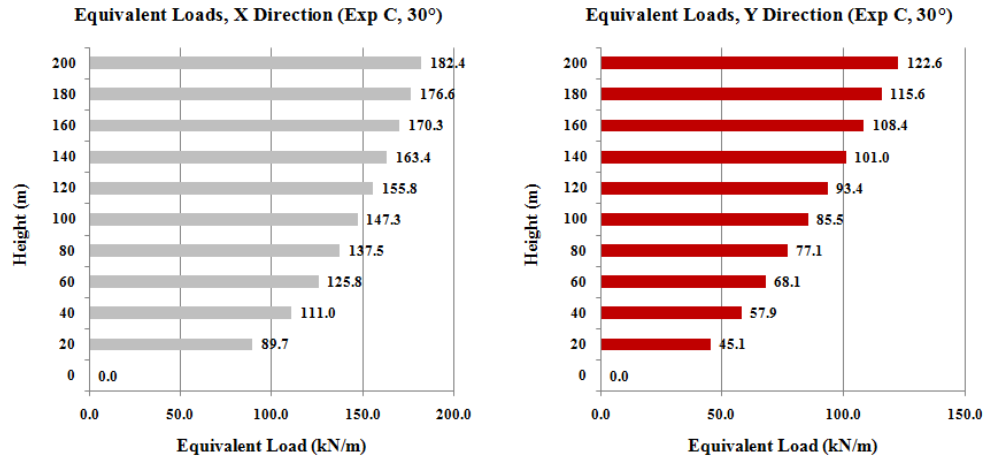
**Figure 4.16 Equivalent loads for exposure C and 30° angle of attack**
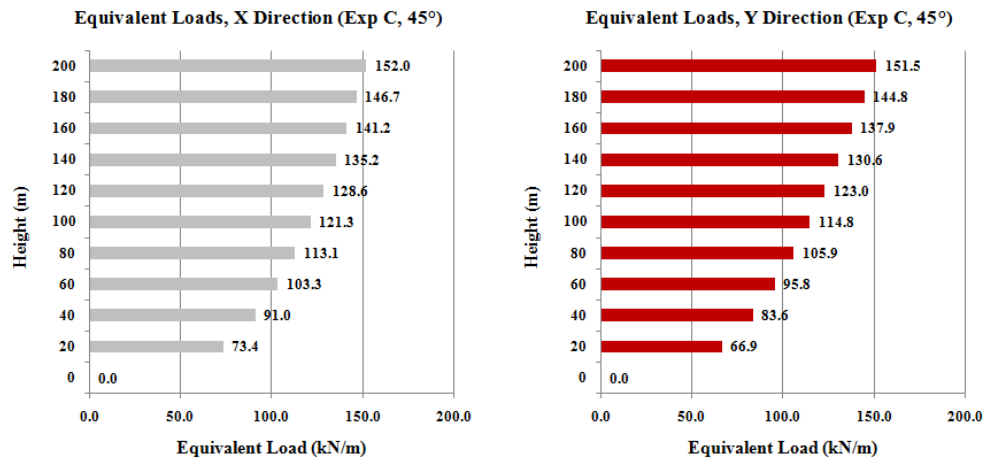


**Figure 4.17 Equivalent loads for exposure C and 45° angle of attack**
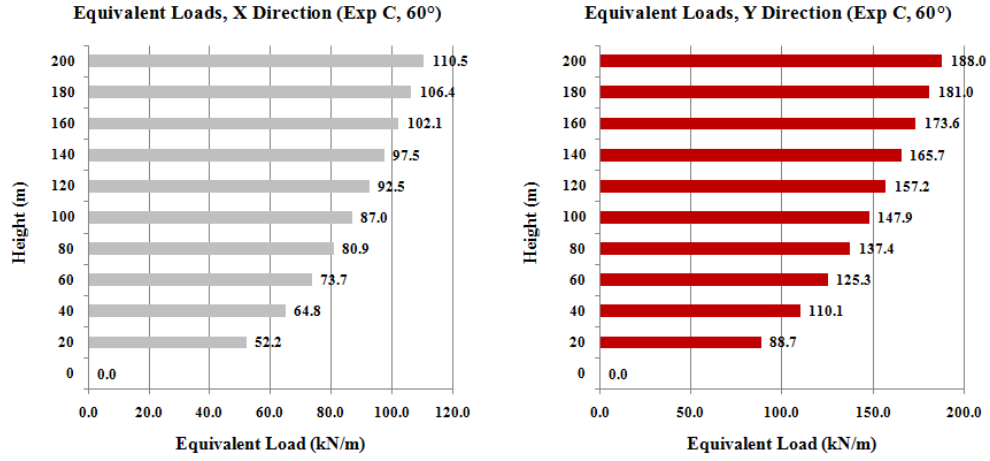
**Figure 4.18 Equivalent loads for exposure C and 60° angle of attack**
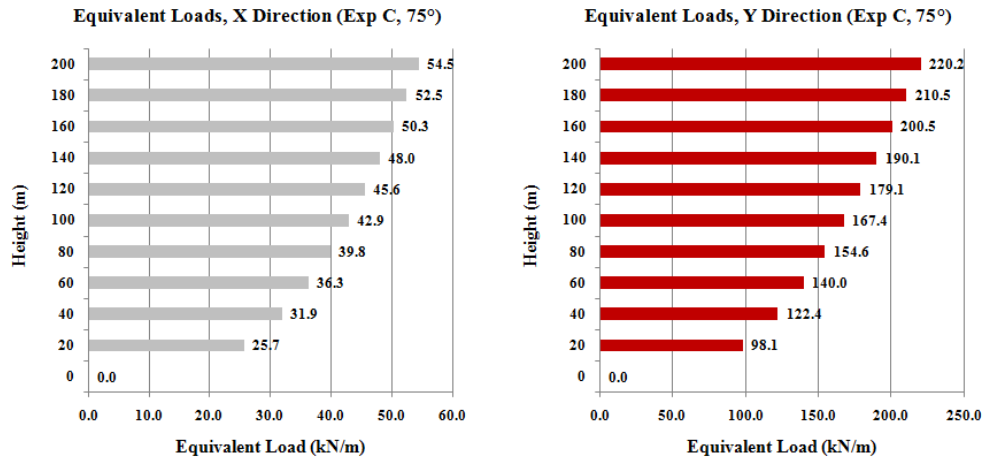


**Figure 4.19 Equivalent loads for exposure C and 75° angle of attack**
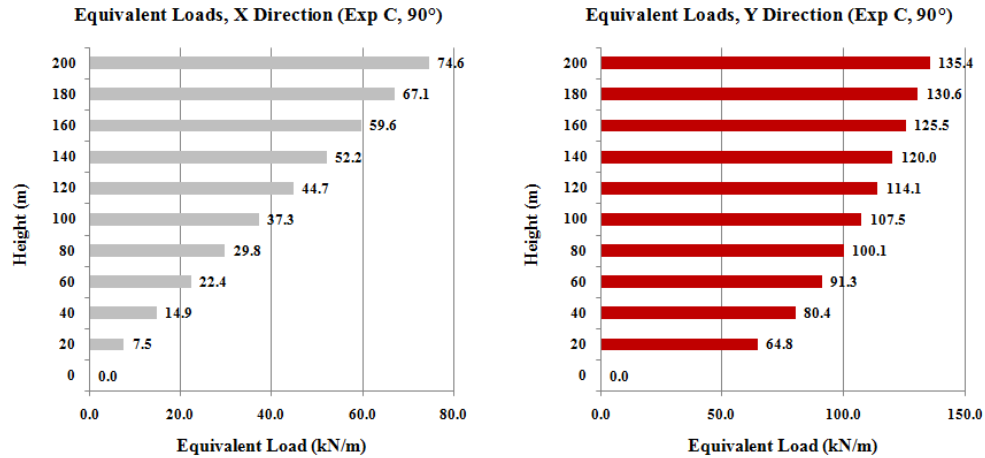
**Figure 4.20 Equivalent loads for exposure C and 90° angle of attack**

In Figures 4.13 to 4.20, equivalent load for every 20 meters of height is presented discretely. Equivalent loads in x direction depend mainly on the mean moment especially for the angles where vortex shedding is not effective in x direction. No significant change in the shapes of the distributions of loads is visualized. The magnitudes of the equivalent loads are directly related with the base bending moments.

*Determination of Top Accelerations*

Calculations are made by using one-hour averaging time, 10 year return period design wind speed (Serviceability design). In order to determine the top accelerations, Equation (2.67) in Chapter 2 is used with a linear mode shape and constant mass per unit height assumptions. In Table top-1, the resultant top accelerations and the resonant component of base moments determined according to serviceability design requirements which are necessary for calculation of top accelerations are given. Moments are in $10^6$ kN.m and accelerations are in mg.

**Table 4.5 Top Accelerations – Serviciability Design**

| Test | X Direction | | Y Direction | |
|------|-------------|-------------|-------------|-------------|
| | $\widehat{M}_R$ | $\widehat{\widehat{Y}}$ | $\widehat{M}_R$ | $\widehat{\widehat{Y}}$ |
| **B-0°** | 0.298 | 1.892 | 0.396 | 2.523 |
| **C-0°** | 0.405 | 2.580 | 0.695 | 4.428 |
| **C-15°** | 0.320 | 2.039 | 0.523 | 3.332 |
| **C-30°** | 0.109 | 0.694 | 0.359 | 2.287 |
| **C-45°** | 0.200 | 1.274 | 0.287 | 1.828 |
| **C-60°** | 0.262 | 1.669 | 0.305 | 1.943 |
| **C-75°** | 0.130 | 0.828 | 0.256 | 1.631 |
| **C-90°** | 0.545 | 3.472 | 0.189 | 1.204 |

In Table 4.5, it is observed that maximum top acceleration occurs in Exposure C and for 0° angle of attack in Y direction which is meaningful since low turbulence intensity magnifies the effect of vortex shedding; increasing D/B ratio results in smaller resonant response; and in across wind (y direction) main reason of response is the resonant components. The maximum top acceleration is calculated as 4.428 mg which corresponds to approximately 0.043 m/s$^2$. In the table of human perception levels Table 1.1 in Chapter 1, it is in level 1 which means that people cannot perceive motion. In order to visualize the change in the top acceleration according to the exposure categories and the angles of attack, Figure 4.21 and Figure 4.22 are prepared. In Figure 4.21, it is seen that top acceleration decreases rapidly as D/B ratio increases especially in y direction. For example, when the angle is 45°, top acceleration in across wind direction is scaled down to approximately 27% of one in 0°. It is also observed in 90° of angle of attack that maximum top acceleration is in x direction which is the across wind direction when the wind flow is along y drection and since the main cause of the top acceleration is the resonant component of response, it is greater in the across wind direction due to vortex sheeding effects. Similarly, in Figure 4.22, top

acceleration in across wind direction in more turbulent exposure category B is around 50% of one in Exposure C.
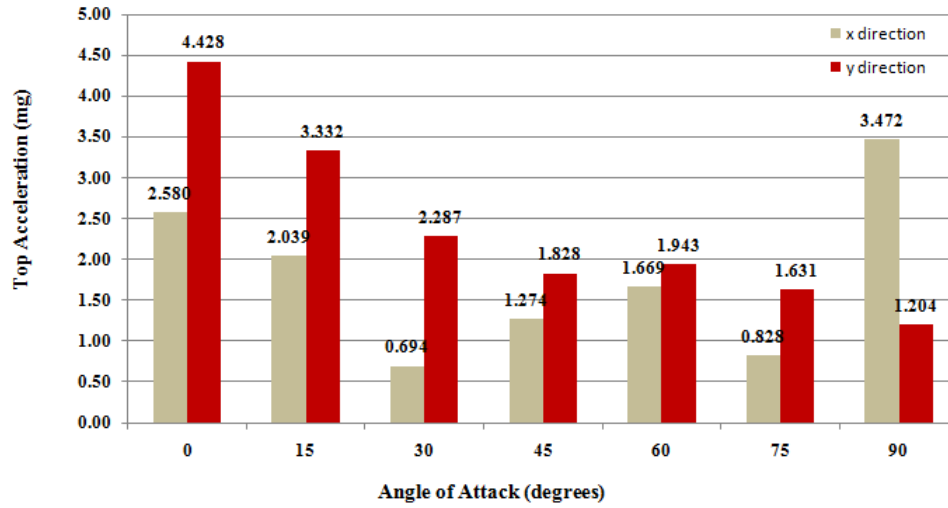


**Figure 4.21 Top accelerations for different angles of attack**
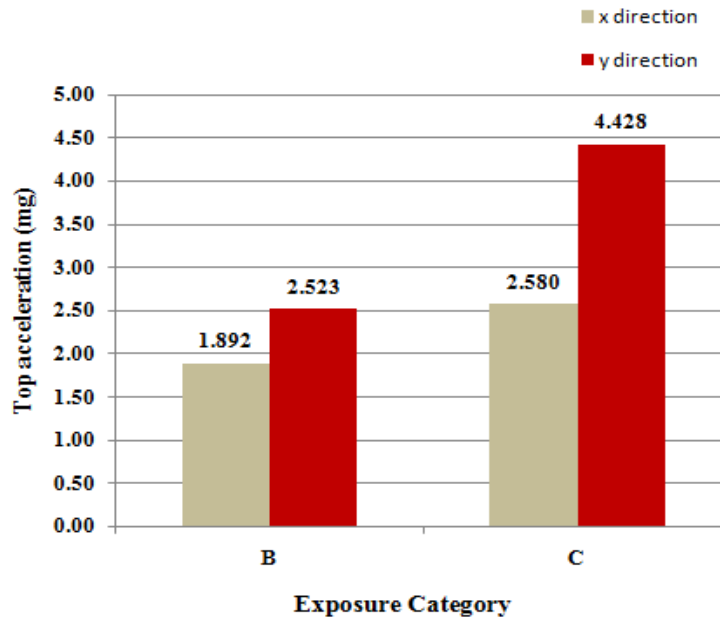


**Figure 4.22 Top accelerations for different exposure categories**

# CHAPTER 5

# COMPARISON OF TECHNICAL SPECIFICATIONS

## 5.1 INTRODUCTION

This chapter is devoted to the determination of wind induced response of buildings using technical specifications ASCE 7-05 (ASCE 7-05, 2005), Eurocode 1 (Eurocode 1, 2005), İstanbul Yüksek Binalar Rüzgar Yönetmeliği (İYBRY) (İYBRY, 2009) and Aerodynamic Loads Database, NatHaz (Kareem, et al., 2000). The conclusions obtained from these standards are compared with the corresponding results of Ankara Wind Tunnel case study. The calculations are performed specifically for the open environment exposure conditions defined accordingly in each of the standards.
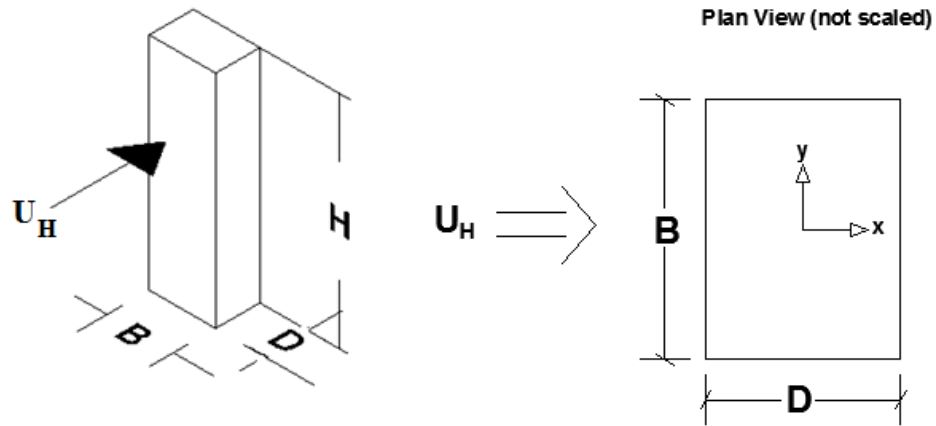


**Figure 5.1 Geometrical properties of the building**

In Figure 5.1, geometrical properties of the building under consideration are given. The along-wind direction is called 'x direction' and the across wind one is 'y direction'. Some assumptions are made regarding the physical properties of the problem. The parameters and coefficients utilized in the calculations are as follows:

- Plan dimension of the building perpendicular to wind, B: 80 m.
- Plan dimension of the building parallel to wind, D: 60 m.
- Height of the building, H: 200 m.
- Fundamental frequency in x direction, $f_{1x}$ : 0.386 Hertz
- Fundamental frequency in y direction, $f_{1y}$: 0.200 Hertz
- Linear mode shape is assumed for both of the lateral directions; $\phi(z) = \frac{z}{H}$
- Building bulk density, $\rho_b$: 250 kg/m$^3$
- Structural damping ratio, $\xi$: 0.02
- Drag coefficient, $C_D$: 1.3
- Air density, $\rho$: 1.25 kg/m$^3$

## 5.2 DETERMINATION OF RESPONSE USING ASCE 7-05

ASCE 7-05 is a technical specification which is published by American Society of Civil Engineers. Exposure category that defines open terrain is exposure C. By using this specification, along-wind response components of the building that involve maximum top acceleration, equivalent static loads and maximum base moment can be calculated. ASCE 7-05 obliges making wind tunnel test for buildings taller than 200 m.

*Wind Profile*

Definition of wind profile related with exposure C is given in Equation (5.1) and the shape is presented in Figure 5.2.

$$V(z) = b * \left(\frac{z}{10}\right)^{\alpha} * V_b \quad \text{(m/sec)} \tag{5.1}$$

In Equation (5.1), b and α are unitless constants which are related with the exposure category and listed in Table 6.2 in the code; $V_b$ is basic wind speed with 3 sec gust at 10 meters above ground in meters/second

d; z is the height given in meters. $V_b$ is taken as 40 m/sec. b and α are 0.65 and 1/6.5 respectively. Thus, Equation (5.1) can be rewritten as;

$$V(z) = 0.65 * \left(\frac{z}{10}\right)^{1/6.5} * 40 = 26 * \left(\frac{z}{10}\right)^{1/6.5} \tag{5.2}$$
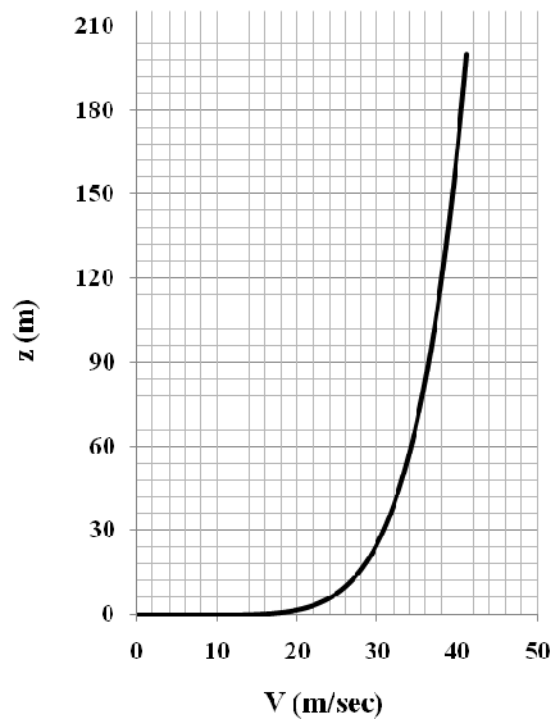


**Figure 5.2 Wind profile definition of ASCE 7-05 for exposure C (ASCE 7-05, 2005)**

*Turbulence Intensity*

Turbulence intensity, $I(z)$ and integral length scale of turbulence, L(z) are defined according to the exposure category as in Equations (5.3) and (5.4) below. There, c and ε are unitless parameters which are related with the exposure category. For exposure C, c is 0.2

85

and $\varepsilon$ is 1/5. $l$ is a parameter of the exposure category but not unitless this time and it is given as 152.4 m.

$$I(z) = c \left(\frac{10}{z}\right)^{1/6} \tag{5.3}$$

$$L(z) = l \left(\frac{z}{10}\right)^{\varepsilon} \tag{5.4}$$
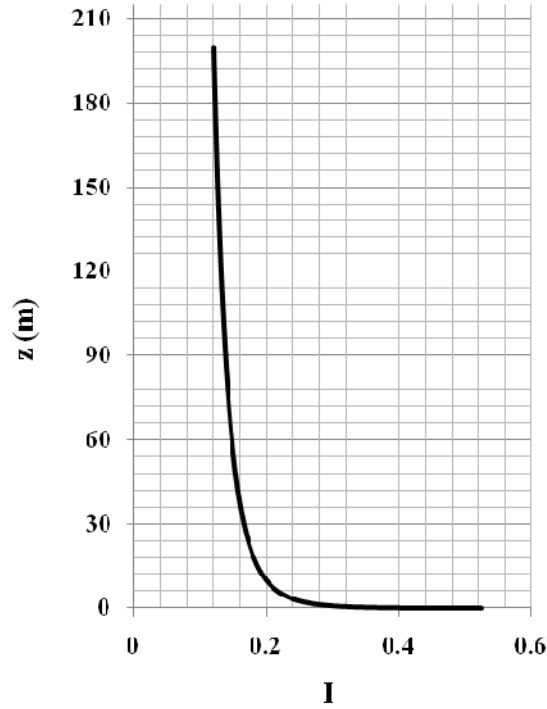


**Figure 5.3 Turbulence intensity definition of ASCE 7-05 for exposure C (ASCE 7-05, 2005)**

*Equivalent static loads in along-wind direction*

In order to determine equivalent static wind loads in along wind direction, Section 6.5.12.2.3 that is given for enclosed and partially enclosed flexible buildings is used. Equation (6-19) given in the code is rewritten in Equation (5.5) below.

$$p = q G_f C_p - q_i \left(G C_{pi}\right) \text{ (lb/ft}^2) \tag{5.5}$$

86

In Equation (5.5), $G_f$ is the gust effect factor defined in Equation (6-8) in the code and Equation (5.6) here; $GC_{pi}$ is internal pressure coefficient; q and $q_i$ are used to designate external and internal velocity pressures respectively. Since the building that is studied is enclosed building, no internal pressure will occur, i.e. $q_i$ is taken as equal to 0. To sum up, equivalent static load is defined as the velocity pressure times a factor, $G_f C_p$. $G_f$ is the same for all but $C_p$ changes according to the orientation of the wall of the building according to wind. (Figure 6.6 in ASCE 7-05) Since L/B is 0.75 (60/80), $C_p$ constants for sidewall, windward and leeward walls can be listed as;

- $C_{p,side} = 0.7$;
- $C_{p,wind} = 0.8$;
- $C_{p,leeward} = 0.5$.

$$G_f = 0.925 \left( \frac{1+1.7I(\bar{z})\sqrt{g_Q^2 Q^2 + g_R^2 R^2}}{1+1.7g_v I(\bar{z})} \right) \tag{5.6}$$

In Equation (5.6), $I(\bar{z})$ term is the turbulence intensity at height $\bar{z}$ where $\bar{z}$ is the equivalent height of the structure and it is defined as 0.6*H; $g_Q$ and $g_v$ are factors that are suggested as 3.4; $g_R$ can be calculated by utilizing Equation (5.7); and Q and R can be determined by using Equations (5.8) and (5.9) respectively.

$$g_R = \sqrt{2\ln(3600n_1)} + \frac{0.577}{\sqrt{2\ln(3600n_1)}} \tag{5.7}$$

In Equation (5.7), $n_1$ is the fundamental frequency of the building which corresponds to the definition of $f_{1x}$ in the beginning of the chapter. Hence, $n_1 = 0.386$ Hertz and $g_R = 3.956$ accordingly.

$$Q = \sqrt{\frac{1}{1+0.63\left(\frac{B+H}{L(\bar{z})}\right)^{0.63}}} \tag{5.8}$$

In Equation (7), B and H are the dimensions of the building. (Figure 5.1); $L(\bar{z})$ is the integral length scale at the equivalent height of the structure. Since H is 200 m, equivalent height, $\bar{z}$ is 0.6*200 that gives 120 m. From Equation (5.4), L(120 m) is equal to 250.501 m. As a result, Q is 0.772.

$$R = \sqrt{\frac{1}{\beta} R_n R_H R_B (0.53 + 0.47R_L)} \tag{5.9}$$

$$R_n = \frac{7.47N_1}{(1+10.3N_1)^{5/3}} \tag{5.10}$$

$$N_1 = \frac{n_1 L(\bar{z})}{V(\bar{z})} \tag{5.11}$$

$$R_l = \frac{1}{\eta} - \frac{1}{2\eta^3}(1 - e^{-2\eta}) \quad for \ \eta > 0 \tag{5.12}$$

where the subscript $l$ in Equation (5.12) shall be taken as H, B, L respectively such that for

- $R_l = R_H; \eta = \frac{4.6n_1 H}{V(\bar{z})}$

- $R_l = R_B; \eta = \frac{4.6n_1 B}{V(\bar{z})}$

- $R_l = R_L; \eta = \frac{15.4n_1 L}{V(\bar{z})}$

In the above equations, $V(\bar{z})$ is the wind speed at the reference height of 0.6H (120 m). In Equation (5.2), z is taken as 120 m and thus $V(\bar{z})$ is calculated as 38.107 m/sec. Therefore, $N_1$ is calculated as 2.535 and hence $R_n$ is 0.077. Since the dimensions of the building (H, B and L) are 200 m, 80 m and 60 m respectively, $R_H$, $R_B$ and $R_L$ becomes 0.102, 0.232 and 0.101 which are put in Equation (5.9) together with the damping coefficient $\beta$ (0.02), and R is determined to be 0.23.

As a result, by putting the relevant parameters in their places in Equation (5.6), gust effect factor ($G_f$) is calculated to be 0.861. The only unknown remained for determination of equivalent loads is the velocity pressure, q which is defined in ASCE 7-05 in Equation (6-15) as in Equation (5.13) below;

$$q(z) = 0.00256 * K_z * K_{zt} * K_d * V_b{}^2 * I \tag{5.13}$$

In Equation (5.13), $K_z$ is the velocity pressure exposure coefficient and can be determined by using the expressions given in Equations (5.14) and (5.15) here and Table 6-3 in the standard. In this expression, $z_g$ is height of the atmospheric boundary layer and defined according to the exposure categories in Table (6-2) in ASCE 7-05. For exposure C, it is stated as 900 ft (274.32 m).

$$K_z = 2.01(z/z_g)^{2/\alpha} \ for \ 15ft \le z \le z_g \tag{5.14}$$

$$K_z = 2.01(15/z_g)^{2/\alpha} \ for \ z < 15ft \tag{5.15}$$

$K_{zt}$ is topographic factor and defined in part 6.5.7.2 in the standard. It is assumed to be 1. $K_d$ is wind directionality factor and can be selected from Table 6.4. However, it is stated that the directionality factor should only be considered in the analysis where load combinations are used. In this study, wind load effects are analyzed without the load combinations. Therefore, $K_d$ is taken as 1. I is importance factor and shall be determined from Table 6-1 based on building and structure categories. For occupancy category II in Table 1-1, corresponding I is 1. As a result, velocity pressure calculated using Equation (5.13) at roof height; H ($q_H$) is 38.545 lb/ft$^2$ (1846 Pa).

In Figure 6.6 in the code, it is stated that external pressures on side walls and leeward wall should have a constant profile proportional to $q_H$ whereas external pressure on windward wall has a parabolic profile proportional to q(z). As a result, Equation (5.5) is applied to windward wall, leeward wall and sidewalls for which corresponding equivalent load profiles are presented in Figure 5.4 below.
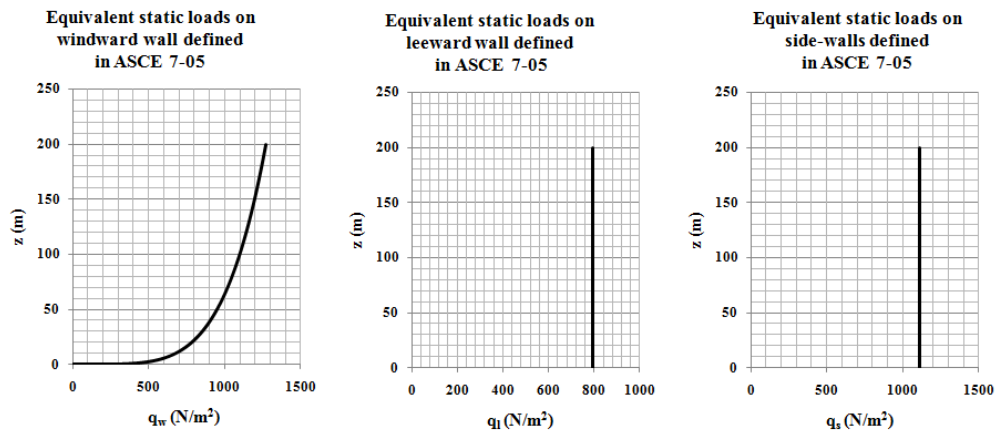


**Figure 5.4 Equivalent static loads on windward, leeward and side walls defined in ASCE 7-05**

*Calculation of mean base bending moment in the along-wind direction*

In order to determine the mean base bending moment in the along wind direction, base moments determined from the application of the equivalent static loads on the windward and leeward walls are superposed. The relevant expression is given in Equation (5.16).

$$M_{along} = \int_0^H B * q_w(z) * z\,dz + \int_0^H B * q_l(z) * z\,dz \qquad (5.16)$$

From Equation (5.16), mean base bending moment in the along-wind direction is calculated as **$3.112*10^6$ kNm**.

### Calculation of maximum along wind acceleration

The maximum along wind acceleration as a function of height above the ground surface is given by equation (C6-13) in the standard and Equation (5.17) here in which $\ddot{X}_{max}(z)$ is maximum acceleration; $g_{\ddot{x}}$ is a factor that is defined in Equation (5.18); $\sigma_{\ddot{x}}(z)$ is root mean square along wind acceleration which is given in Equation (5.19).

$$\ddot{X}_{max}(z) = g_{\ddot{x}} * \sigma_{\ddot{x}}(z) \qquad (5.17)$$

$$g_{\ddot{x}} = \sqrt{2\ln(n_1 T)} + \frac{0.5772}{\sqrt{2\ln(n_1 T)}} \qquad (5.18)$$

In Equation (5.18), $n_1$ is fundamental frequency of the building that is 0.386 Hertz; and T is the length of time over which the maximum acceleration is computed, taken as 3600 seconds to represent 1 hour. Hence, $g_{\ddot{x}}$ is calculated to be 3.956.

$$\sigma_{\ddot{x}}(z) = \frac{0.85\phi(z)\rho BHC_{fx}V(\bar{z})^2}{m_1}I(\bar{z})KR \qquad (5.19)$$

In Equation (5.19), $\phi(z)$ is the fundamental mode shape which is assumed as linear ($\phi(z)=z/H$); $\rho$ is the air density (1.25 kg/m$^3$); B and H are dimensions of the building which are 80 m and 200 m respectively; $C_{fx}$ is drag coefficient that is assumed to be 1.3; $m_1$ is modal mass that is calculated using Equation (5.20); $V(\bar{z})$ and $I(\bar{z})$ are wind speed and turbulence intensity at reference height, $\bar{z}$ respectively; K is a dimensionless coefficient that is expressed in Equation (5.21); R is the resonant response factor determined using Equation (5.9).

$$m_1 = \int_0^H \mu(z)\phi_1(z)^2\,dz \qquad (5.20)$$

In Equation (5.20), $\mu(z)$ is mass per unit height which is assumed to be constant in $\rho_b*B*D$ in amount. Since $\rho_b$ is assumed to be 250 kg/m$^3$, $\mu(z)$ is calculated as $1.2*10^6$ kg/m.

$$K = \frac{1.65^\alpha}{\alpha+\xi+1} \qquad (5.21)$$

In Equation (5.21), $\alpha$ is the exponent parameter of the wind profile expression and it is 1/6.5 for exposure C. $\xi$ is the mode shape exponent so it is taken as 1 due to linear mode shape assumption. As a result, K is calculated to be 0.501.

When Equation (5.19) is written for z=H, $\sigma_{\ddot{x}}$ is calculated as 0.0061 m/sec² which is multiplied by 3.956 to determine maximum along wind acceleration as 0.024 m/sec². If maximum acceleration is normalized by gravitational acceleration that is 9.81 m/sec², it is determined to be 0.002433 g that is **2.433 mg**.

## 5.3   DETERMINATION OF RESPONSE USING EUROCODE 1

Eurocode 1 is a European standard specifically for actions on structures and part 1-4 is particularly about wind actions on structures. Exposure category that defines most approximately the open terrain is category II. By using this specification, along-wind response components of the building that involve maximum top acceleration, equivalent static loads and maximum base moment can be calculated. Like ASCE 7-05, Eurocode 1 obliges making wind tunnel test for buildings taller than 200 m as well.

### *Wind Profile*

Wind profile definition is expressed in Equation (4.3) in the standard as in Equation (5.22) below and it is presented in Figure 5.5. In Equation (5.22), $C_r(z)$ is the terrain roughness and can be determined as in Equations (5.24) and (5.25); $C_0(z)$ is the orography factor that expresses the effects of hills, cliffs, etc and recommended to be taken as 1 unless a special analysis is required; and $V_b$ is the basic wind velocity that is expressed in Equation (5.23).

$$V_m(z) = C_r(z) * C_o(z) * V_b \tag{5.22}$$

$$V_b = C_{dir} * C_{season} * V_{b,0} \tag{5.23}$$

In Equation (5.23), $C_{dir}$ and $C_{season}$ are directional factor and season factor respectively and they are recommended to be takes as 1 unless a different recommendation exists in National Annex. $V_{b,0}$ is fundamental value of basic wind velocity at 10 m above ground for 1 hour

gust. In the previous calculations, basic wind speed was taken as 40 m/sec for 3 sec gust; it is multiplied by 1.05/1.52 to be converted into hourly gust speed using Figure C6-4 in ASCE 7-05 (ASCE 7-05, 2005). Therefore, $V_{b,0}$ is calculated as 27.632 m/sec.

$$C_r(z) = k_r * \ln\left(\frac{z}{z_0}\right) for\ z_{min} \le z \le z_{max} \tag{5.24}$$

$$C_r(z) = k_r * \ln\left(\frac{z_{min}}{z_0}\right) for\ z \le z_{min} \tag{5.25}$$

In Equations (5.24) and (5.25), $z_0$ is the roughness length defined according to the terrain category (For category II it is given to be 0.05 in Table 4.1); $z_{min}$ is the minimum height defined in Table 4.1 in the code (For category II, it is 2 m); $z_{max}$ is stated to be taken as 200 m; $k_r$ terrain factor that depends on $z_0$ as in Equation (5.26) below in which $z_{0,II}$ is the roughness length of terrain category II. Since the category under consideration is II, $k_r$ becomes 0.19.

$$k_r = 0.19 * \left(\frac{z_0}{z_{0,II}}\right)^{0.07} \tag{5.26}$$

As a result, Equation (5.22) can be rewritten as;

$$V_m(z) = 0.19 * \ln\left(\frac{z}{0.05}\right) * 27.632\ for\ 2 \le z \le 200 \tag{5.27}$$

$$V_m(z) = 0.19 * \ln\left(\frac{2}{0.05}\right) * 27.632\ for\ z \le 2 \tag{5.28}$$
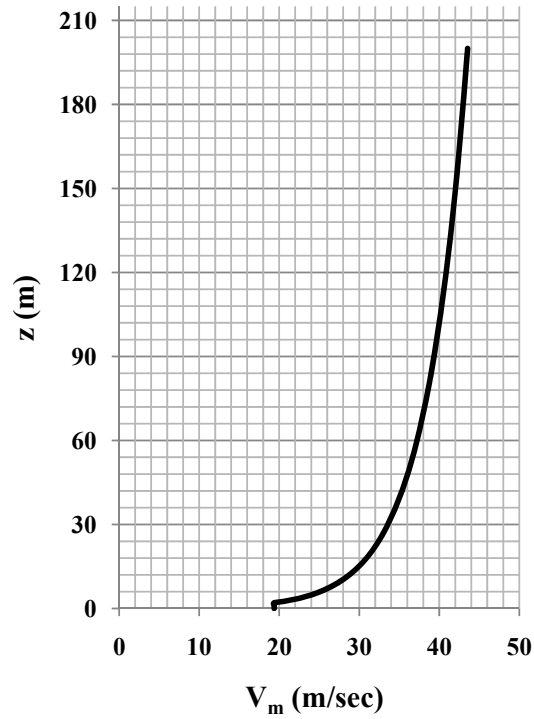
**Figure 5.5 Wind profile definition of Eurocode 1 for terrain II (Eurocode 1, 2005)**

*Turbulence Intensity*

Turbulence intensity, $I_v(z)$ at height z is defined in part 4.4 in the standard and its expression is given in Equations (5.29) and (5.30) here. There, $\sigma_v$ is standard deviation of turbulent component of wind velocity. It can be determined using Equation (5.31) where $k_t$ is turbulence factor. It is recommended to use $k_t$ equal to 1 unless otherwise stated in National Annex. Shape of the turbulence intensity for terrain category II is presented in Figure 5.6.

$$I_v(z) = \frac{\sigma_v}{V_m(z)} \; for \; z_{min} \leq z \leq z_{max} \tag{5.29}$$

$$I_v(z) = \frac{\sigma_v}{V_m(z_{min})} \; for \; z \leq z_{min} \tag{5.30}$$

$$\sigma_v = k_r * V_b * k_t \tag{5.31}$$
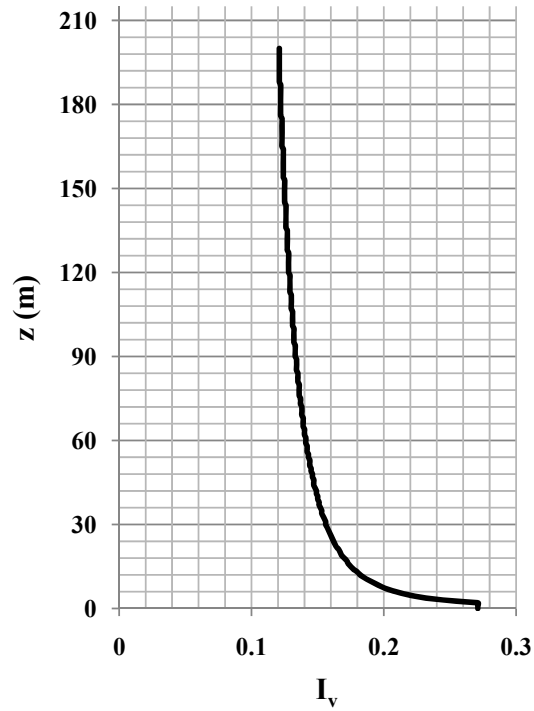
**Figure 5.6 Turbulence intensity definition of Eurocode 1 for terrain II (Eurocode 1, 2005)**

*Equivalent static loads in along-wind direction*

Determination of the equivalent static loads depends on the peak velocity pressure, $q_p$ which is defined in part 4.5 in the standard and given in Equation (5.32) here.

$$q_p(z) = [1 + 7I_v(z)] * \frac{1}{2}\rho V_m^2(z) \qquad (5.32)$$

In Equation (5.32), $\rho$ is the density of air which is taken as 1.25 kg/m$^3$. Change of peak velocity pressure with height is presented in Figure 5.7.
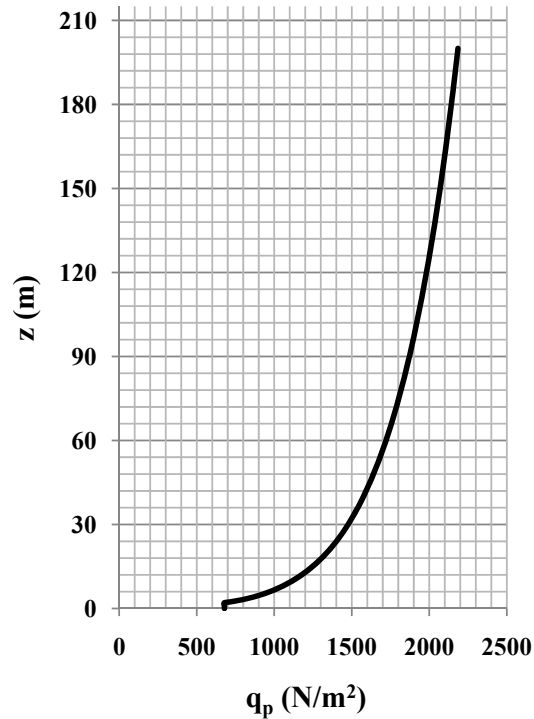
**Figure 5.7 Definition of peak velocity pressure in Eurocode 1**

Wind pressure on surfaces is defined as in Equation (5.33) utilizing only the external pressure. In Equation (5.33), $C_p$ is external pressure coefficient and can be determined according to the geometrical properties of the building.

$$w(z) = q_p(z) * C_p \tag{5.33}$$

Using Table 7.1 in the standard for H/D ratio of 200/60 (3.33), $C_p$ constants for windward and leeward walls can be listed as;

- $C_{p,wind} = 0.800$;
- $C_{p,leeward} = 0.617$.

Wind force, $F_w$ acting on a structure or structural component is determined using the expression (5.3) in the standard and it is given in Equation (5.34) here. In this equation, $C_f$ stands for force coefficient for the structure, i.e. $C_{p,wind}$ and $C_{p,leeward}$ as discussed above. $q_p(z_e)$ is the peak velocity pressure at height, $z_e$. The shape of the wind force should be

such that reference height $z_e$ should be taken equal to B when z is less than B; and it is equal to H for z greater than H-B; in between, it is directly equal to height, z. This is expressed in Figure 7.4 in the code. Remaining term $C_s C_d$ is the structural factor which is explained in Section 6 in the standard.

$$F_w = C_s C_d * C_f * q_p(z_e) * A_{ref}$$ (5.34)

$$C_s C_d = \frac{1 + 2k_p I_v(z_e)\sqrt{B^2 + R^2}}{1 + 7 I_v(z_e)}$$ (5.35)

In Equation (5.35), $z_e$ is taken as 0.6*H that is equal to 120 m and hence $I_v(z_e)$ is the turbulence intensity at 120 m, that is 0.128; $k_p$ is the peak factor defined as the ratio of the maximum value of response to its standard deviation; $B^2$ and $R^2$ are background and resonance response factor, respectively; $A_{ref}$ is reference area which is B*H in along wind direction. For determination of $k_p$, $B^2$ and $R^2$, the following concepts shall be introduced.

*Turbulence length scale, L(z):*

The turbulence length scale is computed with the following equations:

$$L(z) = L_t * \left(\frac{z}{z_t}\right)^\alpha \ for \ z \geq z_{min}$$ (5.36)

$$L(z) = L(z_{min}) \ for \ z < z_{min}$$ (5.37)

In Equations (5.36) and (5.37), $L_t$ is a reference length scale and taken as 300 m; $z_t$ is a reference height which is 200 m; $\alpha = 0.67 + 0.05*\ln(z_0)$ where $z_0$ is 0.05 and so α is calculated as 0.52. Recall that $z_{min}$ is 2 m for terrain II.

*Non-dimensional power spectral density function, $S_L(z,n)$:*

$$S_L(z, n) = \frac{6.8 f_L(z,n)}{(1 + 10.2 f_L(z,n))^{5/3}}$$ (5.38)

$$f_L(z, n) = \frac{n * L(z)}{V_m(z)}$$ (5.39)

In Equation (5.38), $f_L(z,n)$ is a non-dimensional frequency that is determined by using Equation (5.39) where n is the fundamental frequency of the structure (0.386 Hertz). $S_L$ vs $f_L$ graph is presented in Figure 5.8.
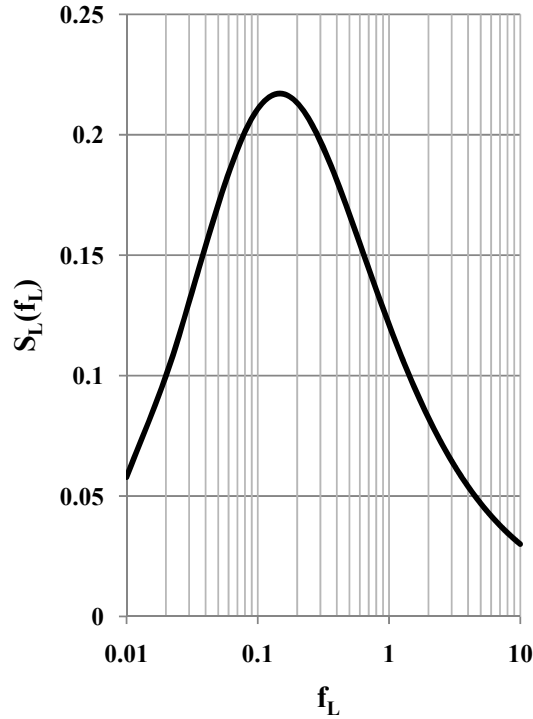


**Figure 5.8 Power spectral density function, $S_L(f_L)$ defined in Eurocode 1**

In Figure 5.8, the power spectral density function of wind speed is presented. It shows the distribution of wind speed over frequencies. It should not be confused with the power spectral density functions and the normalized spectra formed in Chapter 4 because they are created for the response of the building (base bending moments); however, the power spectral density function in Figure 5.8 is given for wind speed itself, not the response.

*Background Response Factor, $B^2$:*

$$B^2 = \frac{1}{1+0.9\left[\frac{B+H}{L(z_e)}\right]^{0.63}}$$

(5.40)

In Equation (5.40), B and H are 80 m and 200 m respectively; $L(z_e)$ is the turbulence length scale at the reference height of 120 m which is calculated as 229.992 m using Equations (5.36) and (5.37). As a result, $B^2$ is determined to be 0.495.

*Resonant Response Factor, $R^2$:*

$$R^2 = \frac{\pi^2}{2\delta} * S_L(z_e, f_{1,x}) * R_h(\eta_h) * R_b(\eta_b)$$ (5.41)

In Equation (5.41), $\delta$ is total logarithmic decrement of damping that can be calculated using Equation (5.44); $S_L(z_e, f_{1,x})$ is non-dimensional power spectral density function that is evaluated at the reference height and the fundamental frequency i.e. $S_L(120, 0.386)$ is calculated as 0.079; $R_h(\eta_h)$ and $R_b(\eta_b)$ are aerodynamic admittance functions that are expressed in Equations (5.42) and (5.43).

$$R_h(\eta_h) = \frac{1}{\eta_h} - \frac{1}{2\eta_h^2}(1 - e^{-2\eta_h}); \ R_h = 1 \ for \ \eta_h = 0$$ (5.42)

$$R_b(\eta_b) = \frac{1}{\eta_b} - \frac{1}{2\eta_b^2}(1 - e^{-2\eta_b}); \ R_b = 1 \ for \ \eta_b = 0$$ (5.43)

where; $\eta_h = \frac{4.6H}{L(z_e)} f_L(z_e, f_{1,x})$ and $\eta_b = \frac{4.6B}{L(z_e)} f_L(z_e, f_{1,x})$

The parameters $\eta_h$ and $\eta_b$ are calculated as 8.691 and 3.476 respectively; and when they are put in Equations (5.42) and (5.43), $R_h(\eta_h)$ is determined to be 0.108 and $R_b(\eta_b)$ to be 0.246.

$$\delta = \delta_s + \delta_a + \delta_d$$ (5.44)

where $\delta_s$ is the logarithmic decrement of structural damping (assumed to be 2%); $\delta_a$ is the logarithmic decrement of aerodynamic damping for the fundamental mode that can be determined through Equation (5.45); $\delta_d$ is logarithmic decrement of damping due to special devices. In this case study, special devices are not utilizes for damping thus $\delta_d$ is neglected.

$$\delta_a = \frac{C_f * \rho * V_m(z_e) * B}{2 * f_{1,x} * \mu_e}$$ (5.45)

In Equation (5.45), $C_f$ is force coefficient which is equal to $C_{fo} * \psi_r * \psi_\lambda$ as stated in Section 7 in the standard. $C_{fo}$ is determined from Figure 7.23 according to the D/B ratio of the

building and by linear interpolation $C_{fo}$ is calculated as 2.35. $\psi_r$ and $\psi_\lambda$ are reduction factor and end effect factor respectively. They are assumed to be 1 from the relevant figures of section 7. As a result, force coefficient is 2.35. $\mu_e$ in the above equation stands for equivalent mass per unit area which is accepted to be the bulk density of the building, $\rho_b$ times the parallel plan dimension, D, i.e. $\mu_e$ is equal to 250*60 which gives 15000 kg/m$^2$. When the parameters are put in place, Equation (38) can be rewritten as;

$$\delta_a = \frac{2.35*1.25*40.862*80}{2*0.386*15000} = 0.829$$

Then,

$$\delta = 0.02 + 0.829 = 0.849$$

When the parameters of Equation (5.41) are put in their places;

$$R^2 = \frac{\pi^2}{2*0.849} * 0.079 * 0.108 * 0.246 = 0.012$$

*Peak factor, $k_p$:*

$$k_p = \sqrt{2\ln(\nu T)} + \frac{0.6}{\sqrt{2\ln(\nu T)}} \tag{5.46}$$

In Equation (5.46), $\nu$ is the up-crossing frequency given in Equation (5.47); and T is the averaging time for the mean wind velocity, T=600 seconds is recommended.

$$\nu = f_{1,x}\sqrt{\frac{R^2}{B^2+R^2}}; \quad \nu \geq 0.08 \, Hz \tag{5.47}$$

Since $f_{1,x}$ is 0.386; and $R^2$ and $B^2$ are 0.012 and 0.495 respectively, $\nu$ is calculated to be 0.08 Hertz. Therefore, $k_p$ is 3.

As a result, Equation (5.35) can be rewritten as;

$$C_sC_d = \frac{1 + 2*3*0.128*\sqrt{0.495+0.012}}{1+7*0.128} = 0.816$$

When Equation (5.34) is applied both for the windward and leeward walls, wind force, $F_w$ is obtained. Equivalent wind force profiles along the height of the structure for both of these cases are drawn in Figure 5.9.
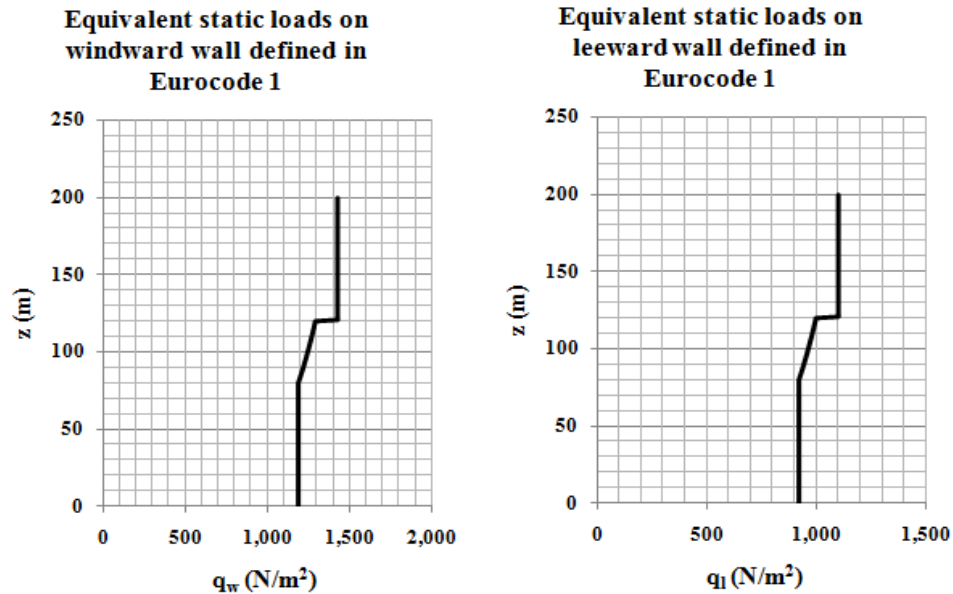


**Figure 5.9 Equivalent static loads on windward and leeward walls defined in Eurocode 1**

*Calculation of mean base bending moment in the along-wind direction*

Mean base bending moment is calculated using Equation (5.16) and the result is determined to be **$3.835*10^6$ kNm**.

*Calculation of maximum along wind acceleration*

Maximum along wind acceleration is defined in part C.4 as the product of the standard deviation of acceleration expressed in Equation (5.48) by the peak factor, $k_p$ calculated for an up crossing frequency, $\nu$ equal to the fundamental frequency of the building. For 0.386 Hertz of up crossing frequency, peak factor is calculated as 3.482.

$$\sigma_a = C_f * \rho * I_v(z_e) * V_m^2(z_e) * R * \frac{K_y * K_z * \phi(z)}{\mu_{ref} * \phi_{max}} \tag{5.48}$$

In Equation (5.48), $\sigma_a$ is the standard deviation of the acceleration; $C_f$ is the force coefficient as defined in the explanations of Equation (5.45), $C_f$ is calculated to be 2.35; $I_v(z_e)$ is the turbulence in reference height of 120 m that is 0.128; $V_m(z_e)$ is the wind speed at 120 m which is 40.862 m/sec; R is the square root of the resonant response, i.e. $\sqrt{0.012} = 0.11$; $\phi(z)$ is the mode shape which is assumed as linear so $\phi(z) = z/H$; $\phi_{max}$ is the mode shape value at the point with maximum amplitude that is equal to 1; $K_y$ and $K_z$ are constants given in C.2 (6) such that for linear mode shape, $K_y$ and $K_z$ are given as 1 and 3/2 respectively; $\mu_{ref}$ is reference mass per unit area which was calculated to be 15000 kg/m$^2$ after Equation (5.45). When these parameters are put in Equation (5.48), the standard deviation of acceleration at top of the building, in other words at z=H is calculated as 6.957*10$^{-3}$ m/s$^2$. Since peak factor is determined to be 3.482, maximum along wind acceleration is 3.482*6.957*10$^{-3}$ which is equal to 0.024 m/sec$^2$. When this is normalized by the gravitational acceleration of 9.81 m/sec$^2$, the resultant value is **2.469 mg**.

## 5.4 DETERMINATION OF RESPONSE USING İYBRY

İstanbul Yüksek Binalar Rüzgar Yönetmeliği (İYBRY) is a special guideline developed by Boğaziçi University, Kandilli Observatory in August 2008 for design of tall buildings under wind loads. Exposure category that defines most approximately the open terrain is category II. By using this specification, along-wind response components of the building that involve equivalent static loads and maximum base moment can be derived whereas there is no explicit procedure recommended for determination of maximum top acceleration.

*Wind Profile*

Chapter 3 is devoted to the wind profile and turbulence intensity definitions in the guideline. Wind profile expression is given in Equation (5.49) where $C_e(z)$ is surface roughness that depends on height; $C_t$ is topography constant and expressed in Equation (5.52); and $V_b$ is basic wind speed that is defined for 10 minute gust. Hence, 40 m/sec of design basic wind

speed for 3 sec gust is converted into 10 minute gust speed simply by multiplying it by 1.06/1.52 so $V_b$ is 27.895 m/sec.

$$V_m(z) = C_e(z) * C_t * V_b \tag{5.49}$$

$$C_e(z) = k_r * ln\left(\frac{z}{z_0}\right) \ for \ z > z_{min} \ ; \ k_r = 0.23 * (z_0)^{0.07} \tag{5.50}$$

$$C_e(z) = C_e(z_{min}) \ for \ z \le z_{min} \tag{5.51}$$

In Equations (5.50) and (5.51), $z_0$ is the surface roughness height and $z_{min}$ is the minimum height where surface roughness is constant. Both of them depend on the exposure category and listed in Table 3.1 in the guideline. Specifically for category II, $z_0$ is 0.05 m and $z_{min}$ is 2 m. Hence, $k_r$ is equal to 0.186.

$$C_t = 1.0 + 0.001\Delta \tag{5.52}$$

In this expression, $\Delta$ is the elevation of the place of the structure from sea level. $C_t$ is assumed to be 1 in this study. Resultant wind profile for category II is presented in Figure 5.10 below.
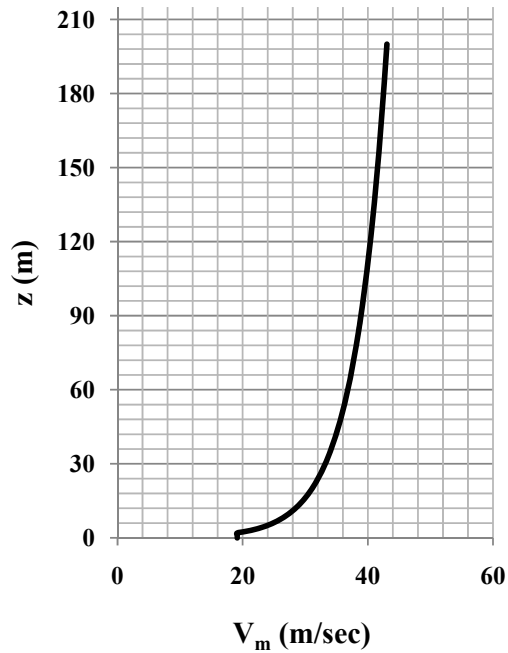


**Figure 5.10 Wind profile definition of İYBRY for terrain II (İYBRY, 2009)**

### Turbulence Intensity and Length:

Turbulence is defined in terms of intensity and length scale as in equations below. Then, plot of turbulence intensity is presented in Figure 5.11.

$$I_w(z) = \frac{\sigma_w}{V_m(z)} = \frac{k_r * V_b}{C_e(z) * V_b} = \frac{k_r}{C_e(z)} \tag{5.53}$$

$$L(z) = 300 \left(\frac{z}{200}\right)^\alpha \, for \, z \geq z_{min} \tag{5.54}$$

$$L(z) = L(z_{min}) \, for \, z \leq z_{min} \tag{5.55}$$

where $\alpha = 0.67 + 0.05\ln(z_0)$
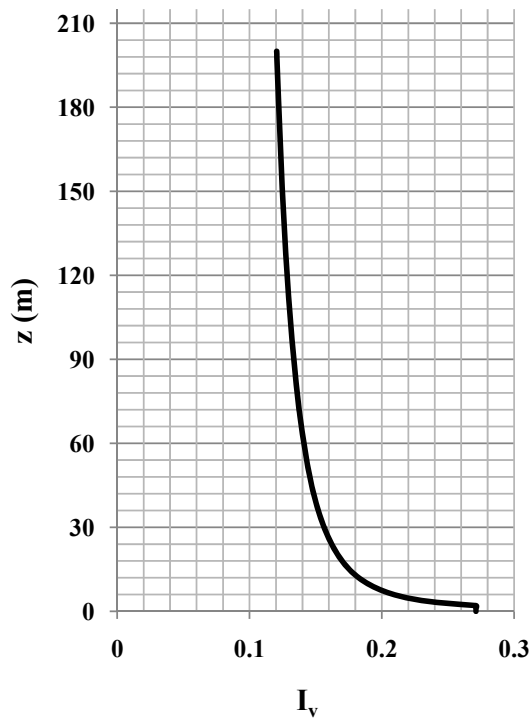


**Figure 5.11 Turbulence intensity definition of İYBRY for terrain II (İYBRY, 2009)**

*Equivalent static loads in along-wind direction*

Wind-induced forces acting on rectangular buildings are explained in part 5 in the guideline. Total force on the building, F is the summation of external force ($F_{ex}$), internal force ($F_{in}$) and frictional force ($F_{fr}$). However, in this study, no openings in the building are considered and main aim is to compare the external force definitions in different standards. Therefore, the expression for $F_{ex}$ will be studied in detail.

$$F_{ex} = C_s C_d \sum_{exposure\ area} q_p(z) C_{pe} A_{ex} \tag{5.56}$$

In Equation (5.56), $q_p(z_e)$ is maximum wind pressure at height, z; $C_{pe}$ is the pressure constant; $A_{ex}$ is exposure area that is equal to B*H; $C_s$ is correlation constant; and $C_d$ is dynamic resonance constant. $F_{ex}$ can be analyzed in two parts one of which is the windward wall and the other is the leeward wall. For each of them, different pressure constants are defined in Figure 4.2 in the guideline. For H/D ratio of 200/60 that is 3.33, on the windward 'D' and leeward 'E' sides, the pressure constants, $C_{p,wind}$ and $C_{p,leeward}$ are calculated as 0.8 and 0.617 respectively.

$$C_s = \frac{1 + 7 I_w(z_r)\sqrt{B^2}}{1 + 7 I_w(z_r)} \tag{5.57}$$

$$C_d = \frac{1 + 7 I_w(z_r)\sqrt{B^2 + R^2}}{1 + 7 I_w(z_r)\sqrt{B^2}} \tag{5.58}$$

In Equations (5.57) and (5.58), $I_w(z_r)$ is turbulence intensity at the reference height, $z_r$ which can be taken as 0.6*H that is 120 m. Using Equation (5.53), $I_w(120)$ is calculated as 0.128. $B^2$ and $R^2$ are background factor and resonant factor respectively. They are expressed in Equations (5.59) and (5.60) below where L($z_r$) is the turbulence length scale at reference height of 120 m. From Equations (5.54) and (5.55), L(120) is determined to be 229.992 m.

$$B^2 = \frac{1}{1 + 0.9\left[\frac{B+H}{L(z_r)}\right]^{0.63}} \tag{5.59}$$

When B=80 m, H=200 m and L($z_r$)=229.992 m are put in the relevant places in Equation (5.59), background factor, $B^2$ is calculated as 0.495.

$$R^2 = \frac{\pi^2}{2\delta} S_L(z_r, f_o) R_h(\eta_h) R_b(\eta_b) \tag{5.60}$$

In the expression of resonance factor, δ is logarithmic decrement; $S_L(z_r, f_o)$ is spectral density function evaluated at the reference height, $z_r$ and fundamental frequency of the building, $f_o$ (0.386 Hertz); $R_h(\eta_h)$ and $R_b(\eta_b)$ are aerodynamic admittance functions in vertical and horizontal directions, respectively.

$$\delta = \frac{2\pi\xi_o}{\sqrt{1-\xi_0^2}} \approx 2\pi\xi_0 \tag{5.61}$$

In Equation (5.61), $\xi_0$ is damping ratio that is 0.02. Thus, δ is calculated as 0.126.

$$S_L(z,f) = \frac{6.8 f_L(z,f)}{[1+10.2 f_L(z,f)]^{5/3}} \; ; \; f_L(z,f) = \frac{f L(z)}{V_m(z)} \tag{5.62}$$

Shape of the power spectral density function is the same as the definition in Eurocode 1. Hence, its plot can be observed in Figure 5.8. At the reference height and fundamental frequency, $f_L(120,0.386)$ is 2.193 and hence $S_L(120,0.386)$ is calculated as 0.078.

$$R_h(\eta_h) = \frac{1}{\eta_h} - \frac{1}{2\eta_h^2}(1 - e^{-2\eta_h}); \; R_h = 1 \; for \; \eta_h = 0 \tag{5.63}$$

$$R_b(\eta_b) = \frac{1}{\eta_b} - \frac{1}{2\eta_b^2}(1 - e^{-2\eta_b}); \; R_b = 1 \; for \; \eta_b = 0 \tag{5.64}$$

where; $\eta_h = \frac{4.6H}{L(z_e)} f_L(z_r, f_o)$ and $\eta_b = \frac{4.6B}{L(z_e)} f_L(z_r, f_o)$

When $f_L(120,0.386)$ which is equal to 2.193 is put in its place in Equations (5.63) and (5.64), $\eta_h$ is evaluated as 8.771; and $\eta_b$ is calculated to be 3.508. Hence, $R_h(\eta_h)$ and $R_b(\eta_b)$ are 0.108 and 0.244 respectively. As a result, Equation (5.60) can be rewritten as;

$$R^2 = \frac{\pi^2}{2 * 0.126} * 0.078 * 0.108 * 0.244 = 0.081$$

When results for the parameters are put in Equations (5.57) and (5.58), $C_s$ and $C_d$ are calculated as 0.86 and 1.03. Their product, $C_s C_d$ is 0.886.

Maximum wind pressure, $q_p(z)$ can be expressed as given in Equation (5.65) and when the relevant parameters are put in their places and Equation(5.56) is written for each windward wall and leeward wall taking $A_{ref}$ equal to B to determine the equivalent static loads per unit height, Figure 5.12 is obtained.

$$q_p(z) = C_q(z) * q_b \; where \; q_b = \frac{1}{2}\rho V_b^2; \; C_q(z) = C_e^2(z)C_t^2[1 + 7I_w(z)] \tag{5.65}$$
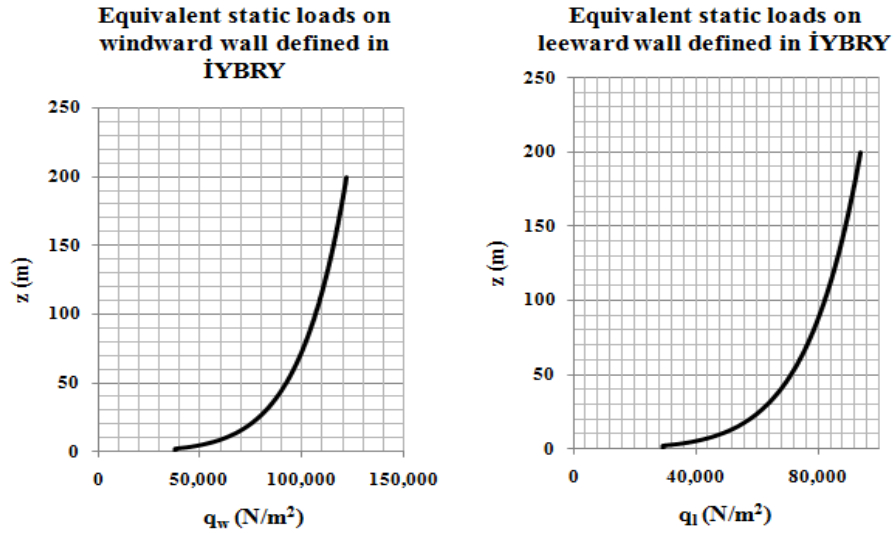
**Figure 5.12 Equivalent static loads on windward and leeward walls defined in İYBRY**

*Calculation of mean base bending moment in the along-wind direction*

Mean base bending moment is calculated using Equation (5.16) and the result is determined to be **$3.925*10^6$ kNm**.

## 5.5 DETERMINATION OF RESPONSE USING NATHAZ

NatHaz is an aerodynamic loads database that is available via internet (Kareem, et al., 2000). Wind tunnel tests performed on various building model geometries in different exposure categories are gathered to give an idea about the response of a similar building as a preliminary design work. Hence, it is a useful tool especially for the preliminary design of a tall building. First of all, shape of the building and the relevant exposure category is chosen. The aspect ratio of the building under consideration is 80x60x200. Since there is not a model in the database that exactly matches with these proportions, most similar one is chosen as 4x6x16. After the selection of relevant model, a property form appears as given in Figure 5.13.

You have selected Shape 03 with a Height 16" tested in Exposure C. These results are applicable to Buildings of this shape with Aspect ratio(B:D:H) of 6:4:16.

Note:

Since Torsional reduced frequency in the Serviceability design is beyond NatHaz Torsional data, the neareast spectrum value is used, instead. It may result in overestimation of Torsional-related accelerations.

**■ Input parameters by user**

| $B$ | 80 m | $D$ | 60 m | $H$ | 200 m |
|---|---|---|---|---|---|
| $f_x$ | 0.386 Hz | $f_y$ | 0.2 Hz | $f_z$ | 0.35 Hz |
| $\beta_1$ | 1.0 | $\beta_2$ | 1.0 | $\beta_3$ | 1.0 |
| $\rho_B$ | 192.082 kg/m³ | $\gamma$ | 18 m | $\zeta$ | 0.02 |
| $\Delta H$ | 5 m | $\rho_A$ | 1.25 kg/m³ | $C_D$ | 1.3 |
| $U_{10}$ | 40 m/s | Place | Continental US | File | w_force |
| Input | Metric(SI) unit | Output | Metric(SI) unit | On-line Unit Converter | |

**Figure 5.13 Screen for data input in NatHaz website**

When the program is analyzed, resultant data and graphs are given in Figures 5.14, 5.15, 5.16 and 5.17.



■ Non-dimensional PSD for alongwind, acrosswind and torsional ($C_M(f) = f \cdot S_M(f) / \sigma_M^2$)
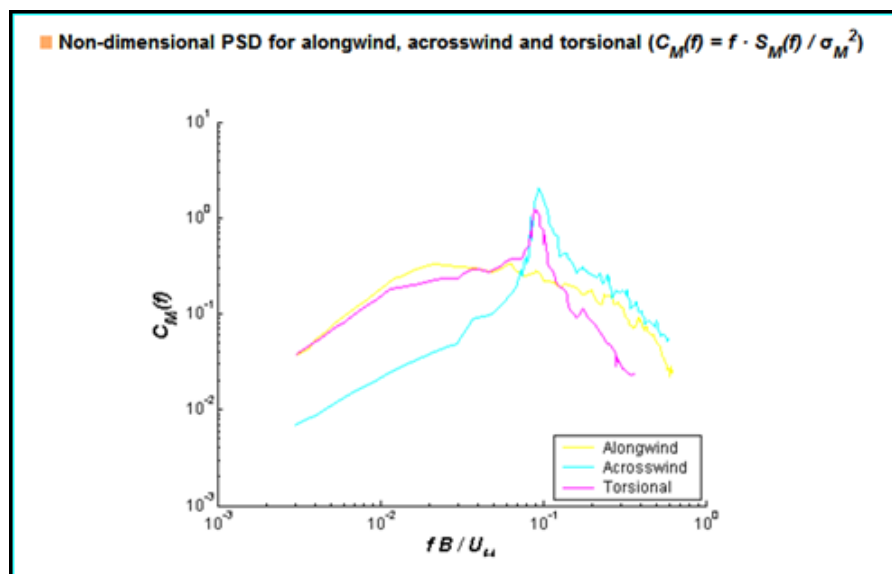
**Figure 5.14 Non-dimensional power spectral density functions for along wind, across wind and torsional directions**

107

| | Peak Accelerations at roof | |
|---|---|---|
| Alongwind | **5.20** *milli-g* | |
| Acrosswind | **12.89** *milli-g* | |
| Lateral Accelerations at Corner Induced by Torsion | **0.00238** *rad/s²* | Alongwind component : **9.69** *milli-g* |
| | | Acrosswind component : **7.27** *milli-g* |
| Total Lateral Accelerations at Corner | Alongwind component : **11.00** *milli-g* Acrosswind component : **14.80** *milli-g* | |

| | RMS Accelerations at roof | |
|---|---|---|
| Alongwind | **1.31** *milli-g* | |
| Acrosswind | **3.40** *milli-g* | |
| Lateral Accelerations at Corner Induced by Torsion | **0.000605** *rad/s²* | Alongwind component : **2.47** *milli-g* |
| | | Acrosswind component : **1.85** *milli-g* |
| Total Lateral Accelerations at Corner | Alongwind component : **2.79** *milli-g* Acrosswind component : **3.87** *milli-g* | |

**Figure 5.15 Serviceability design calculations (accelerations)**
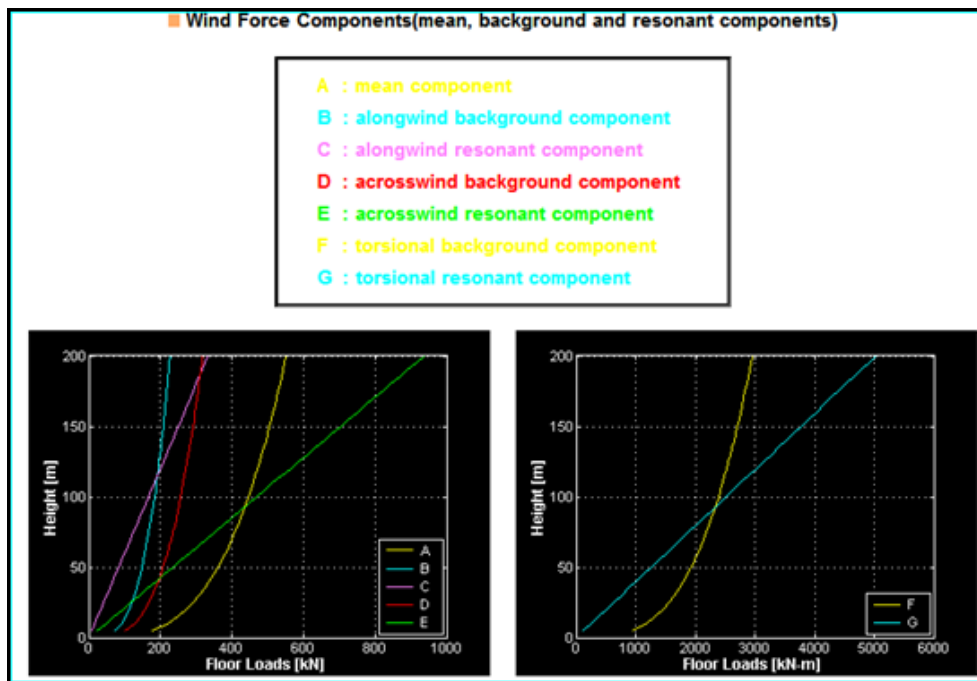


**Figure 5.16 Resultant wind force components**

■ 1-hour mean wind speeds for designs

Survivability design (50-year return period) : $U_H$ = 41.22 $m/s$

Serviceability design (10-year return period) : $U_H$ = 34.62 $m/s$

■ RMS base moment coefficients($\sigma_{CM}$), reduced frequencies($f_1 \cdot B / U_H$) and non-dimensional moment coefficients($C_M (f_1)$)

| | $\sigma_{CM}$ | $f_1 \cdot B / U_H$ | | $C_M (f_1)$ | |
|---|---|---|---|---|---|
| | | 50-year | 10-year | 50-year | 10-year |
| Alongwind | 0.068 | 0.749 | 0.892 | 0.024 | 0.024 |
| Acrosswind | 0.127 | 0.388 | 0.462 | 0.105 | 0.082 |
| Torsional | 0.026 | 0.679 | 0.809 | 0.024 | 0.024 |

■ Survivability Design (50-year wind) : Base moments

| | Base Moment ($10^6$ kN-m ) | | | |
|---|---|---|---|---|
| | $\bar{M}$ | $\hat{M}_B$ | $\hat{M}_R$ | $\hat{M}$ |
| Alongwind | 1.9141 | 0.7878 | 0.8886 | 3.1016 |
| Acrosswind | - | 1.1038 | 2.5018 | 2.7345 |
| Torsional | - | 0.0905 | 0.1006 | 0.1353 |

■ Survivability Design (50-year wind) : Maximum Displacements

| | Maximum Displacements at roof |
|---|---|
| Alongwind | 0.043 $m$ |
| Acrosswind | 0.141 $m$ |

**Figure 5.17 Survivability design calculations**

## 5.6  DISCUSSION OF RESULTS

In this chapter, wind imposed response of the building which was investigated through the wind tunnel tests performed in Ankara Wind Tunnel (AWT) has been analyzed by using several technical specifications which are ASCE 7-05, Eurocode 1, İYBRY and NatHaz Aerodynamic Loads Database. Main difference between these standards appears in definition of the wind profile, not only about its shape but also about its gustiness. For example, in ASCE 7-05, 3 sec gust speed is used whereas in Eurocode and İYBRY, it is converted into 10 minute gust wind speed. In addition, the property definitions of the exposure categories vary. Hence, in ASCE 7-05, the exposure category defined for open terrain (C) is selected and ones in the Eurocode and İYBRY that are most similar to this definition are chosen. (II)   Wind profiles of these three specifications are compared on a graph in Figure 5.18 below. In the figure it is seen that ASCE profile is a bit smaller in magnitude than the other two profiles. İYBRY and Eurocode 1 definitions are approximately the same. Note that in the Ankara Wind Tunnel (AWT) test studies and in NatHaz, wind profile definition of ASCE 7-05 is directly used.
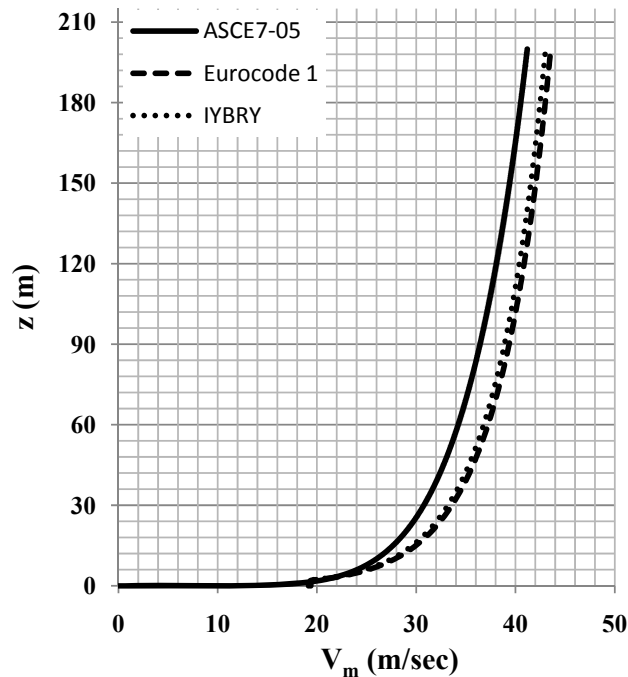


**Figure 5.18 Comparison of wind profile definitions in technical specifications**

Wind response of a tall building mainly comprises of base bending moments, top accelerations and equivalent static load definitions. In the technical specifications, analytical calculations are expressed only in the along-wind direction; however, in AWT tests, response in across wind direction is also achieved which could only be compared with NatHaz solutions. Top acceleration is described in all of the guidelines except İYBRY. As a result, first of all the equivalent wind load definitions in the along wind direction are presented in Figure 5.19. Then, base bending moments in along wind direction are compared for all of the calculation procedures in Table 5.1. After that, in Table 5.2, top accelerations are listed for all except İYBRY. Finally, in Table 5.3, base bending moment components in along and across wind directions obtained in the AWT tests are compared with the NatHaz solutions.
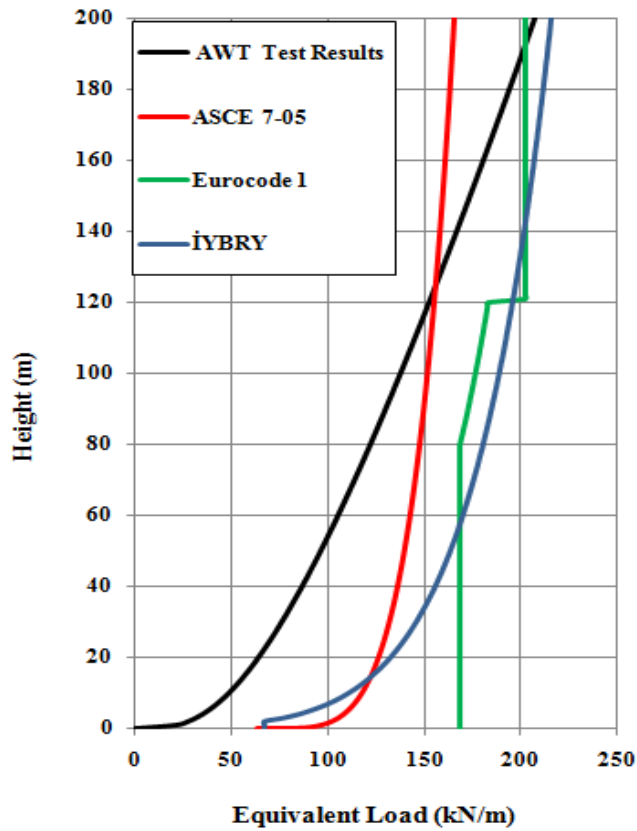


**Figure 5.19 Comparison of equivalent static wind load definitions**

In Figure 5.19, the equivalent wind loads that are calculated by using the technical specifications ASCE 7-05, Eurocode and İstanbul Yüksek Binalar Rüzgar Yönetmeliği and by using the results of Ankara Wind Tunnel tests are presented. They are the ones determined for open environment exposure type for zero degree angle of attack and in along wind direction. In each of them the shapes are quite different. Especially, Eurocode 1 defines a load pattern in a discrete way in which load is constant up to a certain height and changes linearly till another height after which it remain again constant; whereas, in ASCE 7-05 and İYBRY, equivalent static loads have a parabolic shape. Although, from the AWT test results, equivalent load starts from 0 and increases in a more steep manner, in the specifications, load starts from a certain magnitude. The shapes and magnitudes of the equivalent static loads affect the base bending moments presented in Table 5.1. In NatHaz, equivalent static loads are defined such that the equivalent loads obtained from each component of base bending moments are presented. It is compared with the equivalent loads obtained from Ankara Wind Tunnel test result in the same way in Figure 5.20 below.
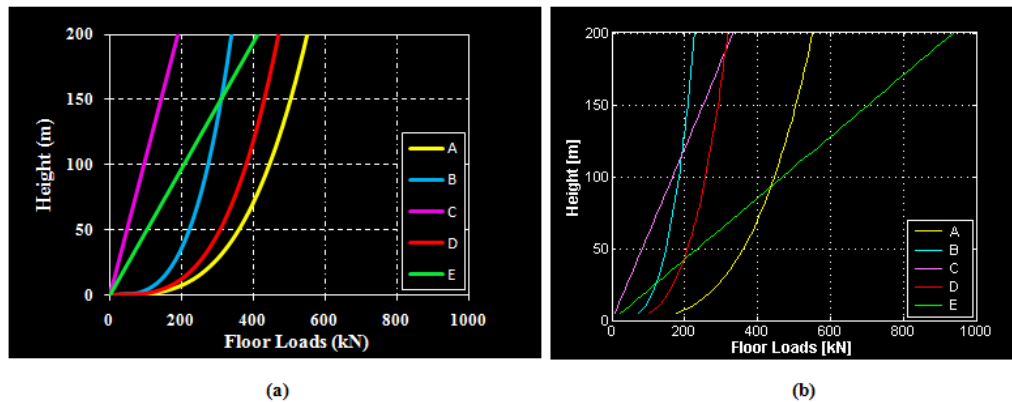


**Figure 5.20 Wind force components (a) from Ankara Wind Tunnel Tests (b) from NatHaz**

In Figure 5.20, wind force components in along and across wind directions are presented. The graph on left is obtained from the Ankara Wind Tunnel test results and the one on right is from NatHaz Aerodynamic Loads Database. The letters in the legends denote the components such that A is the mean components; B is along wind background component; C is along wind resonant component; D is across wind background component; and E is across wind resonant component. The floor loads are calculated by multiplying the

equivalent static load (kN/m) by the floor height which is assumed to be 5 m. It is observed in Figure 5.20 that mean component is almost the same but the others are quite different. Especially the across wind resonant component which is represented by letter 'E' is very divergent in NatHaz from AWT results. It is mainly due to the fact that after a certain normalized frequency, NatHaz assumes the magnitude of the normalized spectra as constant but in AWT results, the shape of the spectra are taken as they are. In addition, the turbulence intensities in NatHaz tests and AWT tests are quite different (Kareem, et al., 2000). The difference between the resonant components in across wind direction affects the top accelerations as it can be observed in Table 5.2.

**Table 5.1 Comparison of base bending moment results**

|  | **Base bending moment** |
|---|---|
| AWT | 3.206 |
| NatHaz | 3.102 |
| ASCE 7-05 | 3.112 |
| Eurocode 1 | 3.835 |
| İYBRY | 3.925 |

*All dimensions are in $10^6$ kN.m*

In Table 5.1, it is seen that maximum base bending moments are calculated in Eurocode 1 and İYBRY which is mainly resulted from the definitions of the wind profiles. Since wind speed is larger for these two, the wind induced pressure and hence the bending moments are calculated around 25% higher in magnitude. Wind speed at maximum height of the building, 200 m in Eurocode profile is around 5% larger than corresponding ASCE definition. Since wind induced force and moment are directly related with the wind pressure and it is related with the square of the wind speed, difference in the results of moments are in an amount of square of the difference in wind speeds. On the other hand, differences in the approach of distributing wind loads to the height have caused minor differences in the results as well. The slight difference between NatHaz and ASCE solutions is because of the fact that there is not a model definition in NatHaz which has exactly the same geometrical

properties with the building under consideration and the most similar one is chosen. Bending moment obtained from AWT tests differ from ASCE and NatHaz solutions in 3% and from Eurocode and İYBRY in 20%. It is unavoidable for getting this much difference with the Eurocode and İYBRY results due to the wind profile variations. The 3% difference of Ankara Wind Tunnel tests is mainly due to change in turbulence intensity which is detailed in Chapter 3.

**Table 5.2 Comparison of top accelerations**

| | Acceleration |
|---|---|
| AWT | 2.580 |
| NatHaz | 5.200 |
| ASCE 7-05 | 2.433 |
| Eurocode 1 | 2.469 |

*All dimensions are in mg*

**Table 5.3 Comparison of results of AWT and NatHaz**

| | Along-wind Direction | | | | | Across-wind Direction | | | | |
|---|---|---|---|---|---|---|---|---|---|---|
| | $\bar{M}$ | $\widehat{M}_B$ | $\widehat{M}_R$ | $M_d$ | $\widehat{\widehat{Y}}$ | $\bar{M}$ | $\widehat{M}_B$ | $\widehat{M}_R$ | $M_d$ | $\widehat{\widehat{Y}}$ |
| **AWT** | 1.917 | 1.182 | 0.512 | ***3.205*** | ***2.580*** | 0.000 | 1.635 | 1.104 | ***1.973*** | ***4.428*** |
| **NATHAZ** | 1.914 | 0.788 | 0.889 | ***3.102*** | ***5.200*** | 0.000 | 1.104 | 2.502 | ***2.735*** | ***12.890*** |

*All dimensions of moments are in $10^6$ kN.m and accelerations in mg.*

In Table 5.3, $\bar{M}$ is average moment; $\widehat{M}_B$ and $\widehat{M}_R$ are background and resonant components of base moment; $M_d$ is the design base moment which is calculated by summing the average moment and the square root of sum of squares of resonant and background components; $\widehat{\widehat{Y}}$ is

114

the top acceleration. In Chapter 3 it is discussed that turbulence intensity in AWT tests has been greater than it is defined in ASCE7-05. In Chapter 4, investigations of the results of wind tunnel tests performed in different exposure categories and hence different turbulence intensities have shown that higher turbulence intensity leads to an increase in the background component of base bending moment and decrease in the resonant component of base bending moment. In Table 5.3, the same phenomenon holds true as well and while background component in AWT tests is greater than the NatHaz results, resonant component is less. Average moments are nearly the same for both. However, these differences affect resultant design base bending moments in the along wind direction with a difference around 3% only. On the contrary, in across wind direction, since main reason for base bending moment occurrence is vortex shedding vibrations (Holmes, 2005); the resonant component is more dominant. Because resonant component in AWT tests is less than the one in NatHaz, the design base bending moment in across wind direction is less compared with NatHaz result in around 40%. This difference affects the top accelerations such that they are 2-3 times less in AWT results.

# CHAPTER 6

# CONCLUSIONS

In this study, series of wind tunnel tests have been performed in Ankara Wind Tunnel. Ankara Wind Tunnel has a comparatively short test section which is not very suitable for building testing because it is very difficult to create atmospheric boundary layer with desired properties. Therefore, in order to create atmospheric boundary layer and simulate the wind profile in nature, special boundary layer creation elements were designed and mounted at the inlet of the test section. Wind speed through the test section height was measured by means of a hot-wire anemometer system during the experiments. Response of a rectangular building model was measured with High Frequency Base Balance system which has been designed and produced specifically for this study. The balance system was able to measure two perpendicular base bending moments of the model. Throughout the tests, effects of different wind profiles and different angles of attack on response of the building have been analyzed. Finally, response of the building has been examined using the procedures defined in some technical specifications such as ASCE 7-05 (ASCE 7-05, 2005), Eurocode 1 (Eurocode 1, 2005), İstanbul Yüksek Binalar Rüzgar Yönetmeliği (İYBRY, 2009) and NatHaz Aerodynamic Loads Database (Kareem, et al., 2000); and they have been compared with the results obtained from Ankara Wind Tunnel tests. At the end of these studies, the following conclusions can be drawn.

- Effects of wind profile and turbulence intensity on the response of tall buildings are very significant. Therefore, during the wind tunnel tests, it is exclusively recommended that wind profile and turbulence intensity should match with their correspondences in the location where the building under consideration will be constructed as much as possible. If these data will be gathered from a national wind guideline instead of a field study, not only wind speeds but also turbulence intensities should be defined clearly under the scope of that guideline during its preparation.

116

- In a wind tunnel whose test section is comparatively short, boundary layer creation elements result in an admissible similitude of wind profile and turbulence intensity.

- Wind induced response of a tall building can be examined in three major components which are mean component, background and resonant fluctuating components. Mean component can easily be calculated in case the drag coefficient is known. Background and resonant components are related with the randomness of wind which depends on turbulence intensity.

- It is observed that turbulence intensity has a negative influence on the vortex generation. In other words, response of the building which is resulted from the vortex generation is less when the turbulence intensity is high. An example for this kind of response can be the resonant components of base bending moments especially in across wind direction.

- Response of a rectangular tall building varies according to its aspect ratio (D/B). As the aspect ratio increases, wind induced actions on the building decreases. Especially, it is observed that vortex shedding effects diminish if dimension of the building parallel to the wind direction is greater than perpendicular one.

- In a rectangular tall building, vortex shedding phenomenon leads to considerable base bending moments in the across wind direction and it may be so dominant if fundamental frequency of the building is close to the vortex shedding frequency. In case of equality, the building can experience resonance. Therefore, during the design process of a tall building, in addition to the analysis in along wind direction, it is strongly recommended that its response in across wind direction should also be studied carefully, especially regarding the resonance issue.

- It is observed during the analysis made for different wind directions that unlike the traditional approaches, maximum base moment does not necessarily occur in the perpendicular directions. Hence, effects of wind angle of attack should be considered in the design of a tall building.

- In order to provide comfort criteria, maximum top accelerations should be studied especially in across wind direction since main cause of the acceleration is the vortex shedding phenomenon which is dominant in across wind direction.

- High frequency base balance system should be designed so that it has a high frequency out of the range of modal frequencies of the building under consideration. Otherwise, it leads to biased results regarding response of the building in the range of fundamental frequency of the system itself.

- Through an improvement in the design of the high frequency base balance system, in addition to the base bending moments, two base shear forces and torsional moment can

also be measured. By the help of base shear force measurements, information about the shape of the distribution of dynamic wind loads in the storeys can be obtained instead of applying the linear mode shape assumption or the definitions in the technical specifications.

# REFERENCES

**ASCE 7-05 ASCE** Minimum Design Loads for Buildings and Other Structures. - United States of America : American Society of Civil Engineers, 2005.

**Baals Donald D. and Corliss William R.** Wind Tunnels of NASA. - Washington, D.C. : National Aeronautics and Space Administration, 1981.

**By the ASCE Aerospace Division Task Committee on Wind Tunnel Studies of Buildings and Structures** Wind Tunnel Studies of Buildings and Structures // Journal of Aerospace Engineering. - 1996. - pp. 19-36.

**Cermak E.J.** Physical Modelling of the Atmospheric Boundary Layer (ABL) in Long Boundary Layer Wind Tunnel (BLWT) - Colorado : Fluid Dynamics and Diffusion Lab, College of Civil Engineering, Colorado State University, 1982.

**Cermak E.J.** Progress in Physical Modelling for Wind Engineering // Journal of Wind Engineering 55. - 1995. - pp. 439-455.

**Cermak E.J., Cochran L.S. and Leffler R.D.** Wind Tunnel Modelling of the Atmospheric Surface Layer // Journal of Wind Engineering 54/55. - 1995. - pp. 505-513.

**Cermak J.E., Sadeh W.Z. and Hsi. G.** Fluctuating moments on tall buildings produced by wind loading // Natural Bureau of Standards Building Science Series 30. - 1970. - pp. 45-59.

**Cermak Jack E.** Wind-tunnel development and trends in applications to civil engineering // Journal of Wind Engineering and Industrial Aerodynamics 91. - 2003. - pp. 355-370.

**Cheung J.C.K. and Melbourne W.H.** Torsional Moments of Tall Buildings // Journal of Wind Engineering and Industrial Aerodynamics 41-44. - 1992. - pp. 1125-1126.

**Clough Ray W. and Penzien Joseph** Dynamics of Structures - Berkeley : Computers & Structures, Inc., 2003.

**Cook N.J.** On Simulating the Lower Third of the Urban Adiabatic Boundary Layer in a Wind Tunnel // Atmospheric Environment 7. - 1973. - pp. 691-705.

**Counihan J.** An Improved Method of Simulating an Atmospheric Boundary Layer in a Wind Tunnel // Atmospheric Environment 3. - 1969. - pp. 197-214.

**Counihan J.** Simulation of an Adiabatic Urban Boundary Layer in a Wind Tunnel // Atmospheric Environment 7. - 1973. - pp. 673-689.

**Davenport A.G.** Gust Loading Factors // ASCE Journal of the Structural Division 93. - 1967. - pp. 11-34.

**Davenport A.G.** Note on the Distribution of the Largest Value of a Random Function with Application to Gust Loading // Proceeding, Institute of Civil Engineers 28. - 1964. - pp. 187-196.

**Davenport A.G.** The Treatment of Wind Loading on Tall Buildings // Symp. on Tall Buildings at the University of Southampton. - 1966. - pp. 3-44.

**Eurocode 1** Actions on Structures - Part 1-4: General actions - Wind actions - Brussels : European Committee for Standardization, 2005.

**Fuji K., Hibi K. and Ueda H.** A new measuring system using electronically scanned pressure sensors (ESP) and some applications of the ESP system to a squared building shape // 9th Symposium on Wind Engineering. - 1986. - pp. 313-318.

**Gamble Scott** Wind Tunnel Testing // STRUCTURE magazine. - 2003. - pp. 24-27.

**Garg R.K., Lou J.X. and Kasperski M.** Some Features of Modelling Spectral Characteristics of Flow in Boundary Layer Wind Tunnels // Journal of Wind Engineering 72. - 1997. - pp. 1-12.

**Hart Gary C. [et al.]** Structural Design Using a Wind Tunnel Test Program and a Risk Analysis // Journal of Wind Engineering and Industrial Aerodynamics 14. - 1983. - pp. 27-36.

**Holmes John D.** Wind Loading of Structures - New York : Taylor & Francis Group , 2005.

**Irwin A.W.** Human Response to Dynamics Motion of Structures // The Structural Engineer. - 1978.

**Irwin H.P.** The Design of Spires for Wind Simulation // Journal of Wind Engineering and Industrial Aerodynamics. - 1981. - pp. 361-366.

**Isyumov N. and Poole M.** Wind Induced Torque on Square and Rectangular Building Shapes // Journal of Wind Engineering and Industrial Aerodynamics 13. - 1983. - pp. 183-196.

**İYBRY** İstanbul Yüksek Binalar Rüzgar Yönetmeliği - İstanbul : İstanbul Büyükşehir Belediyesi, 2009.

**Lythe G.R. and Surry D.** Wind Induced Torsional Loads on Tall Builidings // Journal of Wind Engineering and Industrial Aerodynamics 36. - 1990. - pp. 225-234.

**Mendis P. [et al.]** Wind Loading on Tall Buildings // Ejse Special Issue: Loading on Structures. - 2007. - pp. 41-54.

**Ohya Y.** Wind-Tunnel Study of Atmospheric Stable Boundary Layer over a Rough Surface // Boundary-Layer Meteoroogy 98. - 2001. - pp. 57-82.

**Potter Merle C. and Wiggert David C.** Mechanics of Fluids - USA : Brooks/Cole, 2002.

**Shojaee Nima [et al.]** Design and Analysis of Passive Devices for Atmospheric Boundary Layer Simulation in a Short Aeronautical Wind Tunnel // 5th Ankara International Aerospace Conference. - Ankara : [s.n.], 2009.

**Simiu Emil and Scanlan Robert H.** Wind Effects on Structures - New York : John Wiley & Sons, 1978.

**TS 498** Yapı Elemanlarının Boyutlandırılmasında Alınacak Yüklerin Hesap Değerleri - Ankara : Türk Standardları Enstitüsü, 1987.

**Tschanz T. and Davenport A.G.** The Base Balance Technique for the Determination of Dynamic Wind Loads // Journal of Wind Engineering and Industrial Aerodynamics 13. - 1983. - pp. 429-439.

**Tübitak Savunma Sanayii Araştırma ve Geliştirme** // Tarihçe-TÜBİTAK-SAGE. - 16 April 2011. - http://www.sage.tubitak.gov.tr/aerodinamik/art_tarihce.asp.

**Vickery B.J.** On the Flow Behind a Coarse Grid and Its Use as a Model of Atmospheric Turbulence in Studies related to Wind Loads on Buildings - [s.l.] : National Physical Laboratory (U.K.) Aero Report 1143, 1965.

**Wirsching Paul H., Paez Thomas L. and Ortiz Keith** Random Vibrations - New York : John Wiley & Sons, Inc., 1995.

**Zhang W.J., Xu Y.L. and Kwok K.C.S.** Torsional Vibration and Stability of Wind-Excited Tall Buildings with Eccentricity // Journal of Wind Engineering and Industrial Aerodynamics. - 1993. - pp. 299-309.

**Zhou Yin, Kiyewski Tracy and Kareem Ahsan** Aerodynamic Loads on Tall Buildings: Interactive Database // ASCE Journal of Structural Engineering. - 2003. - pp. 394-404.

http://www.modernsteel.com/Uploads/Issues/August_2005/30744_davenport.pdf., last access on 17/04/2011

http://www.cppwind.com/about/people/principals/cermak.htm., last access on 17/04/2011

http://aerodata.ce.nd.edu/., last access on 29/05/2011

http://www.nd.edu/~nathaz/doc/ak-resume-May%202009.pdf., last access on 20/04/2011

# APPENDIX A

# DEFINITIONS

- *Stationary Process*: It is a kind of a process statistical properties of which do not change with time. In other words, it implies that a process continues from the infinite past to infinite future. Obviously, encountering exactly real stationary processes in nature is impossible but many environmental problems are practically assumed to be stationary in case the natural periods of the systems are too short compared with the duration of loading (Wirsching, et al., 1995). Wind loading problems on tall buildings are accepted to be stationary processes.

- *Gaussian (Normal) Distribution*: It is a most widely used kind of continuous probability distributions. Random variables that are formed by superposition of many other random variables approach to Gaussian distribution (Wirsching, et al., 1995). Therefore, wind as a natural event is reasonably accepted to fit normal distribution.

- *Mean*: It is the average value of a random process. In other words, it is the summation of the variables divided by the number of the variables of a random process.

- *Standard Deviation*: It is measurement of variability in statistics. It reflects how much dispersion exists from the mean.

- *Autocorrelation Function*: It is a mathematical tool that is used to find the similarities between the processes with themselves within a time interval.

- *Fast Fourier Transform (FFT)*: It is a special algorithm used to compute discrete Fourier transform (DFT). In DFT or specifically FFT, it is aimed to transfer a time dependent process into frequency domain by decomposing it into its components of different frequencies. It provides the transition between time and frequency domains.

- *Spectral density function*: It is used to characterize a stationary random process in the frequency domain. It is basically Fourier transform of the autocorrelation function. It can be numerically computed by Fast Fourier Transform (FFT).

# APPENDIX B

# ANKARA WIND TUNNEL TEST RESULTS

In this part of the study, results of the tests conducted in Ankara Wind Tunnel are presented. Time dependent base bending moment graphs and their Fast Fourier Transforms in the two perpendicular directions of the building (X and Y) are presented.
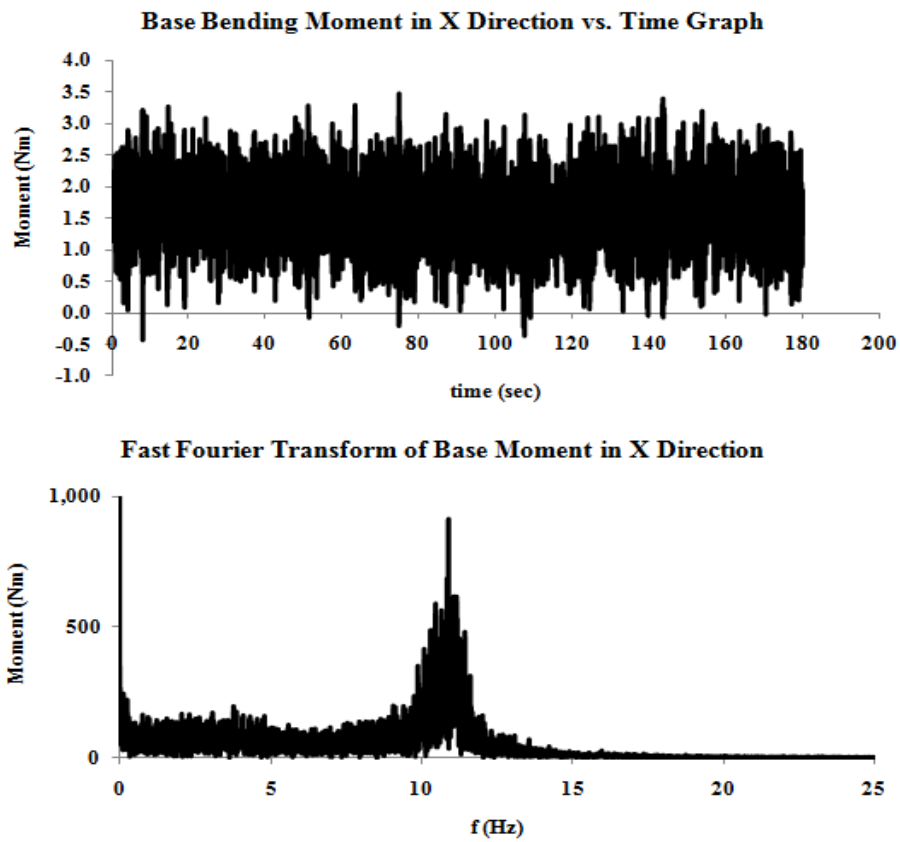


**Figure A. 1 Base bending moment and its FFT for the test in Exposure C and 0° angle of attack in X direction**

**Base Bending Moment in Y Direction vs. Time Graph**



**Fast Fourier Transform of Base Moment in Y Direction**
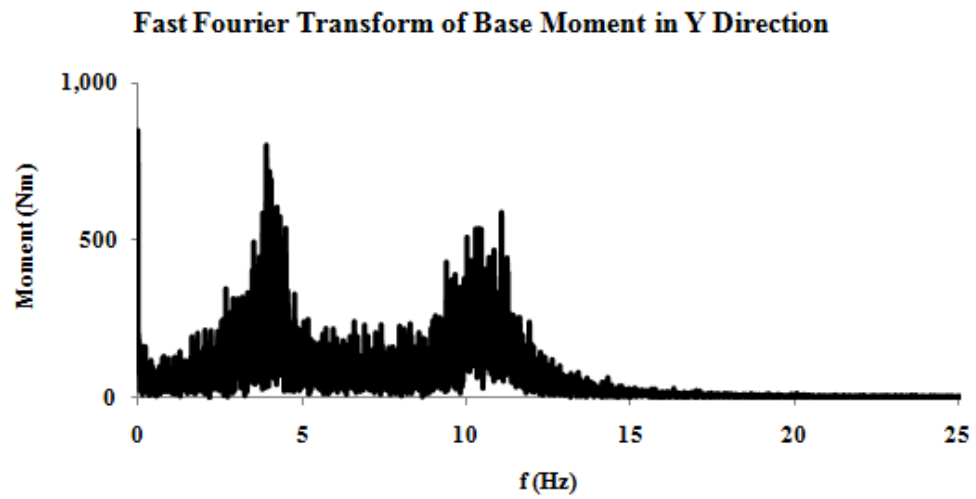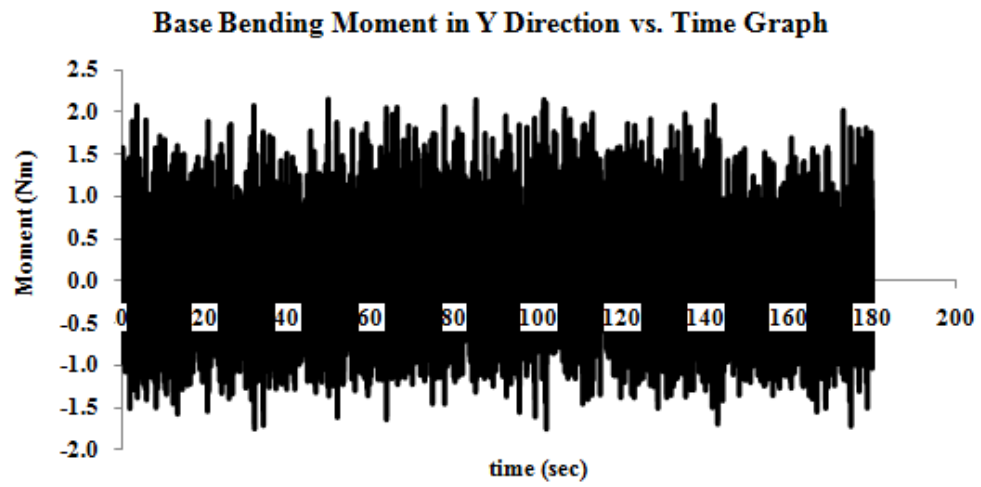


**Figure A. 2 Base bending moment and its FFT for the test in Exposure C and 0° angle of attack in Y direction**

**Base Bending Moment in X Direction vs. Time Graph**



**Fast Fourier Transform of Base Moment in X Direction**
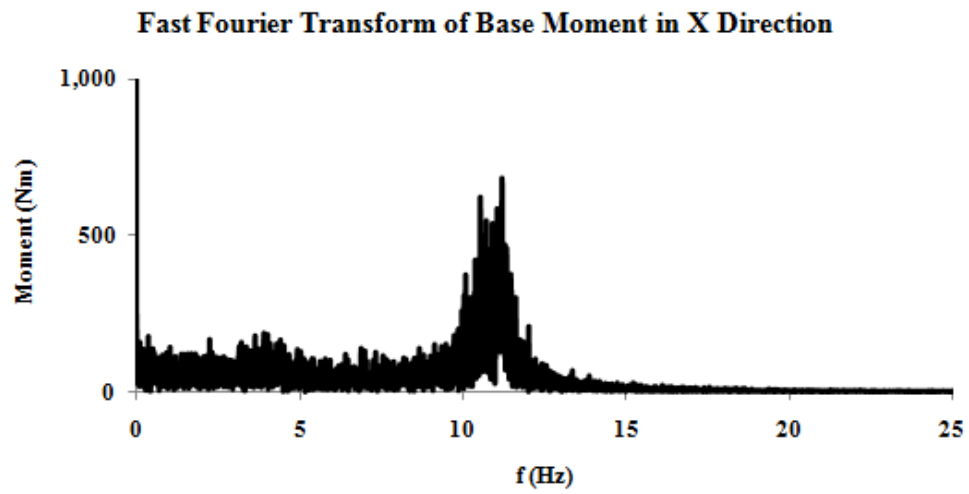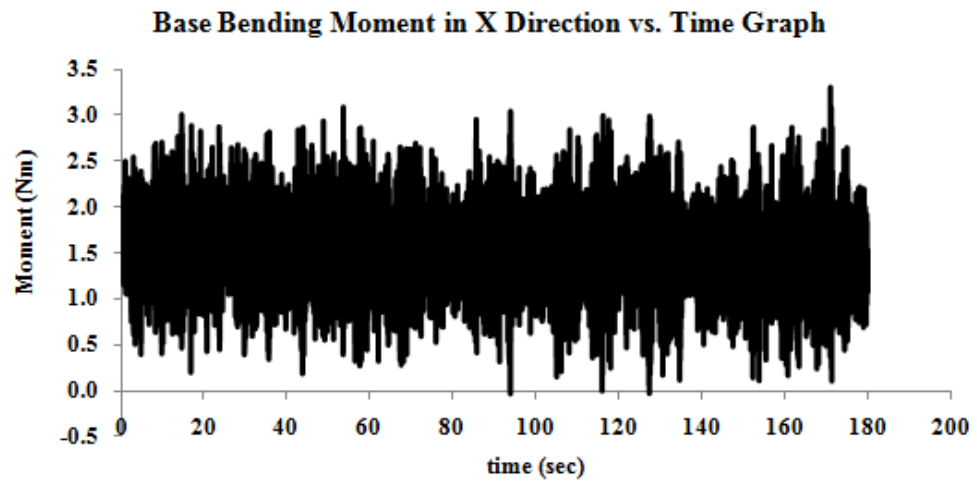


**Figure A. 3 Base bending moment and its FFT for the test in Exposure C and 15° angle of attack in X direction**

## Base Bending Moment in Y Direction vs. Time Graph



## Fast Fourier Transform of Base Moment in Y Direction
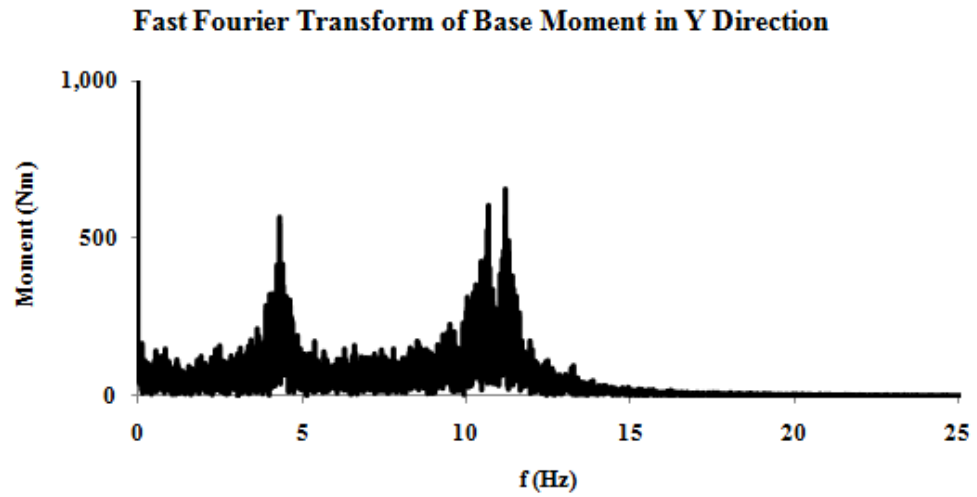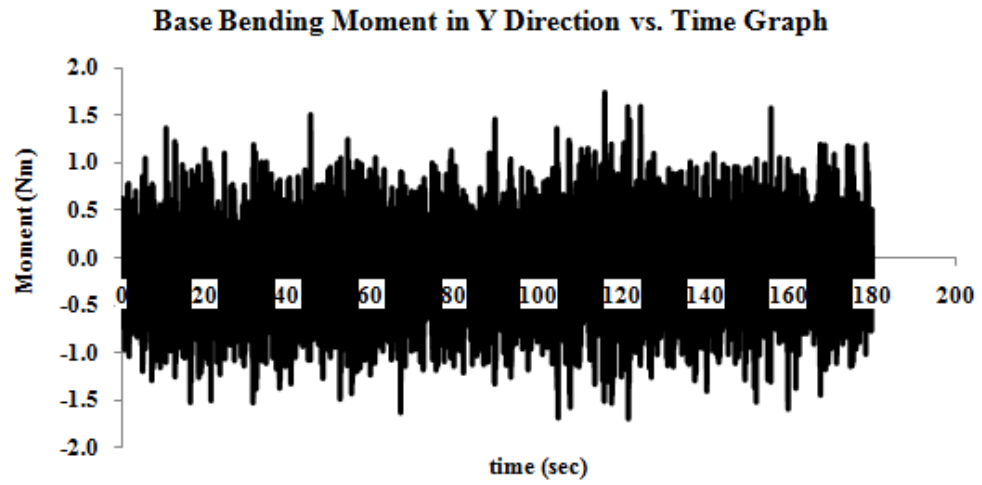


**Figure A. 4 Base bending moment and its FFT for the test in Exposure C and 15° angle of attack in Y direction**
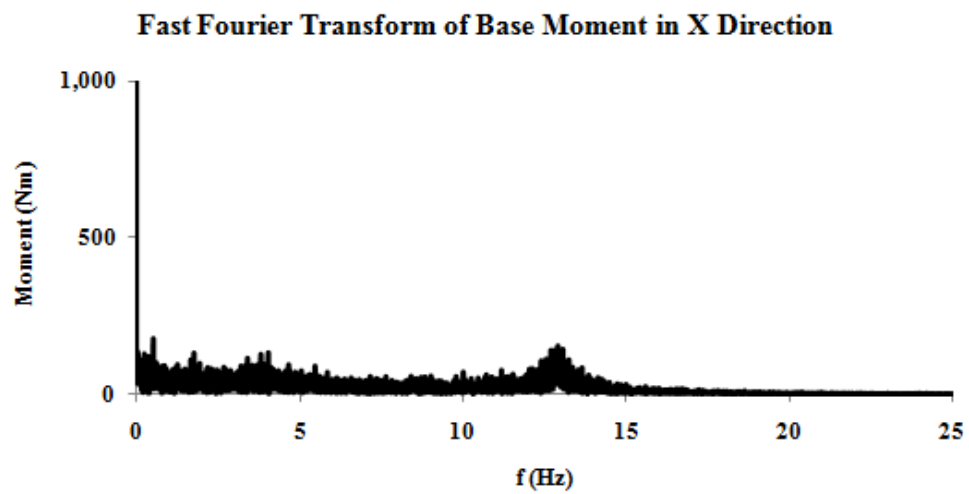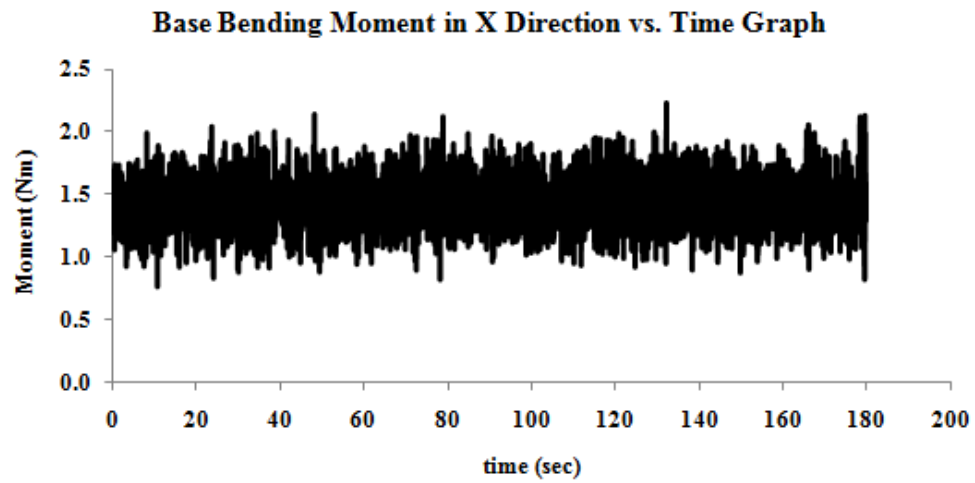
**Figure A. 5 Base bending moment and its FFT for the test in Exposure C and 30° angle of attack in X direction**
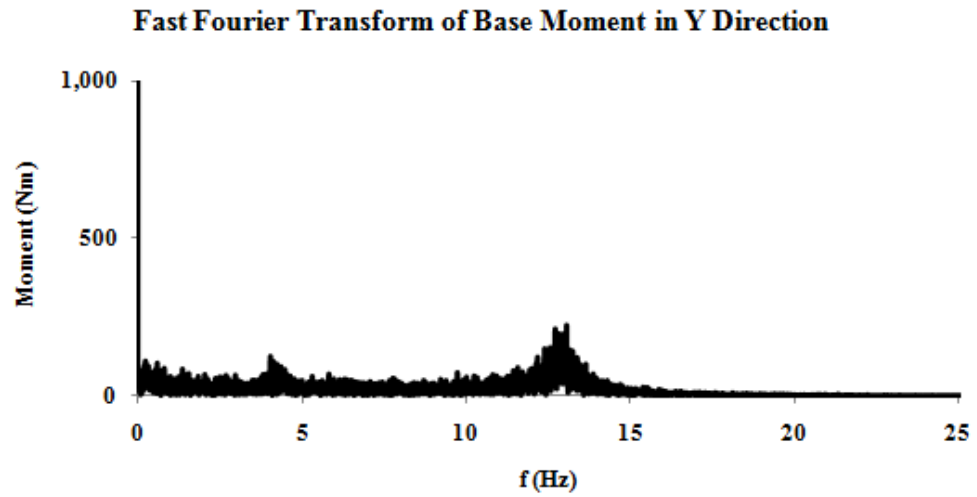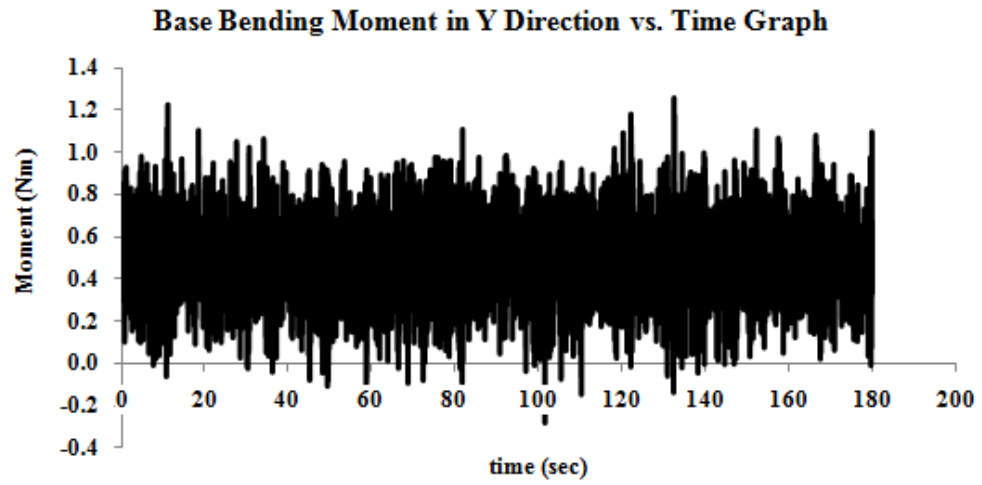
**Figure A. 6 Base bending moment and its FFT for the test in Exposure C and 30° angle of attack in Y direction**

## Base Bending Moment in X Direction vs. Time Graph



## Fast Fourier Transform of Base Moment in X Direction
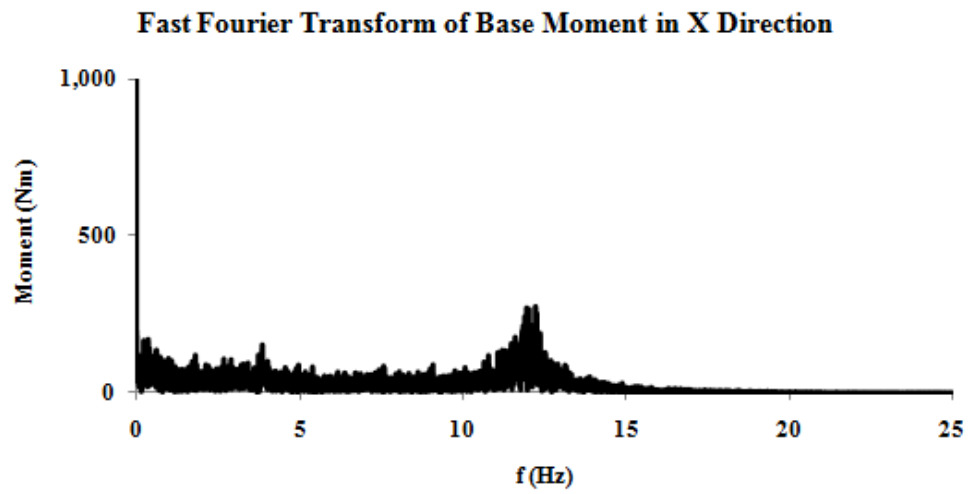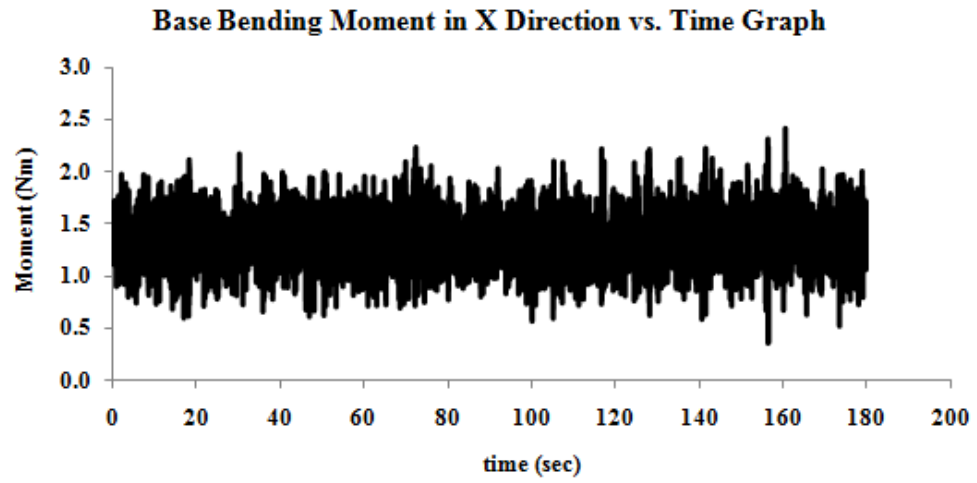


**Figure A. 7 Base bending moment and its FFT for the test in Exposure C and 45° angle of attack in X direction**

## Base Bending Moment in Y Direction vs. Time Graph



## Fast Fourier Transform of Base Moment in Y Direction
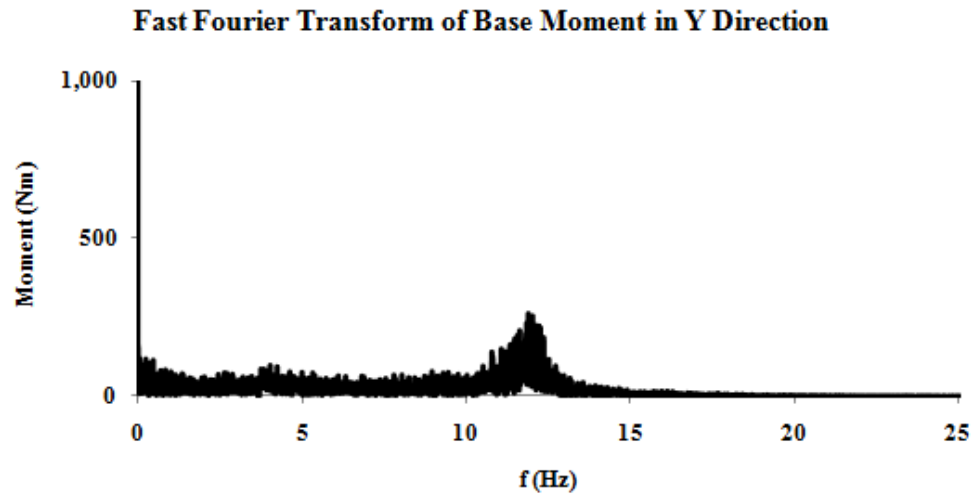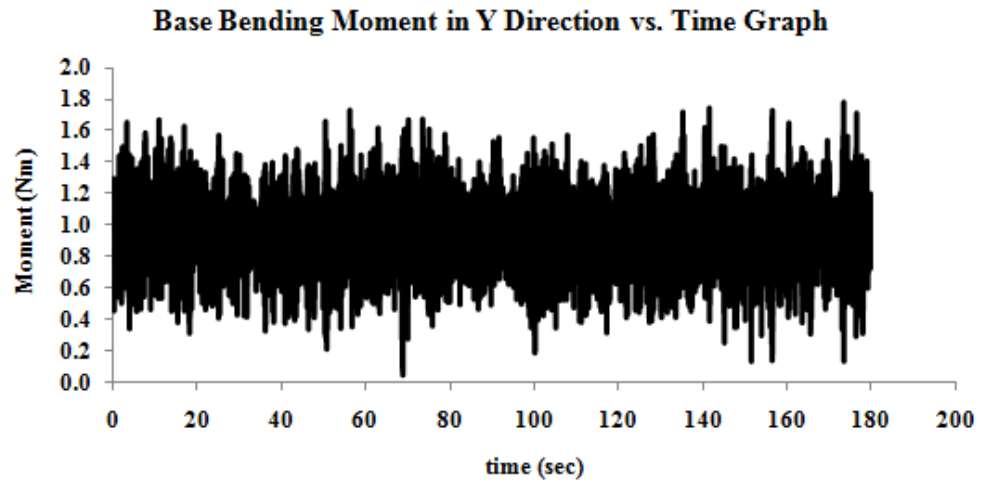


**Figure A. 8 Base bending moment and its FFT for the test in Exposure C and 45° angle of attack in Y direction**
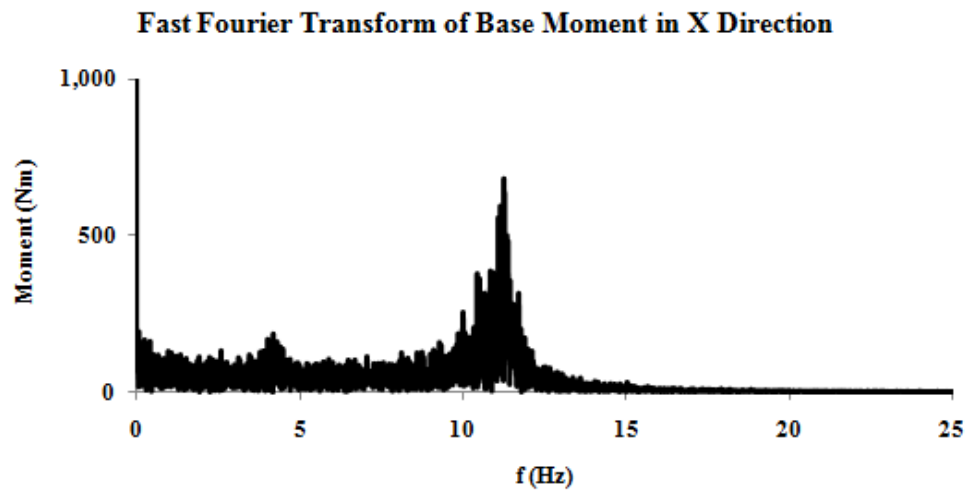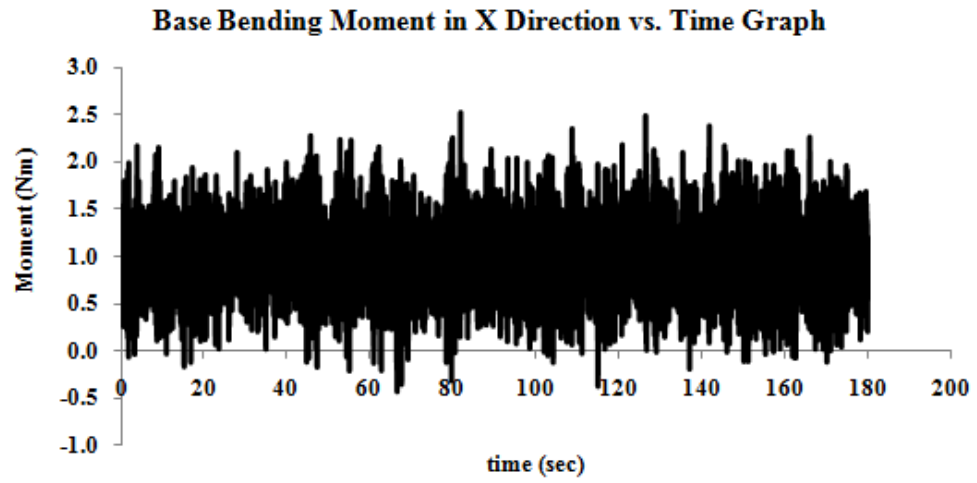
**Figure A. 9 Base bending moment and its FFT for the test in Exposure C and 60° angle of attack in X direction**
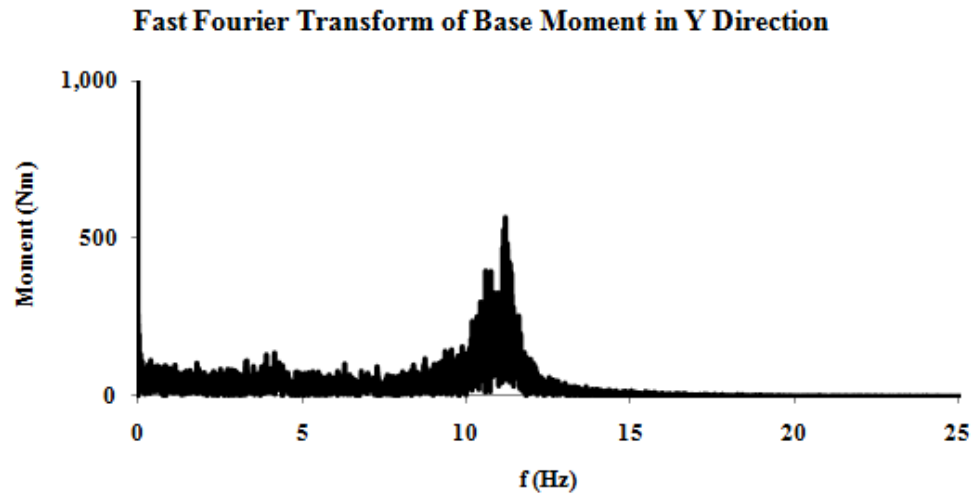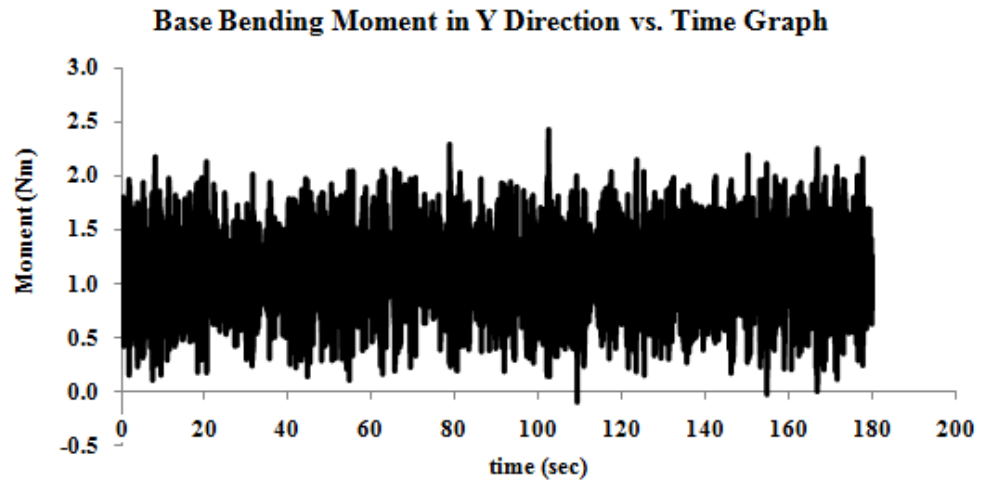
**Figure A. 10 Base bending moment and its FFT for the test in Exposure C and 60°
angle of attack in Y direction**
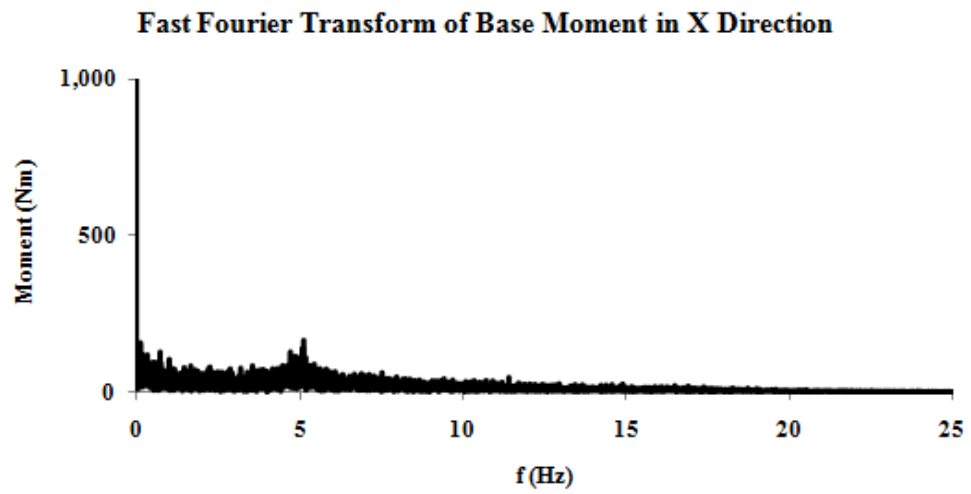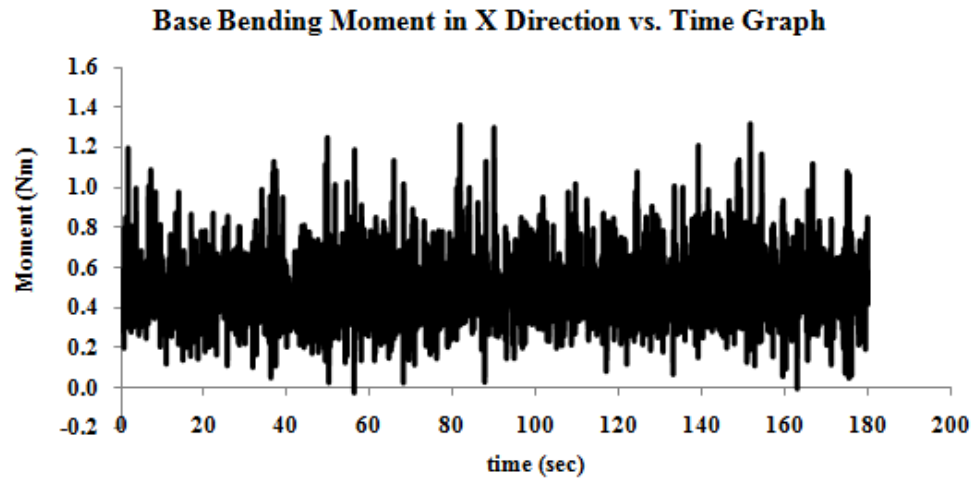
**Figure A. 11 Base bending moment and its FFT for the test in Exposure C and 75°
angle of attack in X direction**
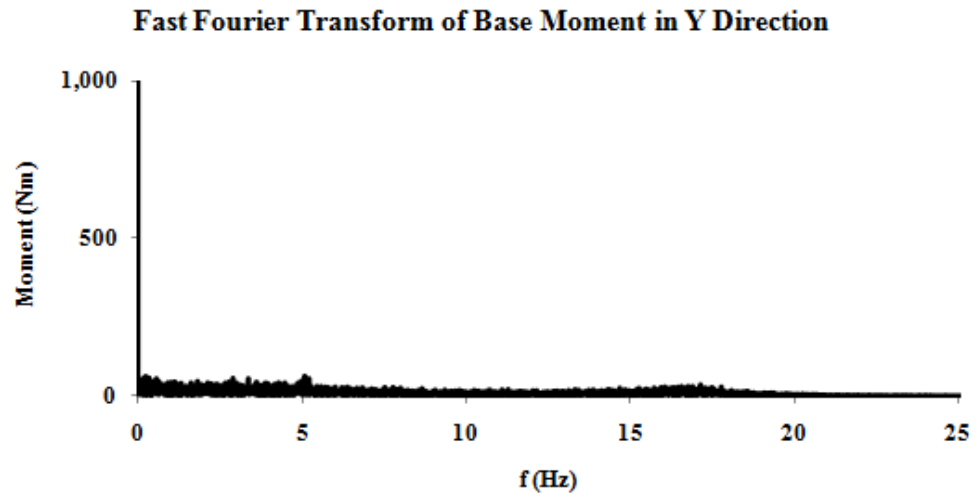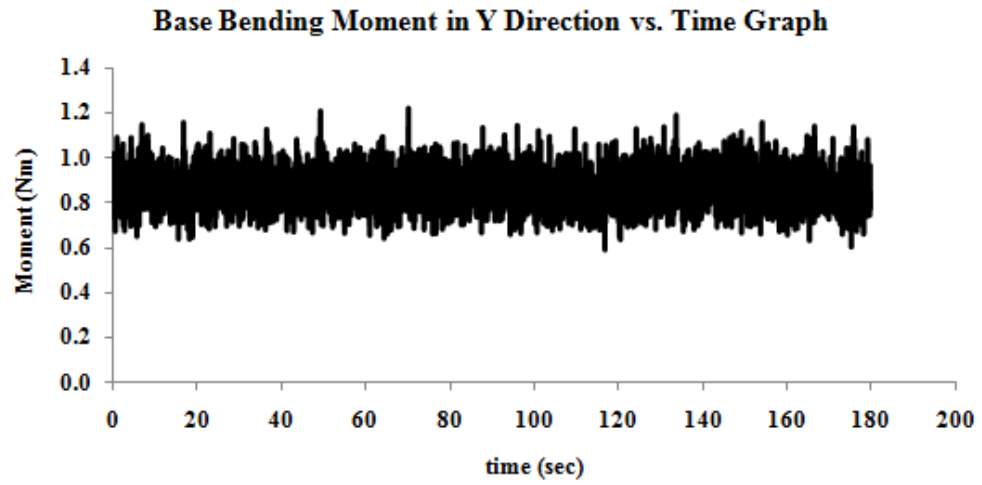
**Figure A. 12 Base bending moment and its FFT for the test in Exposure C and 75°
angle of attack in Y direction**
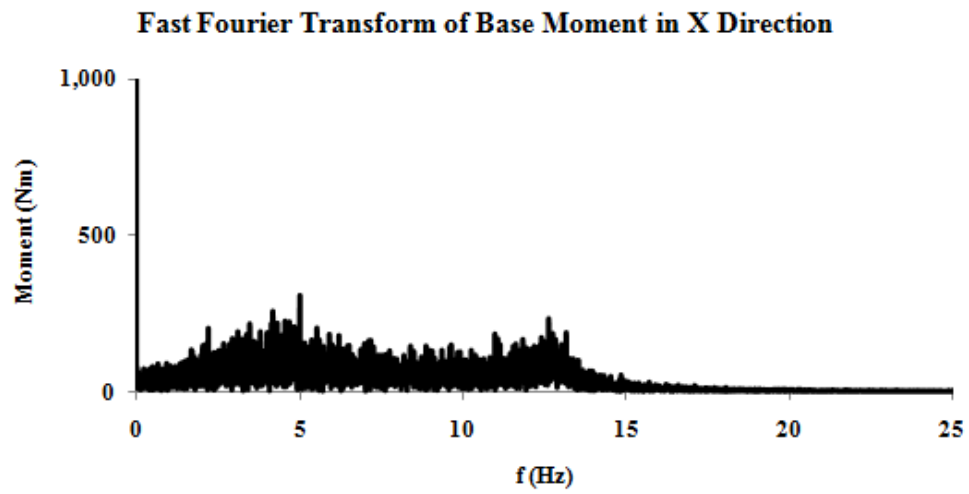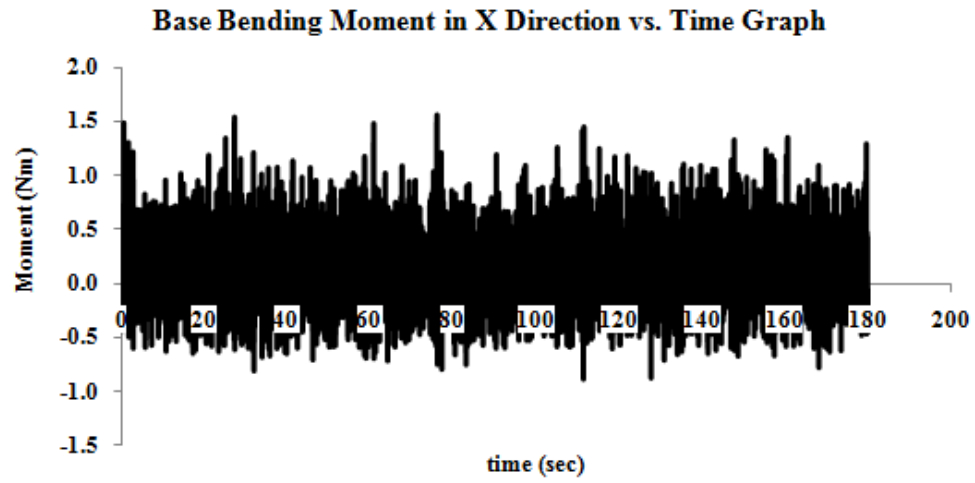
**Figure A. 13 Base bending moment and its FFT for the test in Exposure C and 90°
angle of attack in X direction**
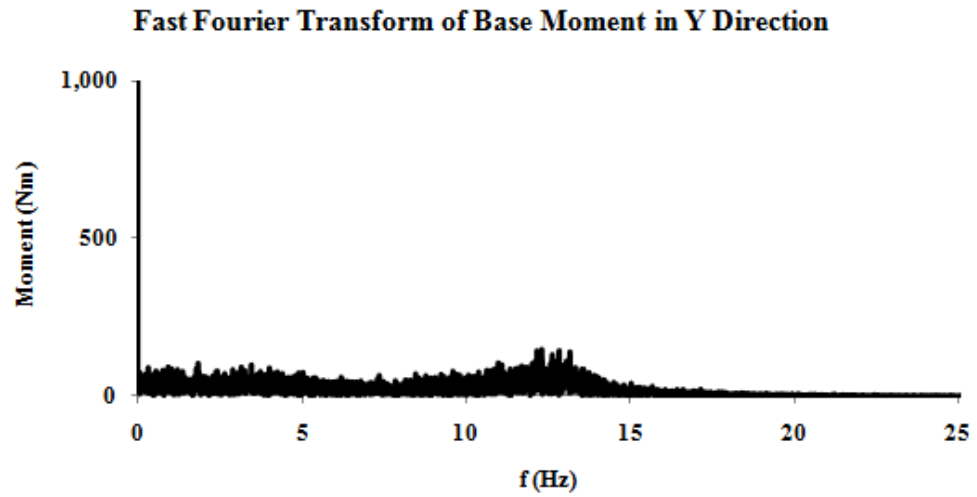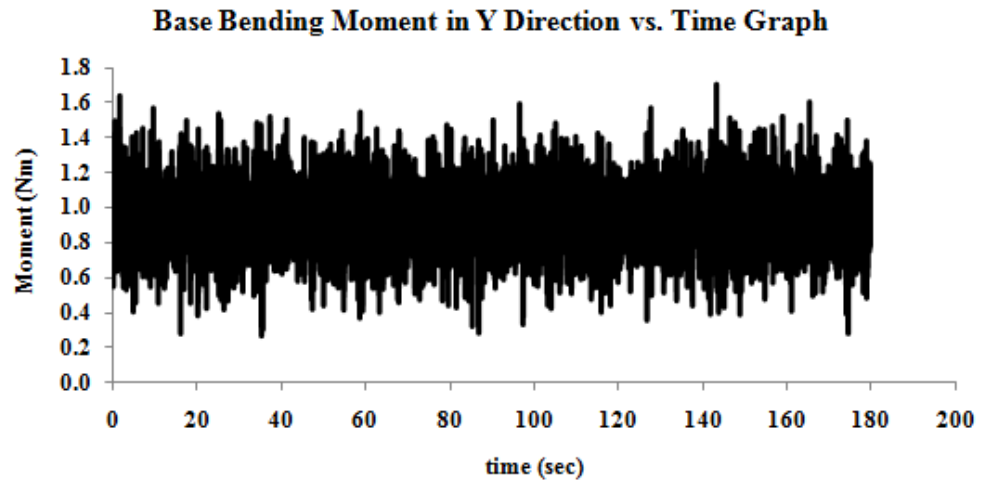
**Figure A. 14 Base bending moment and its FFT for the test in Exposure C and 90°
angle of attack in Y direction**
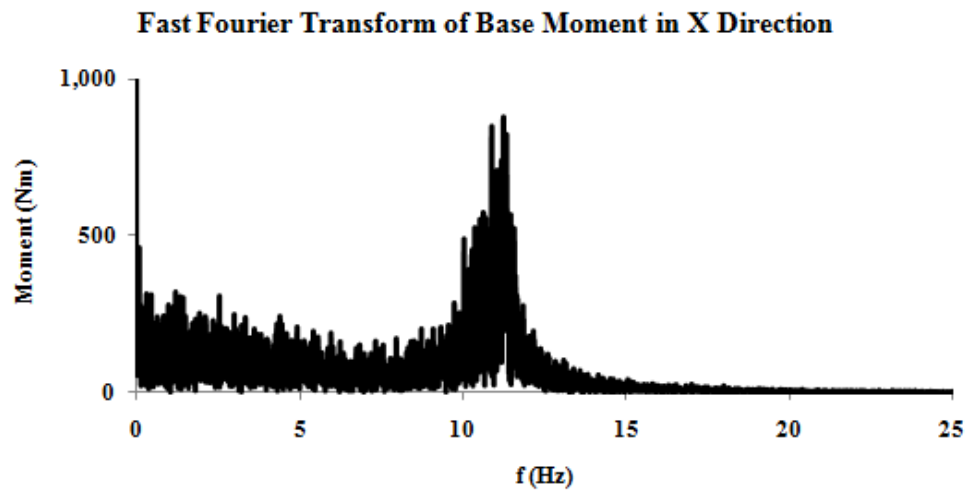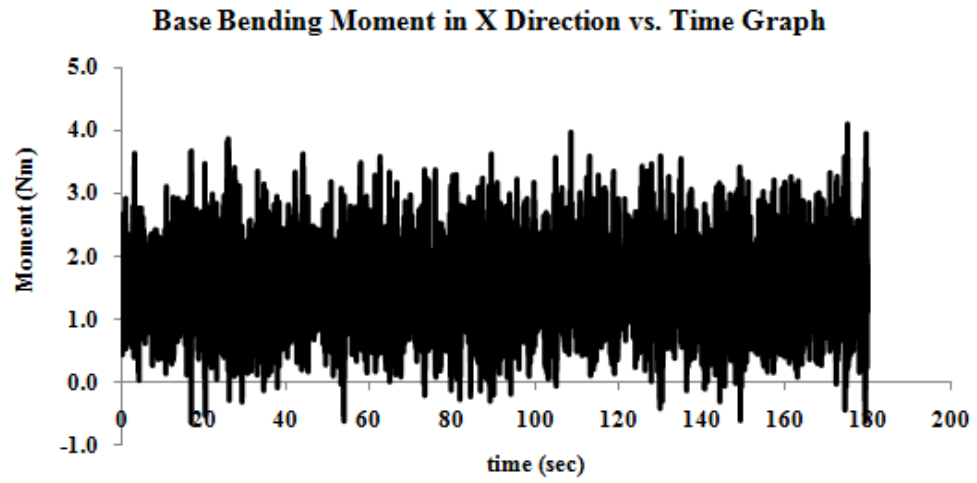
**Figure A. 15 Base bending moment and its FFT for the test in Exposure B and 0° angle of attack in X direction**
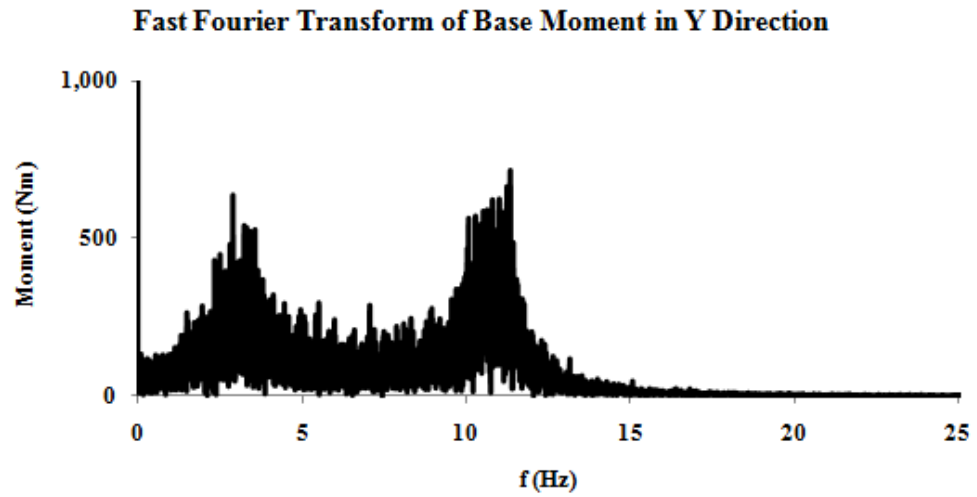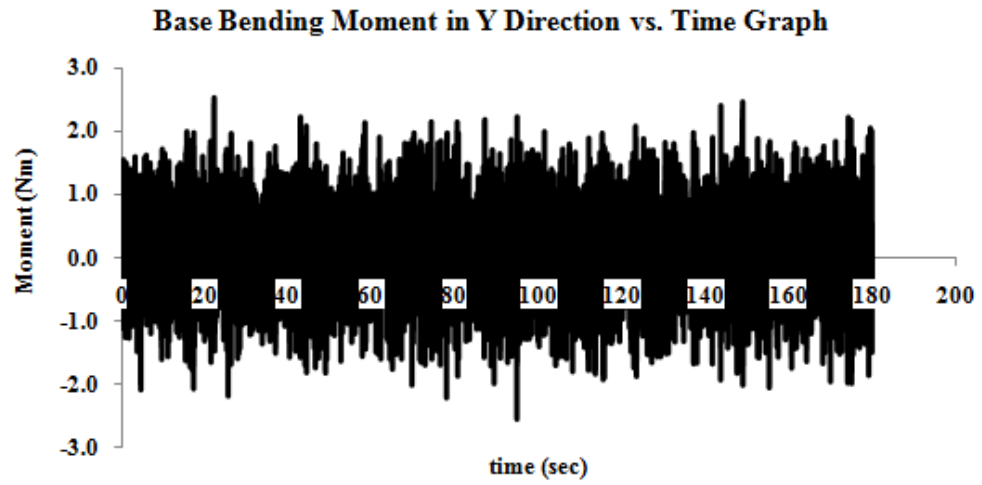
**Figure A. 16 Base bending moment and its FFT for the test in Exposure B and 0° angle of attack in Y direction**